Electrocatalytic Approaches for CO_2 Reduction and Hydrogen Generation

This Thesis is Presented for the Degree of

Master of Science

By

Finn Connaughton B. Sc.

Under Supervision of

Dr. Mary Pryce and Prof. Johannes G. Vos

at

Dublin City University,

School of Chemical Sciences,

Glasnevin,

Dublin 9.

September 2019

I hereby certify that this material, which I now submit for assessment on the programme of study leading to the award of Master of Science, is entirely my own work, and that I have exercised reasonable care to ensure that the work is original, and does not to the best of my knowledge breach any law of copyright, and has not been taken from the work of other save and to the extent that such work has been cited and acknowledged within the text of my work.

Signed: _____

Finn Connaughton

Candidate I.D. No.: 58538239

Date: 12/09/2019

Table of Contents

Table of Figures

Abbreviations:

ABAB	A porphyrin with two different groups in the meso position
ACN	Acetonitrile
ADP	Adenosine diphosphate
Ag/AgCl	Silver/silver chloride reference
Ag/Ag^+	Silver/silver ion reference
ATP	Adenosine triphosphate
AU	Absorbance Unit
BID	The Barrier Ionization Discharge
BNAH	1-BENZYL-1,4-DIHYDRONICOTINAMIDE
BODIPY	Boron-dipyrromethene
BPG	Basal-plane pyrolytic graphite
Cat	Catalyst
CH3CN	Acetonitrile
CH4	Methane
CO	Carbon monoxide
CO_2	Carbon dioxide
CoPc	Cobalt phthalocyanine
CoTNP	Cobalt 5,10,15,20-tetrakis(4-nitrophenyl)porphyrin
CuPc	Copper phthalocyanine
CuTNP	Copper 5,10,15,20-tetrakis(4-nitrophenyl)porphyrin
DCM	Dichloromethane (methylene chloride)
DDQ	2,3-Dichloro-5,6-dicyano-1,4-benzoquinone
DFT	Density functional theory
DMF	dimethylformamide
DMSO	Higher polarity solvents
DNA	Deoxyribonucleic acid
EDTA	Ethylenediaminetetraacetic acid
FE	Faradic efficiency
FeTNP	Iron 5,10,15,20-tetrakis(4-nitrophenyl)porphyrin
FLP	Frustrated Lewis pair
TPP	Tetraphenylporphyrin
FT-IR	Fourier Transform Infrared spectroscopy
G3P	glyceraldehyde 3 phosphate
GC	Gas chromatography
GCE	Glassy carbon electrode
HCOOH	Formic acid
HNMR	Proton Nuclear magnetic resonance spectroscopy
HOMO	Highest occupied molecular orbital

IPCC	Intergovernmental panel for climate change
IR	Infra-red
ITO	Indium tin oxide
LED	Light emitting diode
LUMO	Lowest unoccupied molecular orbital
LWE	Long wave energy
MEOH	Methanol
MgTPP	Magnesium tetraphenylporphyrin
MnTPP	Manganese tetraphenylporphyrin
NADPH	Nicotinamide adenine dinucleotide phosphate
NF	Nafion
NMR	Nuclear magnetic resonance spectroscopy
NO2	Nitro
P(VP-St)	Poly(4-vinylpyridine:styrene)
PVP	Polyvinyl pyridine
RE	Renewable energy
RGO	Reduced graphene oxide
SCE	Saturated calomel electrode
SWE	Short wave energy
TBAP	Tetra butyl ammonia phosphate
TEA	Triethylamine
TEOA	Triethanolamine
TEP	4,4',4",4'"-(porphyrin-5,10,15,20-tetrayl)tetrabenzoate
TFA	Trifluoroacetic acid
TMS	Trimethylsilane
TNP	5,10,15,20-tetrakis(4-nitrophenyl)porphyrin
TOF	Turnover frequency
TON	Turnover number
TPC	Palladium tetraphenylchlorin
TPP	5,10,15,20-tetraphenylporhyrin
TW	Tera watts
USA	United States of America
UV	Ultraviolet
UV-Vis	Ultraviolet- Visible
ZnTNP	Zinc 5,10,15,20-tetrakis(4-nitrophenyl)porphyrin
ZnTPP	Zinc 5,10,15,20-tetraphenylporhyrin

Abstract
Finn Connaughton

Electrocatalytic Approaches for CO_2 Reduction and Hydrogen Generation

This monograph aims to describe the research performed to identify sustainable catalysts for the recycling of CO2 emissions and H_2 generation .

Chapter one consists of a general overview of both electrocatalytic and photocatalytic routes towards CO_2 reduction and hydrogen evolution, the basis of the research presented in this thesis. Additionally, chapter one introduced is the background and theory of the various techniques that were used throughout the research; with a focus on the principles of photochemistry and electrochemistry.

Chapter two commences with a literature review of the use of macrocyclic systems for the reduction of CO_2 and hydrogen production; through both photochemical and electrochemical pathways. The syntheses of the porphyrin and metalloporphyrin catalysts used are discussed; and the subsequent investigation of these porphyrins for their ability to function as either photo- or electrocatalysts for both CO_2 reduction and hydrogen evolution is described. The catalysts were characterised using ^{1}H NMR, ^{13}C NMR, Mass spectroscopy, UV-vis spectroscopy, emission spectroscopy and IR spectroscopy where applicable.

Chapter three contains a literature review of the application of BODIPY systems focussing on the reduction of CO_2 and hydrogen production. The syntheses of several boron dipyrromethene (BODIPY) systems are reported. Additionally, they were characterised with the usual range of spectroscopic techniques. The aforementioned systems were investigated for their ability to function as a photosensitiser for both hydrogen production and CO_2 reduction.

Dedicated to my loving family, who have been my rock when everything else was gravel.

Acknowledgements

I would like to firstly acknowledge and thank Dr Mary Pryce, who gave me so much guidance and help over the last number of years. I am not sure I would be where I am today without you giving me this opportunity in the first place and for that I will be forever grateful.

Secondly, I would like to thank the Technical Staff in DCU. Whenever I had a hair brained idea, they always welcomed it and helped be bring it to life . I have never met a more enthusiastic and willing to help group in all my life and are an inspiration to me going forward.

I would like to thank all of the people I shared my time with in DCU. Liam, Disha, Suzanne, Laura, Nive and Jen just to name a few. You all made it a very special place for me to be and I don't think I would have survived the process without you all.

Finally, I would like to thank my family. This has been a long time coming down a long and windy road. However, at no point did I feel like I had to do that walk alone. That will mean more to me than anyone can every understand.

1. Chapter 1: Introduction

Chapter one provides an introduction to the research topic of this thesis. The aim of this chapter is to make a persuasive argument for the need to remove CO_2 from the atmosphere, how worldwide and EU legislation drives the need for this area of investigation and the current understanding of the means and methods to achieve it, and why the existing solutions have been deemed unsuitable. This chapter further proposes an alternate solution to reducing CO_2 levels which the remaining chapters of the thesis evaluate. This solution is to reform CO_2 into products that are more energy dense such as methanol or methane. To support and contextualise this proposal an overview of the literature pertaining to the dyes used for photo and electrocatalytic reduction of CO_2 and the evolution of hydrogen are also included.

1.1. Global warming

The depletion of fossil fuel resources and rising global temperatures are of worldwide concern and are the two major driving forces for a reduction in CO_2 emissions. The depletion of fossil fuels is a result of their use in internal combustion engines and power stations.[1–3] Given industry's reliance on these depleting reserves, concerns over the supply of fossil fuel resources have arisen, thereby leading industry to search for alternative fuel sources. One solution to this looming issue has been the discovery of large reserves of shale gas worldwide. Shale gas refers to gas trapped in nonporous shale rock formations.[4] It is estimated that by 2035 50% of all natural gas used in The United States of America will come from gas liberated from shale rock formations.[5,6] However, the recent push to develop these sources of shale gas both in the United States and abroad via hydraulic fracturing has drawn a great deal of public criticism. Hydraulic fracturing, or fracking as it is commonly known, is a technique for accessing gas reserves which would otherwise be inaccessible. It involves drilling horizontally

through a layer of rock and injecting a pressurised mixture of water, sand, and other chemicals that fractures the rock and facilitates the flow of oil and gas. The process involved in hydraulic fracturing also involves the clearing of large land masses for well pads and the construction of access roads and other structural resources such as pipelines. Millions of gallons of water are used in the process and wastewater removal must also be considered. Human resources are also vital to the process and each of these factors contributes to the potential economic, environmental, social, and health impact of the decision to access shale gas. Whilst opponents of this course of action cite health and environmental concerns, proponents argue that economic growth and more secure energy supplies will facilitate a rapid transition away from carbon-based electricity generation.

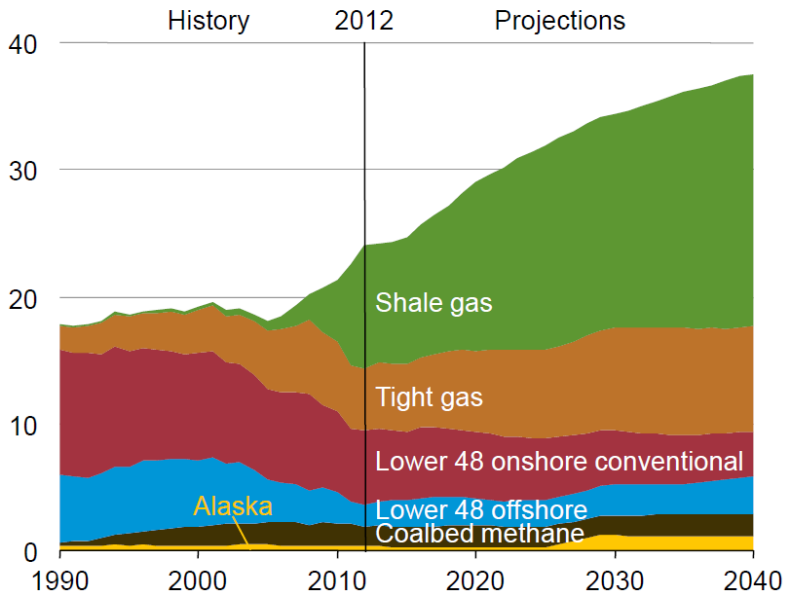

Figure 1: Relative amounts from different methods of Natural gas within the USA [7]

However, purely accessing further fossil fuel sources ignores the looming issue of global warming. Greenhouse gases are the leading cause of global warming, which is one of the greatest challenges to affect mankind in many years, and will continue to be a major concern until a viable new fuel source is identified.[8] With copious amounts

of greenhouse gases still being released into the atmosphere every day and the temperature of the planet steadily rising, the effects of climate change are becoming more apparent as time goes on. Greenhouse gases are a combination of several types of gases, but there are three main gases that account for the majority of all greenhouse gasses emitted (CO_2, CH_4 and NO_2). In terms of their approximate contribution to global warming, CO_2 accounts for (72 %), CH_4 (7 %) and NO_2 (19 %).[9] In the past 30 years each decade's average temperature has exceeded all previous recorded temperatures.[10] Data for atmospheric CO_2 concentration has been recorded for the previous 400,000 years and since 1950, CO_2 concentration has been greater than that previously recorded. As of January 2019, it reached 410.83ppm,[11] which is 37% higher than that recorded in the past half a million years.

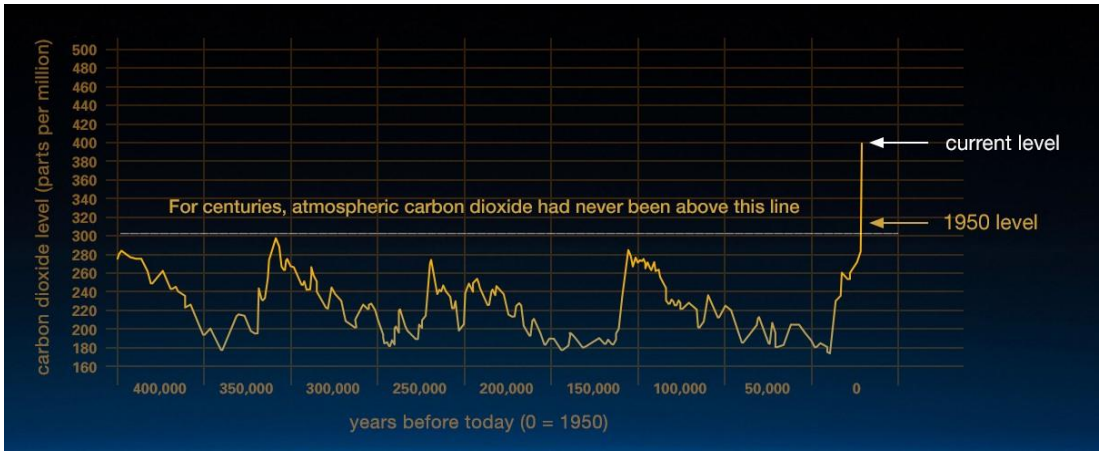

Figure 2: CO_2 levels in the atmosphere over the past 400,000 years[12]

CO_2 is of primary concern due to the fact that as global warming worsens, and temperatures rise, more CO_2 is released into the environment from non-anthropogenic sources. This is due to the release of CO_2 from the top meter of soil which houses approximately twice as much CO_2 compared to the atmosphere. It is thought that as the earth's temperature rises, it will force more CO_2 out of the soil into the atmosphere causing a feedback loop leading to an accelerated increase in global temperature and

thus accelerating global warming.[13] In the period 1870-2004, average increases in atmospheric CO_2 levels were approximately 1.4 mm per year. Based on current trajectories, this statistic is expected to double over the next 100 years. Many recent climate simulations now predict that an increase of 6^{o}C could be observed by the end of the century if action is not taken. This would reduce the amount of farmable land by approximately 17 % thus leading to many heavily inhabited zones no longer being habitable[14] and could cause an ice-free Antarctica by the end of the century.[15]

Due to the reasons discussed above a proactive measure must be taken in order to counteract the issue of climate change.[16,17] EU and worldwide directives have called for the reduction of emissions and a commensurate move to renewable energy sources to solve the issue. The Paris Accord holds 150 nations responsible to a long-term goal of keeping the increase in global average temperature to well below 2°C above pre-industrial levels. Ideally, this temperature rise would be capped at 1.5°C, since this would significantly reduce risks and the impacts of climate change.[18] In support of these aims the Renewable Energy Directive establishes an overall policy for the production and promotion of energy from renewable sources in the EU.[19] Supporting this policy, the 2020 climate & energy package legislates for the EU to achieve a 20% cut in greenhouse gas emissions from 1990 levels (to be achieved through the attainment of individual national targets ranging from 10%-49%), source 20% of EU energy from renewables and improve energy efficiency by 20%.[20] All EU countries must also ensure that at least 10% of their transport fuels come from renewable sources by 2020.[18] The Paris Accord broadly aims to achieve this by undertaking rapid reductions in emissions in accordance with the best available science. Researchers have identified a multi-pronged approach to address the impact of global warming

1. Eliminate the production of new CO_2 streams

2. Reduce current production of CO_2
3. Actively reduce CO_2 concentration in the atmosphere powered by renewable sources

A study by Armour *et al.* has suggested that even if all greenhouse gas emissions were eliminated, a rapid rise in temperature of ~ 0.9 ^{o}C would still occur due to aerosols in the atmosphere reflecting sunlight.[21] It was also estimated that it would take centuries for CO_2 levels to fall back to 40% of its peak, still leaving it higher than pre-industrial revolution CO_2 concentrations and it would take hundreds of thousands of years to equilibrate completely.[21] With the United Nations issuing a directive to 195 member countries to reduce their greenhouse gas emissions by 50 % by 2050, option one alone may no longer be sufficient. However, actively reducing atmospheric CO_2 by converting it to other fuels or storable liquids has been shown to be a viable alternative.

Product	# e⁻	Product	# e⁻
Formate 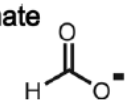	2	Acetaldehyde 	10
Carbon monoxide 	2	Ethanol 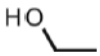	12
Methanol 	6	Ethylene	12
Glyoxal 	6	Hydroxyacetone 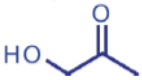	14
Methane 	8	Acetone 	16
Acetate 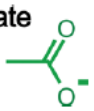	8	Allyl alcohol 	16
Glycolaldehyde 	8	Propionaldehyde 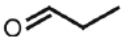	16
Ethylene glycol 	10	1-Propanol 	18

Figure 3: reported products from the reduction of CO2.[22]

The process of global warming involves short and long wave energy. When short wave energy (SWE) is emitted by the sun it is absorbed for the most part by the atmosphere and the planet or reflected by the atmosphere and clouds. The SWE that are absorbed by the planet is subsequently reemitted as long wave energy (LWE). A proportion of the LWE is then reflected and absorbed by the atmosphere causing back radiation as observed in Figure 4 below. As mentioned previously, CO_2 is one of the main constituents of greenhouse gases, and the focus of this thesis.

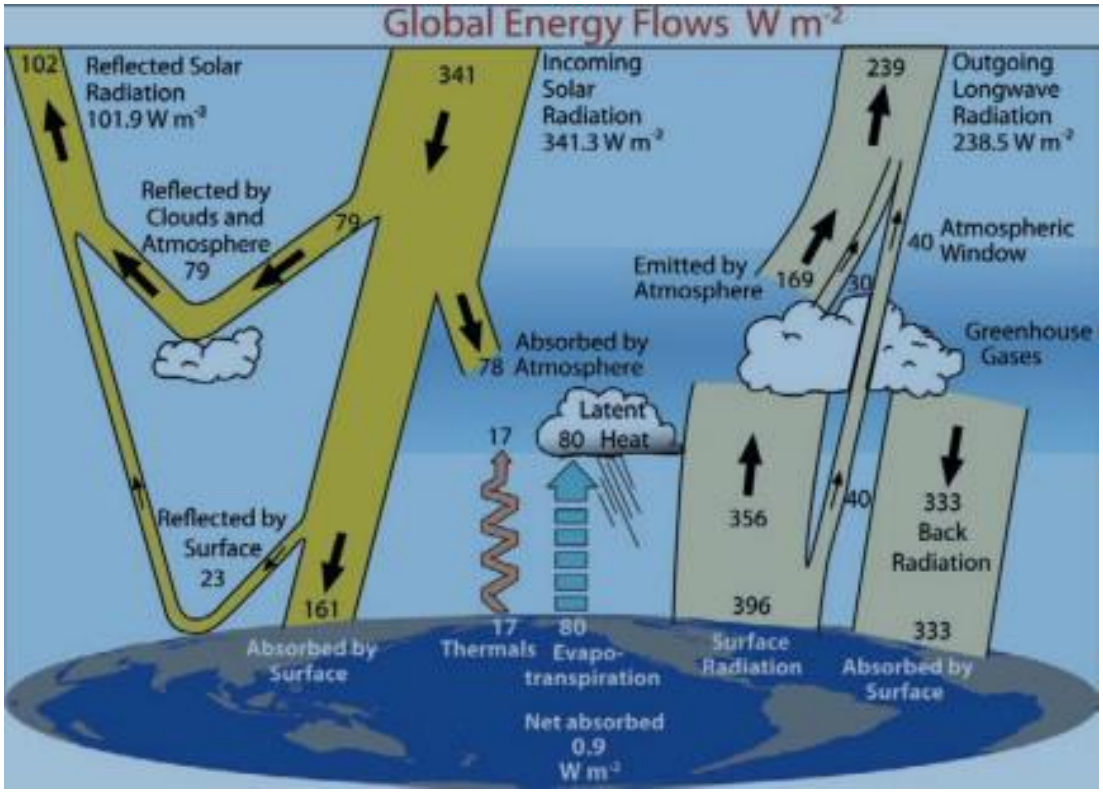

Figure 4: An approximation of the earths mean energy budget. [23] **This figure identifies the modes in which energy is dispersed within the atmosphere and by the planet.**

CO_2 has three forms of vibration; symmetric stretching, asymmetric stretching and bending. Symmetric stretching is not infra-red (IR) active. Asymmetric stretching is IR active and occurs at approximately 2300-2600 cm^{-1}. [24] Bending is also IR active occurring at 550 cm^{-1}. Recent studies have shown a large contribution to global warming is made by water vapour in the atmosphere. Water is considerably more IR active than CO_2, showing strong vibrations in the region of 3000-3600 cm^{-1} caused by asymmetric and symmetric stretching. Water is also shown to be IR active at ~1650 cm^{-1} which is associated with the bending motion. A final vibration is observed at ~600 cm^{-1} which is associated with a liberation motion. It is these vibrations that are

a major factor in the increase of global temperatures. As global temperature increase, the amount of water vapour in the atmosphere will increases in parallel.[23] Additionally, the volume of CO_2 in the top meter of soil is approximately twice that of the CO_2 in the atmosphere. Again, as global temperatures rise, more CO_2 will be driven out of the soil thereby increasing the concentration of CO_2 in the atmosphere.[13] These both could potentially lead to a feedback loop. Thus resulting in an increases in global temperature and then driving more greenhouses gasses out of the soil. It is therefore preferable to move away from the use of fossil fuels which will continue to exasperate this issue and could cause unexpected, and unrepairable damage to the planet.

1.2. Renewable energy

With the ever-increasing concerns about global warming, renewable carbon neutral sources of energy are required. Three common and widely known forms of these are solar, hydroelectric and wind energy. These account for approximately 8.68 % of the worlds energy supply as of the end of 2015.[25] Due to the intermittent nature of wind energy and solar energy and the lack of efficient storage solutions these renewable sources are impractical solutions for large parts of the world. Researchers attempting to improve the range of storage solutions available have suggested water electrolysis and CO_2 reduction as alternatives. These methods allow energy generated by renewable sources to be stored in the form of chemical energy for controlled release at a later time.

Given the limitations associated with the use of both fossil fuels and renewable energy sources to meet the EU targets of reducing CO_2 emissions we sought an alternate solution which would incorporate use of electro- and photocatalysts for CO_2 reduction

and hydrogen evolution. We propose employing catalysts to reduce the activation energy required to produce desired products.

1.3. Photocatalysis

1.3.1. Photosynthesis

One method of removing atmospheric CO_2 is photosynthesis. It is one of the most crucial chemical processes that occur every day. It involves the reaction of CO_2 with H_2O and photons of light to form carbohydrates and O_2.[26,27] Nearly all living organisms rely on photosynthesis to survive. Autotrophs such as bacteria and plants directly use photosynthesis to produce energy. While others such as mammals feed on the organisms that use photosynthesis to survive and are referred to as heterotrophs.

Photosynthesis is separated into two sets of reactions; light dependent reactions and the light independent reactions.[26] The light dependent reaction involves two stages separated into photosystem 1 and photosystem 2. Stage 1 (photosystem 2) involves the excitation of an electron by a photon of energy of light from the sun. This electron is then carried through the electron transport chain by mobile electron carriers. In order to equilibrate the charge from losing the electron, O_2 and H^+ ions are formed within the chlorophyll. The production of protons increases the charge within the thylakoid; the membrane bound compartment within the chloroplast. As the charge increases, the protons repel each other and are forced through an enzyme called ATP synthase which converts ADP (adenosine diphosphate) to ATP (adenosine triphosphate). ATP is one of the major energy carriers for photosynthesis. This leads to photosystem 1 (stage 2) which involves the excitation of electrons which are then transported to an enzyme

(ferredoxin-$NADP^+$ reductase) where $NADP^+$ (Nicotinamide adenine dinucleotide phosphate) is combined with 2 electrons and one proton to form NADPH, the other major energy carrier of photosynthesis.[28]

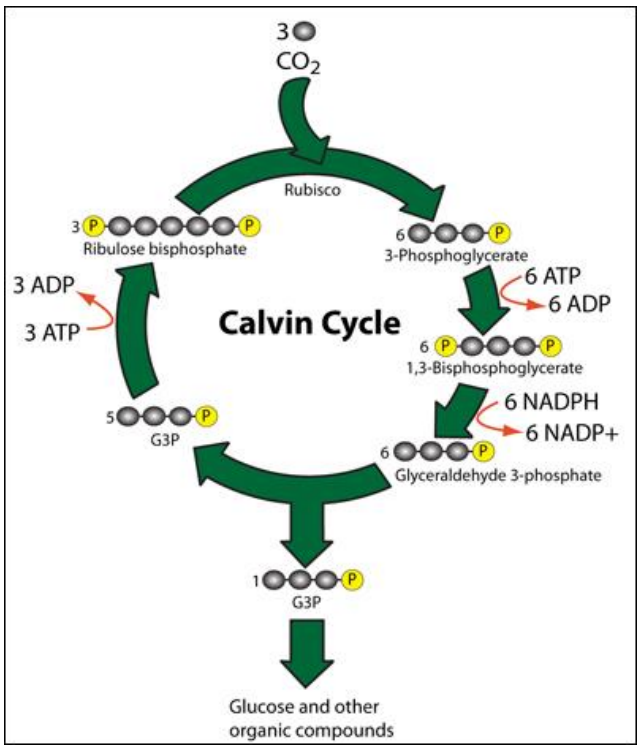

Figure 5: Diagram of the Calvin Cycle[27]

The light independent reactions primarily involve the Calvin Cycle, which is depicted in Figure 5. Previously the light independent reactions were referred to as the dark reactions. However, this was regarded as misleading as these reactions do not take place during the night. Typically, they will take place during the day along with the other parts of photosynthesis. Part one of the Calvin cycle involves carbon fixation. This is the process in which CO_2 is bound to the ribulose bisphosphate with help from the enzyme ribulose bisphosphate carboxylate. As the CO_2 binds the molecule becomes unstable, causing the molecule to break apart into two, three carbon chains. These carbon chains are referred to as phosphoglycerates. Each phosphoglycerate then reacts with an ATP molecule to form 1, 3 bisphosphoglycerate which then reacts with

NADPH to form glyceraldehyde 3 phosphate (G3P). This is the final building block of photosynthesis.G3P is found in all sugars and carbohydrates. Two G3P molecules combined together will form one glucose molecule. However, due to the cyclic nature of the Calvin cycle five out of six G3Ps produced must stay in the Calvin cycle in order to reform the initial ribulose bisphosphate so that the cycle can continue. One of the six G3P leaves the cycle and goes on to form organic compounds such as glucose and carbohydrates.[28]

1.1.1. Photocatalytic CO_2 Reduction

The utilization of photochemistry for CO_2 reduction opens a world of possibilities compared to the other methods discussed here (electrochemical) which require large amounts of energy to power electrolysis. Furthermore, without the use of renewable sources of energy powering these experiments the amount of CO_2 reduced must be offset by the amount produced in running the conversion. An ideal photocatalytic system would simply harness the most abundant source of energy that is currently available, the sun. It is estimated that with just 0.16 % of the earth's surface covered in solar panels which are 10 % efficient, 20 TW of power could be provided. This is 33 % more energy than is estimated that the world will require by year by 2030.[29,30]

However, with an abundant energy source there are still certain unavoidable barriers associated with the reduction of CO_2 to more favourable carbon based molecules (e.g. methanol and methane) including the high over potential required to break the inherent stability in the CO_2 molecule. A possible solution to this is to use molecular catalysts which can be used to stabilize the transition products (the CO radical). Most commonly photochemistry setups consist of 3 parts; a photosensitiser a catalyst and a sacrificial donor. The photosensitiser absorbs light in order to enter an excited state; the excited electron is then transferred to the catalyst through either a bridging ligand

or through space allowing the catalyst to reduce CO_2. Sacrificial donors then replenish the lost electron within the system allowing the system to continue to turnover. [31]

The first reported incident of CO_2 reduction to CO with the use of visible light was reported by Lehn *et al.* in 1982.[32] This was carried out with the use of ruthenium trisbipyridine as the photosensitiser and cobalt dichloride as the catalyst in a mix of acetonitrile and water with trimethylamine (TEA) as the sacrificial donor. Both CO and H_2 were produced with turn over numbers (TON) of less than 10. However, this was later increased to 33 by the use of dimethylformamide (DMF) and triethanolamine (TEOA) instead of acetonitrile, water and trimethylamine.[32] Lehn and Ziessel further increased the TON to 48 with the use solely of rhenium bipyridine tricarbonyl chloride.[33] In 1984 it was shown that with the same photocatalyst as Lehn *et al.* and cobalt tetraazamacrocycles as the catalyst a TON of over 531 could be reached. However, this had poor selectivity for CO with hydrogen evolution being the dominant product.[34] Both Hori et al,[35] and Takeda et al,[36] added triethyl phosphite and a mix of triphosphite compounds respectively to rhenium bipyridine tricarbonyl chloride in similar conditions as Lehn et al had done over a decade previously. However, considerably lower TON were achieved with a maximum TON of 7.5 (0.47 h^{-1})[35] and 6.2 (0.47h^{-1}) respectively.[37]

With the addition of chloride to their earlier protocol, Lehn and Ziessel recreated their earlier results[32] but improved the efficiency.[33] Their research was continued in 1989, and 15 % water was added to the DMF/TEOA solution utilising $Ru(Bipy)_3^{2+}$ as the catalyst and no formal photosensitiser was present. It was observed that once water was added, the catalyst would preferentially produce formate. This was an indication for the requirement of a proton source for formate production. With 15 % water in DMF a TON of 18 was achieved (9.5 h^{-1}) Also within this work, it was recorded that

with a 4:1:1 mix of DMF/TEOA/water, a TON of 43 (21.5 h^{-1}) was achieved, more than double what had previously been obtained. However, the greatest TON was observed with a DMF:TEOA (4:1) mix achieving a TON of 161 (80.5 h^{-1}) which at date of publication was the highest result obtained for homogeneous formate production in the literature.[38] In the same time period, Craig et al. published a similar experiment in aqueous medium with an ascorbate sacrificial donor. It was found that $Ru(Bipy)_3^{2+}$ did not produce CO, however it was not clear if the sample was examined for formate. [39] Although it was noted that upon the addition of nickel tetraazamacrocycle compounds, the solution became active for reduction of CO_2 to CO.

Ishida et al was one of the earliest to instigate the use of BNAH as a sacrificial donor which would later become a common substituent in many photocatalytic papers. They used a 9:1 DMF:H_2O mix, with $[Ru(Bipy)_3]^{2+}$ and $[Ru(Bipy)_2CO_2]$ as the photosensitiser and catalyst respectively. There were two major products formed, CO with a TON of 120 (12 h^{-1}) and formate with a TON of 150 (15 h^{-1}).[40] Kimura et al, investigated a ruthenium tris phenanthroline and a nickel cyclam system for both inter and intra molecular studies. Studies were carried out in an aqueous solution with ascorbic acid as a sacrificial donor. It was observed that neither inter or intra CO_2 reduction performed, achieving TONs of approximately 1 were observed in both cases.[41]

Matsuoka et al. used p-terphenyl as a photosensitiser with a Cobalt cyclam catalyst in a CH_3CN MEOH mix of 4:1 and a TEOA sacrificial donor.[42] The system was shown to produce both methane and formate however, due to degradation of the p-terphenyl (photosensitiser) the system was left non-functional. A total TON of 30 was achieved prior to the catalytic system ceasing to function.[42] In 2000 and 2002 Grodkowskie et

al. published work investigating corrin, pathalcyanines, corroles and porphyrins systems with varying success.[43,44] In both bodies of work Grodkowskie added p-terphenyl to TEA to supplement the photosensitiser. This appeared to follow on from Matsuko's work, as they reported the use of p-terphenyl was used previously as a photosensitiser. It was found that with a tert-butyl pthalocyanane in CH_3CN at a wavelength >310 nm, both CO and formate were produced with a combined TON of 50 (8.33 h^{-1}). In the same work a cobalt corrin system (vitamin B_{12}) was investigated under the same conditions mentioned previously with the addition of 10 % MeOH. In this case H_2 was produced in addition to CO and formate with a total TON of 100 (3.33 h^{-1}). In 2002, a pentafluorophenyl corrole was examined under similar condition to the work carried out in 2000 with a combined TON of 300 (37.5 h^{-1}) for both CO and H_2. In the same study a Co tetra 3-methylphenyl porphyrin was also examined under similar conditions achieving a combined TON of 300 (37.5 h^{-1}) for both CO and H_2.[44,45]

Between 2005 and 2009 Ishitani and co-workers published a number of papers in the area of homogenous CO_2 reduction. These focused on both intra and inter molecular approaches to CO_2 reduction using Ru and Re systems. Gholamkhass et al.[46] investigated a similar system to that of Ishida et al.,[40] in the use of BNAH. Visible light was used extensively in this case (>500 nm). It was thought that BNAH could aid in electron transfer by mediating charge between the photosensitiser and catalyst. In 2005 with $RuDMB_3$ (dimethyl bipyridine) as a photosensitiser and [(Re $DMB(CO_3)Cl$)] as a catalyst, it was observed that the intramolecular system performed better under the same conditions with a TON of 170 (10.6 h^{-1}) for CO, whereas the intermolecular system achieved a TON of 101 (6.3 h^{-1}). An experiment with identical conditions was subsequently carried out in in which the chloride on the

[(ReDMB$(CO)_3$Cl)] complex was replaced by a triethyl phosphite ligand. This showed a significant change as the TON went from 170 to 232 (36% increase).[46–49]

Numerous papers using porphyrins for CO_2 reduction have been published.[50–52] In nearly all cases the porphyrin has been used as the photosynthesizer. Premkumar et al.,[53] published a paper using Nafion membranes dip coated in different porphyrins and phthalocyanines, with the aim of reducing CO_2 to formic acid. The system used is an aqueous solution of 0.1M $NaClO_4$ and 0.1M TEOA. Premkumar et al., achieved turn over numbers in the region of 18000 for combined products for CoTPP after 40 minutes. This equates to approximately a TON of 27000 per hour. There is some crucial information missing however. Premkumar et al. does not specify what wavelength of light that was used. The results quoted were estimates as they were interpreted from graphs. Schneider et al.,[54] investigated the use of three different systems palladium TPP, palladium tetraphenylchlorin (TPC) and ruthenium tris bipyridine. It was found that after 4 hours irradiation in a DMF/TEOA (5:1) system a TON of 3 was achieved for a 1:1 solution of PdTPP and [BpyRe- $(CO)_3$(Pic)][PF_6]. When PdTPP was replaced with PdTPC at the same ratio a TON of 9 was achieved, and when the $[RuBpy_3]^{2+}$ was investigated under the same conditions it gave a TON of 10. One dyad was synthesized using PdTPP and [BpyRe-$(CO)_3$(Pic)][PF_6]. When investigated the poorest result published in this paper was achieved with a TON of 2. Schneider et al. used a broad wavelength light source (>420 nm) for all the experiments mentioned above.

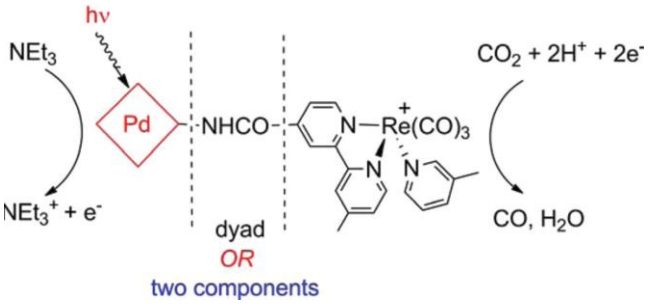

Figure 6: Mechanism proposed by Schneider et al[54].

Windle et al.,[55] carried out similar work to Schneider et al.,[119] studying both inter and intra approaches for $CO_{2\ reduction}$. Similarly, to the previous studies their work was also carried out in DMF/TEOA in a ratio of 5:1. All experiments were irradiated at > 520 nm. It was found that the greatest TON was achieved by the inter molecular configuration of ZnTPP and $[Re(CO)_3(Picoline)Bpy]$. Over a 2 hour irradiation period a TON of 100 was achieved. Where the intramolecular studies were less successful (dyad 1 and dyad 2) under the same condition a TON of 20 and 10 respectively were achieved as seen below in Figure 6.

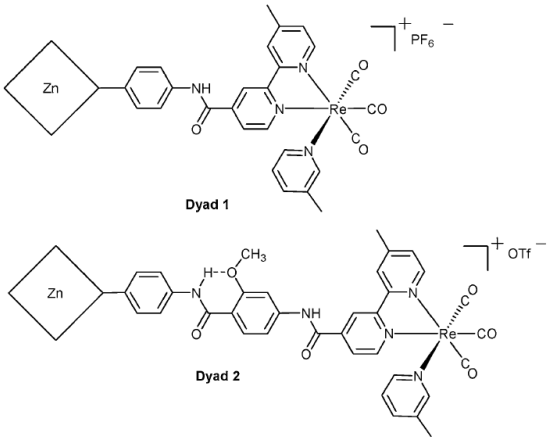

Figure 7: Two intramolecular molecules synthesized by Windle et al[55] for CO_2 Reduction

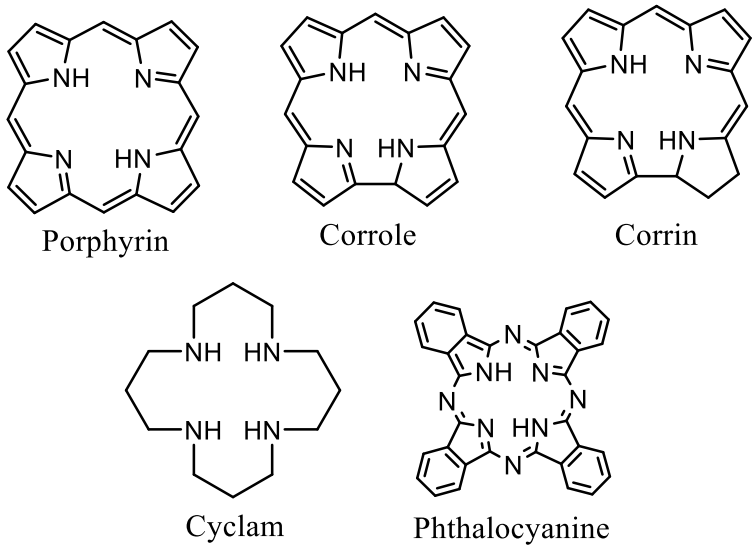

Figure 8: generic structure of different macrocycles

The use of BODIPY based systems for photocatalytic reduction of CO_2 and hydrogen evolution is a newly emerging area of research with approximately 70% of all papers on the topic published in the past three years. Despite their promising photophysical properties Yadav et al.[56] produced the only report of BODIPYs used in a heterogeneous environment where a graphene BODIPY photocatalyst was synthesised. It was proposed that the photocatalyst enters an excited state and excites and protonates Rhodium bipyridine which in turn regenerate NAD^+ in solution to NADH finally allowing for the formate dehydrogenase to convert CO_2 into formate. This was done in an attempt to mimic nature with the multi-step approach. Given the multiple steps involved, the system's ability to regenerate NAD^+ to allow the formate dehydrogenase to function is of great importance.

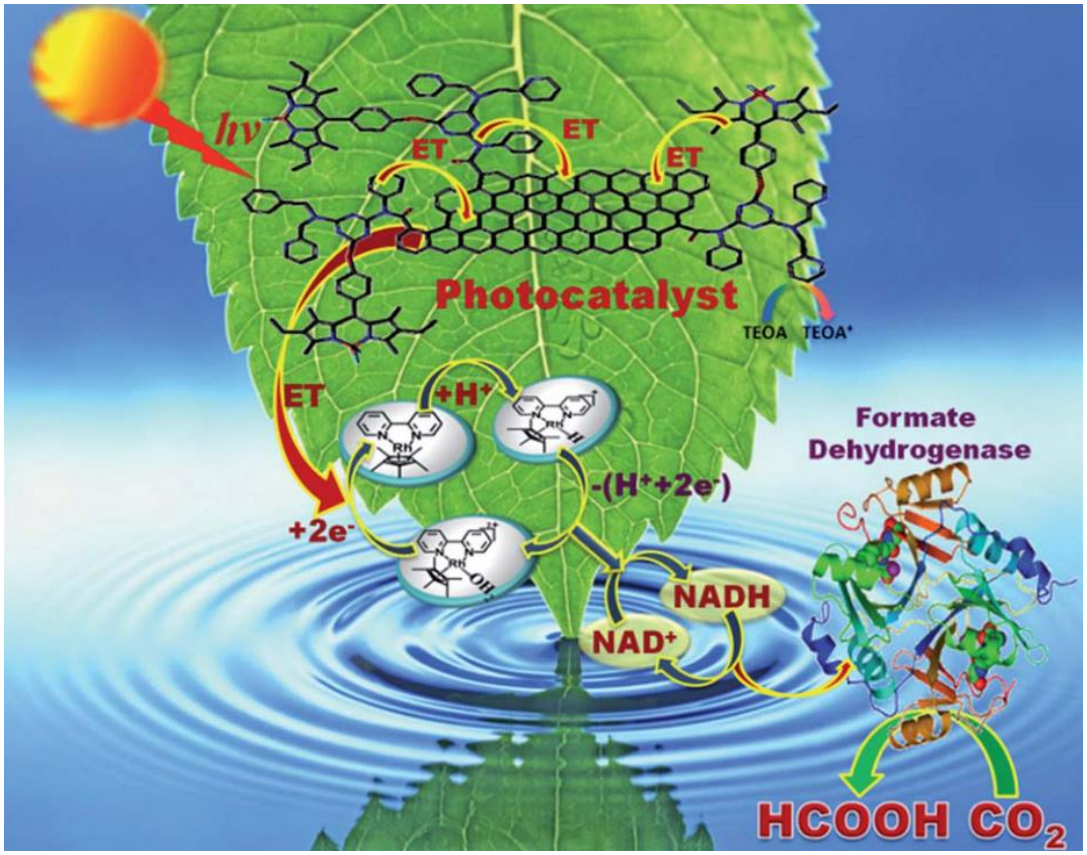

Figure 9: Proposed Mechanism by Yadav et al.[56]

This system achieved a regeneration yield of 54% for NADH and produced 144.2 µmol of formate. To date this is the best result for CO_2 reduction utilizing BODIPY moieties. Yadav et al.[14] suggests that this is a new bench mark for the area of artificial photosynthesis.

Rosenthal and co-workers[57,58] have studied intramolecular photocatalytic systems employing both rhenium bipyridine tricarbonyl chloride catalytic centres and BODIPY photosensitiser systems. In both cases BODIPY cores are bound covalently to the bipyridine ring of the catalytic center. The first of the two systems studied consisted of two BODIPY light harvesting moieties attached to the rhenium bipyridine tricarbonyl chloride (Figure 10)

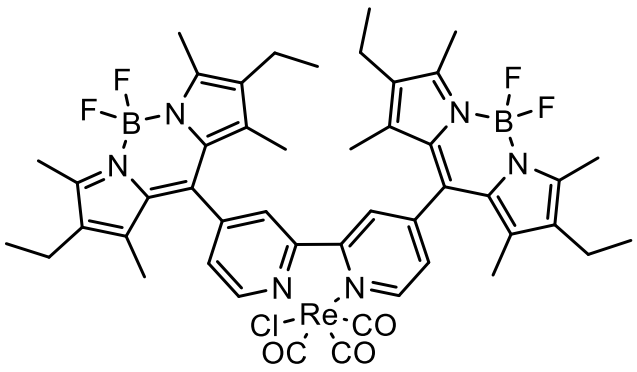

Figure 10: DiBODIPY Rhenium bipyridine tricarbonyl chloride molecule utilised by Rosenthal et al.[58]

However, even with the observed quenching of the BODIPY based fluorescence by the rhenium bipyridine tricarbonyl chloride, when excited at $\lambda > 500$ nm only negligible amounts of CO were produced. DFT measurements indicated that the HOMO electron density was located on the pyrrolic rings of the BODIPY structure however the LUMO electron density was located on the central rhenium bipyridine tricarbonyl chloride. This paper suggests that the rhenium bipyridine tricarbonyl chloride acts as the catalytic centre with charge being funnelled towards it. However, by the fact that it failed to produce any desirable products it would seem the BODIPYs were deactivating the catalyst completely rather than aiding it. This was further supported, given rhenium bipyridine tricarbonyl chloride's well documented ability to reduce CO_2. Rosenthal et al. indicated their surprise at the results of this study due to a previous study carried out by the same group.[57]

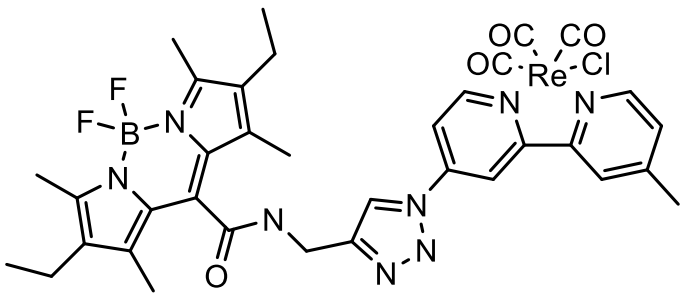

Figure 11: BODIPY Rhenium bipyridine tricarbonyl chloride molecule utilised by Rosenthal et al.[57]

Similar studies were carried out on the molecule in Figure 11. It was found that the di-nuclear system showed negligible amounts of CO formation at $\lambda > 500$ nm iradiation, as reported for the previous system also, however, again when the system was irradiated at $\lambda > 400$ nm, a TON of 20 (TOF = 5 h^{-1}) was achieved over 4 hours. Furthermore, when rhenium bipyridine tricarbonyl chloride was investigated alone a TON of 22 was achieved. This indicated that the BODIPY did not enhance CO_2 reduction but did not hinder the rheniumsystem to any significant level. The effect of the bridging ligand was investigated by Schulz et al.[59] The lack of a bridging ligand in the complex in Figure 10, could cause faster charge recombination, therefore inhibiting the catalytic center from entering an excited state that is sufficiently long lived to reduce CO_2.

Reithmeier et al.[60] implemented a catalytic system that used Iridium terpyridine monophenylpyridine chloride as demonstrated in Figure 12. The outer pyridine rings acted as a photosensitiser that passed the charge to the Iridium catalytic center. A acetonitrile TEOA mixture was used with TEOA acting as the sacrificial donner. Irradiation was carried out at 450 nm and no standalone photosensitiser was used. TONs of 135 were achieved

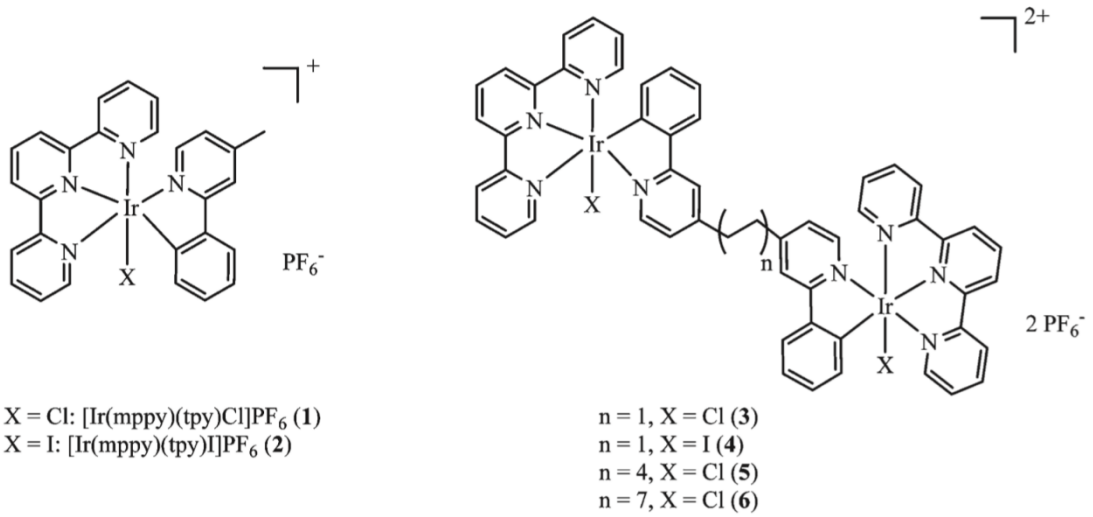

Figure 12:Catalytic systems utilised by Reithmeier et al.[60]

Hernandez and co-workers reported two separate highly active CO_2 catalysts.[61,62] The initial work was carried out investigating a range of catalysts, the most productive of which is referenced in **Figure 13**. This was paired with a iridium based photosensitiser that was kept constant throughout the paper. A TON of 421 was achieved when the system was irradiated with 400-700 nm mercury lamp in N-methyl-2-pyrrolidone and TEOA (5:1). Results reported here were taken after 45 minute irradiation cycles.[62] Hernandez et al. further advanced this work by investigating the photosensitiser and keep the catalyst reported previously consistent. The photosensitiser reported was a copper based **Figure 13**. Under the same conditions as reported previously the TON increased by 15% to 487. Additionally, a small amount of hydrogen was observed with the change in photosensitiser.

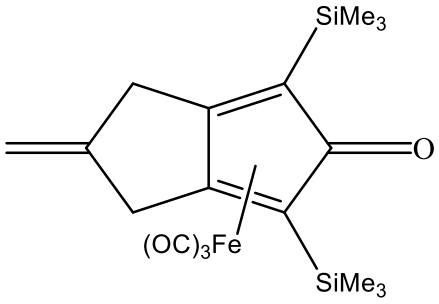

Figure 13: Catalyst utilised by Hernandez et al.[62]

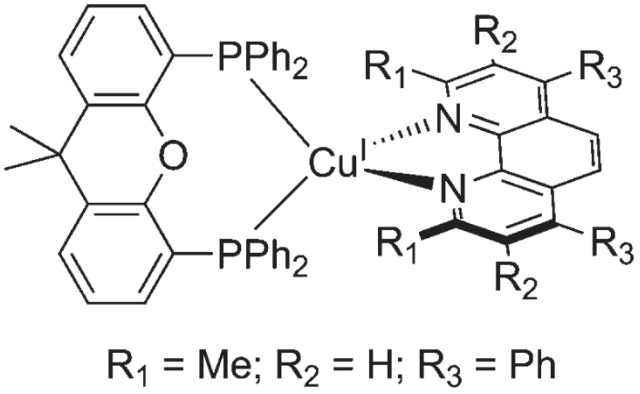

Figure 14: Photosensitiser utilised by Hernandez [2017] et al.[61]

1.4. Electrocatalysis

1.4.1. Electrocatalytic Hydrogen Evolution

Due to the scope of electrochemistry this section focuses on the area of hydrogen generation. Reports containing porphyrins and BODIPYs are excluded from the following section as they are discussed later in detail.

Kaneko and co-workers published numerous reports on proton reduction between 1997-2001.[63–67] Abe and colleagues investigated the use of "Prussian white"($K_4Fe^{2+}{}_4[Fe^{2+}CN_6]_3$).[63] both a platinum electrode and a basal-plane pyrolytic

graphite (BPG) electrode. This was carried out through electrodeposition at 0.5 V (vs a silver/silver chloride (Ag/Gal) electrode). The Pt coated electrode was shown to produce 12 times the amount of hydrogen at -0.4 V (vs Ag/Gal) in a 1.35 pH buffer, with a turnover number (TON) of $1.8x10^3$ h^{-1} with a faradaic efficiency (FE) of 80 %. The BPG coated electrode did not perform as well under the same conditions achieving a TON of 6.7 h^{-1} with no FE reported. The coated BPG electrode performed 27 times better however then the bare BPG electrode.

Polymers assist with electron transport to and from the catalyst.[68] This mechanism allows for much greater regeneration of the catalytic centre. Nafion is one such polymer that is commercially available and has gained much interest over the past 17 years.

Abe et al. also investigated the use of Ruthenium Red ($Ru_3O_2(NH_3)_{14}Cl_5$).[64] With a BPG electrode coated in Nafion and Ru-red, Nafion was coated by drop casting the Nafion onto the electrode and allowing it to dry in open air. The dry electrode was then dip coated in an aqueous solution of Ru-red. In a 1 pH buffer solution at a potential of -0.7 V, a TON of 10 h^{-1} was achieved with a FE of over 90 %. The experiment was repeated at -0.6 V achieving a pH of 183 h^{-1}. Sudden changes in the UV after cyclic voltammetry scans were noted and it was suggested that the Ru-red is degrading to form 3 distinct Ru species.

Also in 2000 Abe, Takahashi et al.,[65] investigated the use of a BPG Nafion electrode coated with a bis (2,2' bipyridine) platinum(II) catalyst at varying potentials as well as a bare BPG electrode coated with platinum black electrode. They reported that at -0.6 V and -1.5 V (vs Ag/AgCl), TONs of 6000 and 23000 were achieved respectively. However, at a -1.5 V (Vs Ag/AgCl) carbon based electrodes are capable of proton

reduction. Values for blank electrode reduction of protons were not reported. The platinum black electrode showed a similar response to that of the $Pt(bpy)_2$ with a TON of 5000. No results were presented for the investigation of platinum black coated BPG electrode at -1.5 V.

Continuing on from this work Abe et al. investigated the use of $[Pt(bpy)_2]^{2+}$ and $[Pt(terpy)Cl]^{+}$ on a indium tin oxide electrode.[66] It was observed that with an ITO electrode coupled with Nafion and $[Pt(bpy)_2]^{2+}$, a TON of 238 h^{-1} was achieved. Alternatively, under the same conditions, the $[Pt(terpy)Cl]^{+}$ electrode performed significantly worse. Obtaining a TON of 55 h^{-1}, the ITO electrodes were coated utilising a similar method to that reported above. [64]

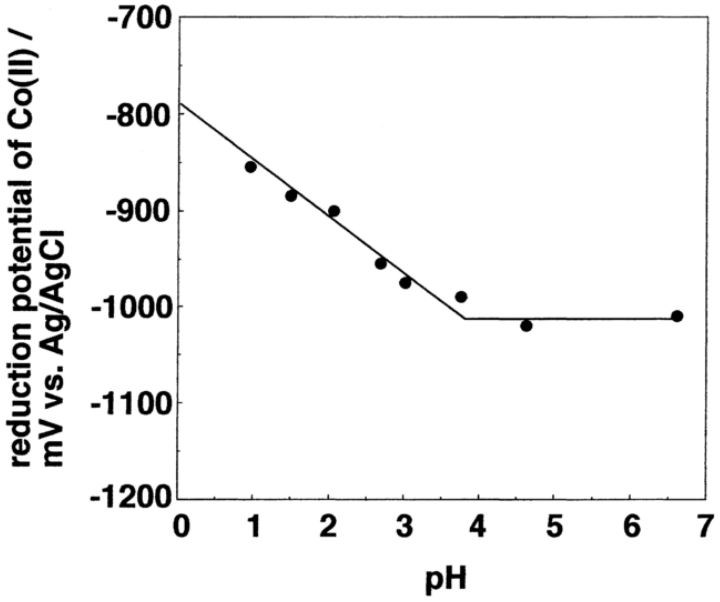

Figure 15: Reduction potential of Co (II/I) vs pH of the buffer. (vs Ag/AgCl) as reported by Abe, Kaneko 2001 et al.[67]

Abe, Kaneko and colleagues investigated the pH effect on a BPG electrode coated with Nafion and a bis (2,2':6',2'' terpyridine) cobalt (II) catalyst.[67] It was observed that at pH > 3.8 the Co (II) state was not protonated and therefore not active for proton reduction. Therefore, in order to obtain the two electron reduction required for

hydrogen evolution at pH >3.8 transition to Co (0) was required. However, at a pH < 3.8 the Co (II) state becomes active. This allows for hydrogen evolution to proceed at a Co (I) state. It can be observed in Figure 15 that as pH decreased the reduction potential of the Co(II) / Co(I) process appeared at more positive potentials. At pH 2.9 a potential of -1 V was applied achieving a TON of 14 h^{-1} whereas, as a pH of 7 a potential of -1.45 V was applied achieving a TON of 21 h^{-1}.

Abe et al. also reported the use of a dimetalic system that incorporated the use or ruthenium and iron in the form ferric ruthenocyanide .[65] These were combined to form ruthenium purple ($Fe_4[Ru(CN_6)]_3$). This catalyst was deposited on a basal plane electrode with an Ag/AgCl reference electrode and a platinum wire couther electrode. At -0.8 V in an acidic buffer (pH 1.5) buffer a TON of $5x10^4$ was achieved.

Berben et al. reported the use of a cobalt tetramine. The author investigated the use of this catalyst in both neutral and acidic pH buffers.[69] It was found that at a neutral pH, no significant change was observed when compared to the blank electrode. However, in an acidic pH, an increase of 2 orders of magnitude was observed. The catalyst was investigated over a 7-hour period, at -0.9 V vs SCE on a modified glassy carbon electrode in a pH 2 phosphate buffer a TON of $5x10^5$ was achieved yielding a TOF of 1190 per minute.

Hu et al. investigated a similar system to that of Berben et al.[69,70] However, it was found that the rate of production was considerably less. TON of 5 were observed in the first hour, afterwards, the catalyst continued to turn over however the faradaic efficiency was reduced to approximately 20 %. Quantifiable depreciation was

observed after the second turnover. This is attributed to a potentially unstable intermediate in the catalytic mechanism.

Jacques et al. investigated the use of numerous nickel and cobalt diamine systems at low over potentials.[71] Additionally, the use of different proton sources was also investigated. Cobalt systems were shown to achieve a greater TON and faradaic efficiency. This group reported that $[Co(dmgBF_2)_2(CH_3CN)_2]$ achieved the greatest TON at the lowest over potentials. A TON of 50 was recorded over 3 hours (TOF of 17) in a CH_3CN solution containing tetrabutylammonium tetrafluoroborat as a supporting electrolyte and p-$CN(C_6H_4)NH_3(BF_4)$ as a proton source at -0.92 V vs Fc/Fc^+. This combination achieved a faradaic efficiency of approximately 100 %. Other proton sources were investigated with other catalysts and TON for a 3-hour experiment ranged from 4-40 TONs. The order of effectiveness based on TON were ranked as follows p-Toluenesulfonic acid < TFA < $PhNH_3(BF_4)$ < p-$CN(C_6H_4)NH_3(BF_4)$.

Pantani et al. reported on the use of cobalt and nickel glyoximes for the reduction of protons in an acid media.[72] No conclusive reports were made, however, the current density was reported and compared to that of a platinum catalyst; with a current density of 2 mA cm^{-2}. The catalyst with the greatest current density reported was catalyst 1 as labelled below. This was dispersed in nafion on a carbon black electrode. A range of potentials were investigated ranging from -0.45 V to -1.2 V vs a SCE reference electrode.

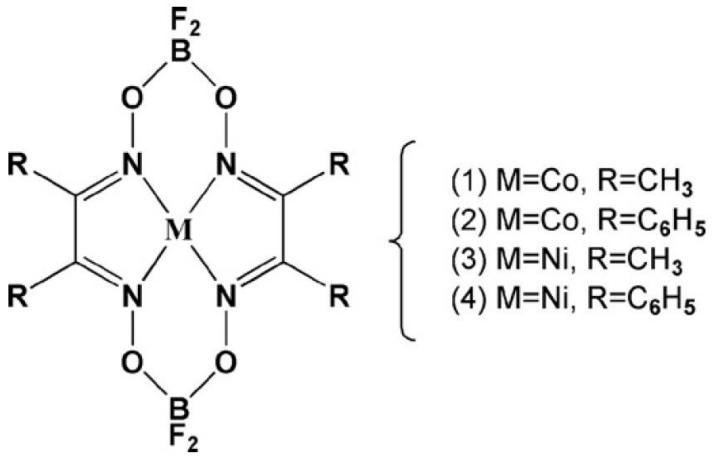

Artero et al. investigated the use of pyridil substituted cobaloximes as hydrogen evolving catalysts.[73] This was carried out in dichloroethane with a $(n\text{-}Bu_4N)BF_4$ electrolyte and triethylammonium chloride as a proton source. Over 3-hour electrolysis a TON of 100 was achieved (TOF of 33). UV-Vis spectrums were obtained to measure the degree of catalyst degradation. After 3 hours of electrolysis the TOF decreased dramatically, however, the catalyst remained intact. The decreases were thus attributed to the design of the electrochemical cell.

Hu, Cossairt et al. established "the most positive potential that has been reported for catalytic hydrogen evolution by a well-defined synthetic catalyst system" by achieving hydrogen evolution at -0.28 V vs SCE reference electrode with a glassy carbon working electrode and a platinum reference electrode.[74] No quantifiable results were published for the cobalt difluoroboryl-diglyoximate catalyst at -0.28 V. However, results were published for the same system containing a proton source of CF_3COOH, a TON of 20 was achieved with this system at -0.73 V vs SCE.

DuBois et al. investigated a cobalt diphosphine catalyst. The catalyst achieved a TOF of 90 per second in acetonitrile solution at -1V vs Fc/Fc^+ and a p- bromoanilinium

tetrafluoroborate electrolyte at a glassy carbon electrode. It is proposed that with the addition of triflic acid, an active catalyst is formed by loss of aphosphate ligand. This system was compared to a similar nickel based system that achieved superior TONs (a TOF of 350 per second) however, at a greater potential (-1.65 V Vs SCE reference electrode).

Jacobson et al. proposed the use of a cobalt phosphate complex with pendant amides.[75] It was observed with the addition of the amide pendants that the catalyst became more active. It was proposed that the amides stabilize the hydrogen intermediate allowing for TOFs of 90 s^{-1} at -1.1 V vs Fe/Fe^{+} in CH_3CN with a tetraethylammonium tetrafluoroborat electrolyte. Varying concentrations of triflic acid were added as a proton source. A clear increase in the foot of the wave was observed with acid concentration. However, little difference was reported in the TOF suggesting there are different limiting steps in the catalytic process.

Manton et al.[76] investigated both photocatalytic and electrocatalytic H_2 generation utilising 3-pyridine and 4-pyridine BODIPY bound directly to the metal center of a cobaloxime and investigated the systems hydrogen generating capabilities. Photocatalytic studies showed no evidence for the photocatalytic evolution of hydrogen, for either inter or intra molecular studies. Following computational chemistry studies, it was proposed that during intramolecular studies the cobaloxime pyridine bond was severed, stopping electronic communication between the photosensitiser and the catalyst. As the coordination of the cobaloxime quenched the fluorescence of the BODIPY moiety, studying the increase in fluorescence of the system over time following irradiation further confirmed the cleavage of the cobaloxime-pyridine bond. A similar mechanism was observed in a study containing porphyrins.[52] The structures proposed by Manton et al. .[76] can be seen in Figure 16

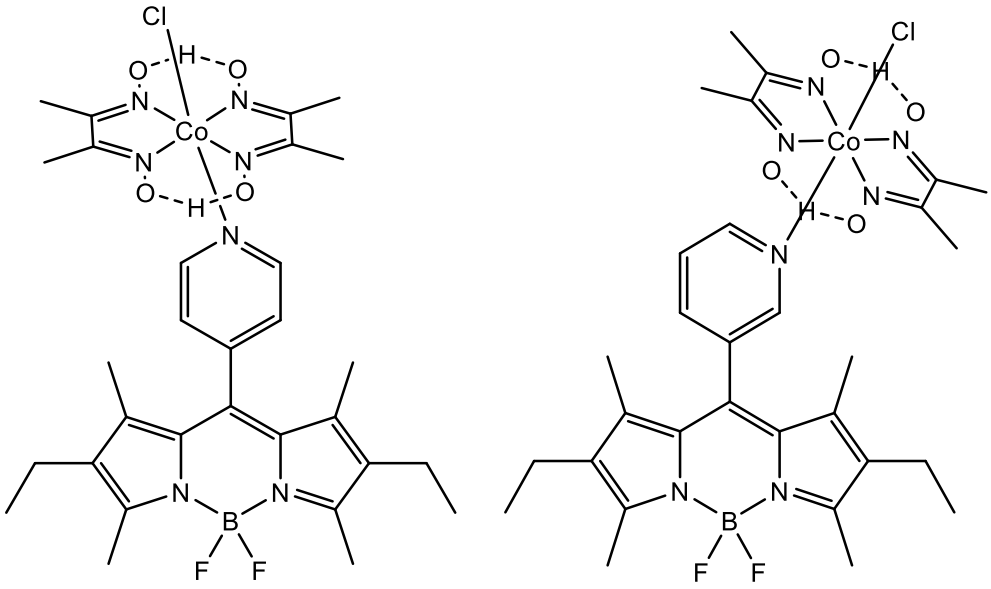

Figure 16: Structures proposed by Manton et al.[76]

Yu et al. and Mahmood et al. both reported carbon nitride (C2N) based catalysts.[77,78] Mahmood et al. investigated a ruthenium immobilized C2N lattice. They showed that a Ru-C2N performs similarly to platinum carbon electrode. The Ru-C2N displayed an overpotential of 30 mV where the Pt-C catalyst displayed an overpotential of 27. The ruthenium based catalyst also had a greater current exchange then that of the Pt-C. At a potential of 50 mv in 0.5 M H_2SO_4 and 1M KOH the Ru-C2N produced a TOF per second of 1 where the Pt-C catalyst still performed better at 2 turnovers per second. However, when the number of active sties were investigated it was found that the Ru/C2N catalyst outperformed the Pt-C catalyst per site. The Ru-C2N increased from 1 TOF per second to 3 TOF s^{-1}. Whereas, the Pt-C catalyst decreased to from 2 TOF 2 TOF $s^{-1\ to\ 1}$ TOF s^{-1}. Yu et al. carried out similar work investigating the effect that the level of coverage of the metal on the surface of the C2N has. It was observed that Mn anchored with coverage of approximately ½ of the potential coverage was the optimum coverage. The Gibbs free energy required for the HER was observed lower

than that of Pt catalysts here. Indicating that C2N catalysts may potentially be an alternative to expensive Pt based catalysts in the future and warrants further study.

Tong et al. investigated the effect of acids equivalents added on two bimetallic thiolate bridged catalysts (CoCo and CoFe).[79] It was found that both catalysts displayed a dependent nature on stronger acids (TFA) performing significantly worse in weak acids (acetic acid). Each experiment was carried out in DCM with a Bu_4NPF_6 electrolyte.

1.5 Macrocycles

1.5.1 Zinc containing catalysts:

Zinc phthalocyanines have been studied for their ability to generate H_2 electrocatalytically. Due to their lack of an observable electrocatalytic zinc based process they are less attractive for use as a molecular electrocatalyst although, they can cause a shift in the catalytic onset. Chebotareva et al.[80] investigated several metal centres for the oxidation of water and hydrogen evolution utilising a basic phthalocyanine (Pc). It was observed that the addition of Zn to the Pc had a very minor effect on the potential onset of the catalytic current with a shift of approximately 50 mV when compared to the unmetalated and bare electrode. This was then supported by the relative inactivity observed, with ZnPC performing marginally better than was observed for the freebase Pc.

Zhao et al., [81] using the same system years later on a basal plane graphite electrode observed that when the ZnPc was placed in a polymer that the catalyst became active. It was observed that with ZnPC and a poly vinylpyridine-co-styrene mixture yielded a TON of 2.92×10^4, and this TON was increased by 31% when changing the polymer

to Nafion 4.33 x 10^4. However, it was observed that the bare electrode in within these parameters produced up to 33% of that observed for the catalytic systems.

Koca et al.,[82] also investigated the use of three different ZnPc on a glassy carbon electrode with Nafion. No TON or moles of hydrogen produced were quoted here however it was noted that only one of the ZnPc compounds showed any activity with it being only marginally greater than that of a Nafion coated bare electrode.

Given the lack of literature based on ZnPC and the large success of other metal centres it would be of interest to see the effect of some more active metal centres in the system proposed by Zhao et al.[81] With the use of an iron centre it is possible that much great results could be obtained at less negative potentials as suggested by Chebotareva et al.[80]

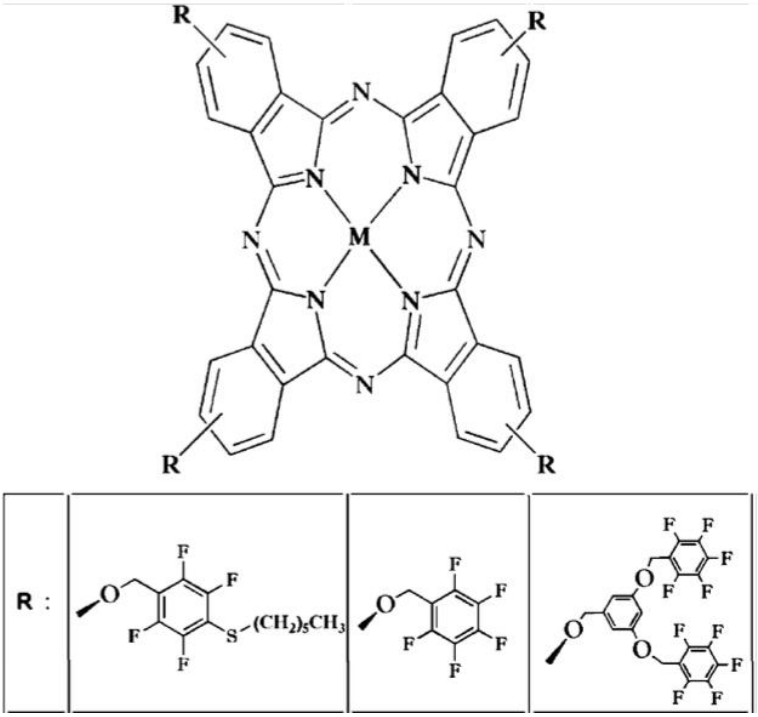

Figure 17: Catalysts reported by Koca et al.[83]

1.5.2 Copper containing catalysts

Copper macrocycles are rarely utilized for electrochemical hydrogen evolution. This is likely due to their lack of a metal process within the solvent window leading them to be less favourable when compared to iron and cobalt.

However, Koca 2009 et al.,[84] investigated the effect of copper (II) phthalocyanine tetrakis (1,1- (dicarboxy)-2-(4-biphenyl)-ethyl)-tetrachloro. Two different catalyst coating techniques were investigated; electropolymerisation and drop casting. It was found that when the catalyst was electropolymerised the electrode showed greater activity than that observed for the bare electrode, however the activity was still less than that of the bare electrode coated with Nafion. The most positive onset and largest catalytic current were observed in a Nafion CuPc coated glassy carbon electrode, reaching approximately three times that of the polymerized catalyst coating method. Three different pHs (3.4, 5.6 and 10.0) were examined with the more acidic the pH the earlier the onset of the catalytic current. Whereas, the more basic the solution the greater the current achieved. The amount of H_2 produced was not quantified therefore it is not possible to quantify the success of the different parameters.

Chebotareva et al.,[80] investigated the use of CuPc. There was very little discussion of the effectiveness of CuPc. Based on the catalytic onset displayed it would appear a very similar performance to that of by ZnPc was obtained. Due to a lack of results reported it is difficult to make comparisons between this and other catalysts. However, based on the catalytic onset and catalytic current reported it would suggest the catalyst may not be an efficient catalyst under these conditions.

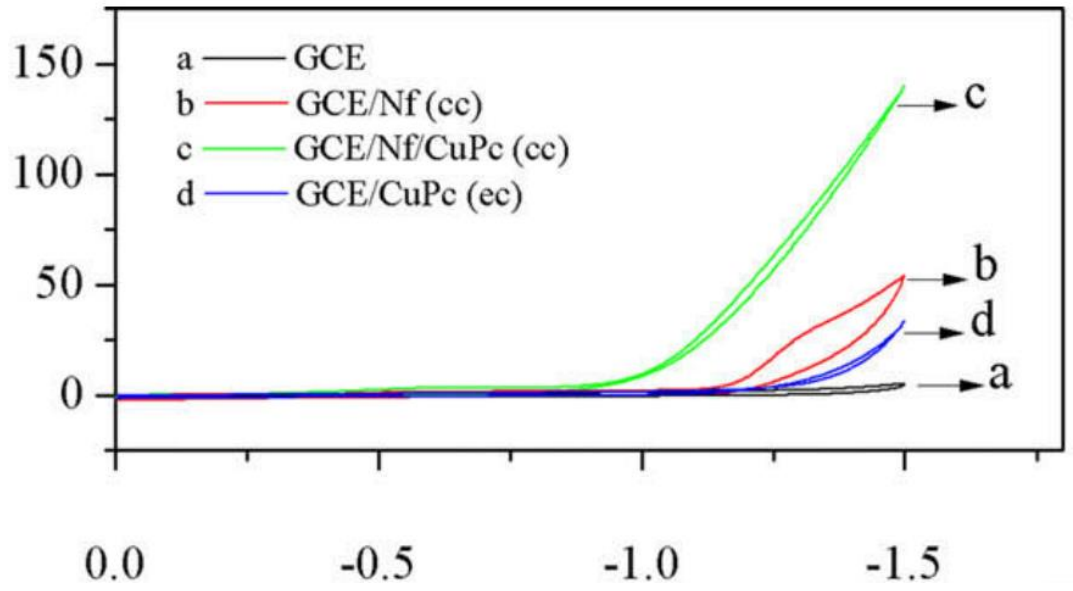

Figure 18: Relative catalytic onsets under different condition reported by Koca 2009 et al.[84] where GCE: glassy carbon electrode, NF: nafion, CuPc: copper phthalocyanine

Sirbu et al,[85]. had success with a copper tetra substituted ferrocene porphyrin. When compared to the copper tetraphenyl porphyrin it was shown that the iron metal centres and the electron donating nature of the ferrocene moved the catalytic onset more positive leading to an enhancement in the number of moles of hydrogen being produced. A TOF of 6100 s^{-1} was reported and the Catalyst was shown to be stable for up to 1.2 hours at which point it is likely the catalyst begins to degrade. Unlike all other hydrogen evolution experiments mention here this was carried out homogeneously as opposed to surface immobilisation in DMF with 0.1 mM catalyst concentration. This leads to the opportunity to run at much greater potentials with up to -1.7V vs Ag/AgCl being used during this bulk electrolysis compared to approximately -1 V in the other papers mentioned above. This is due to the nature of homogenous studies. As these are carried out in solvents with much greater potential windows and small percentages of water they are less favourable than when carried

out in buffer solutions. For the cost benefit analysis to be equal they must produce considerably larger amounts of H_2 at more negative potentials.[86]

1.5.3 Cobalt containing catalysts:

Cobalt centred macrocycles are well documented to be effective for hydrogen evolution. This is partially due to their Co(III) to Co (II) and Co(II) to Co(I) oxidation states which take place at < -1.2 V vs Fc/Fc^+.[80,83,87–91]

Chebotareva et al.,[80] found that the greatest results for hydrogen evolution was achieved using CoPC, achieving efficiencies of 100%. Cobalt demonstrated the largest positive shift of approximately 200 mV, which is assigned to Co(II) to Co(I) oxidation states. It was reported that the hydrogen concentration increased in a linear fashion.

Kellet et al.,[88] investigated three different cobalt porphyrin systems; meso-tetrakis(N,N,N-trimethylanilinium-4-yl)porphine chloride, meso-tetrapyrid-4-ylporphine, and meso-tetrakis(N-methylpyridinium-4-yl)porphine chloride (Figure 19). All 3 catalysts showed high efficiencies for H_2 evolution of >90% at a bulk electrolysis potential of -0.95 V Ag/AgCl.

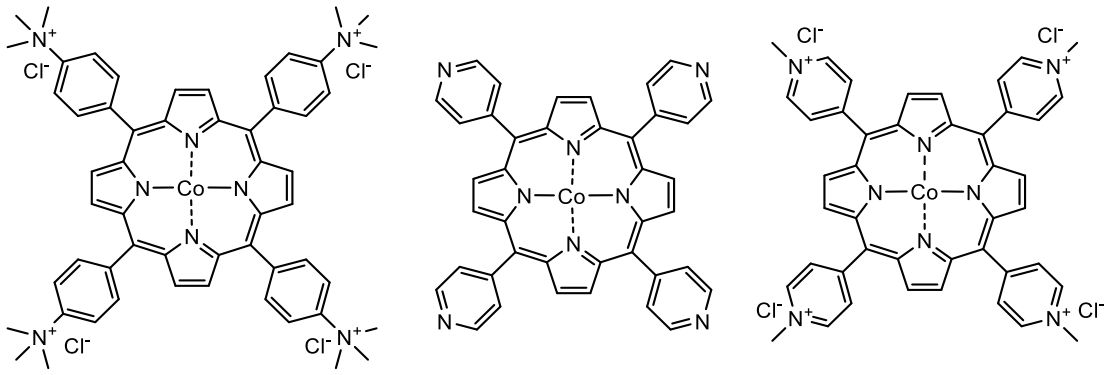

Figure 19: Structures utilised by Kellet et al [88].

This work was carried out homogenously in DMSO, 0.1 M TFA and 0.1 tetra butyl ammonia phosphate (TBAP). Research was conducted to construct a mechanism for

hydrogen production. It was observed that by electrolyzing the system at -0.3 V vs Ag/AgCl (potential associated with Co (III) to Co (II) reduction) no hydrogen was produced. However, when the potential was set to -0.7 V, production of H_2 was observed suggesting that the active catalyst was the reduction of Co(II) to Co(I). The greatest efficiency achieved was at -0.95 V.

Osmanbas et al.,[90] probed the effect of pH and electrodes on the catalytic onset of hydrogen evolution utilizing thiophene metallophthalocyanines. The mechanisms in both basic and acid solutions were also investigated. It was observed that by increasing the pH, the catalytic activity decreases due to an increased separation between first and second reductive processes. The increased gap allows for deprotonation to occur prior to the final reduction step required to form molecular hydrogen. In neutral solutions the protonation becomes less favourable due a lack of H^+ ions so therefore the stable hydride intermediate is less likely to form.

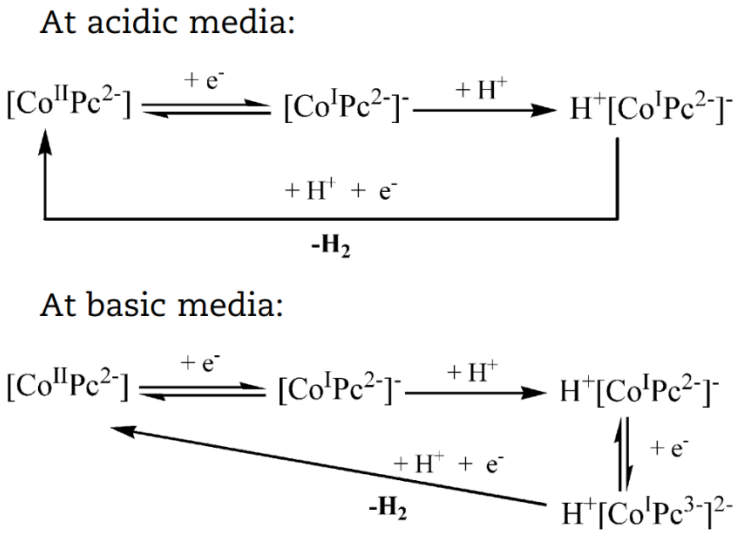

Figure 20: Proposed mechanism for hydrogen evolution [92] **.**

As the solution becomes more basic the catalytic activity begins to increase, this may be due to the additional reduction step observed in the proposed mechanism above.

Osmanbas et al.,[92] further investigated the catalytic onset when using a glassy carbon electrode (GCE) and indium tin oxide (ITO) electrode. Within this experiment various immobilization methods; polymerization, drop and dip coating were compared on GCEs. It was shown that the polymerized coating induced a stronger current. However, the concentration was not compared between polymerised and dip coated. Dip coated electrodes showed much more visible reduction peak for CoPc. It both cases a catalytic onset of approximately -1 V vs Ag/AgCl was observed. When compared to ITO electrodes drop coated had an onset of -0.6 V was observed, and when Nafion was added to the electrode the onset was pushed further positive achieving an onset of -0.4 V. No TON or numbers of moles of hydrogen produced were reported, however the authors indicated that H_2 was successfully produced.

Zhao 1999 et al.,[91] investigated three different CoPc, an unsubstituted cobalt phthalocyanine, cobalt octocyanophthalocyanine, and a cobalt tetrasulfonatophthalocyanine. These catalysts were all immobilized onto graphite electrodes using poly vinylpyridine-co-styrene. The greatest TON was produced by the unsubstituted CoPc ($2.5x10^5$), this decreased by 75% when using the cobalt octocyanophthalocyanine and decreased by a 95% when utilizing the cobalt tetrasulfonatophthalocyanine. TON values remained constant as concentration increased suggesting that the electrode is not being pacified by the thickness of the catalytic layer.

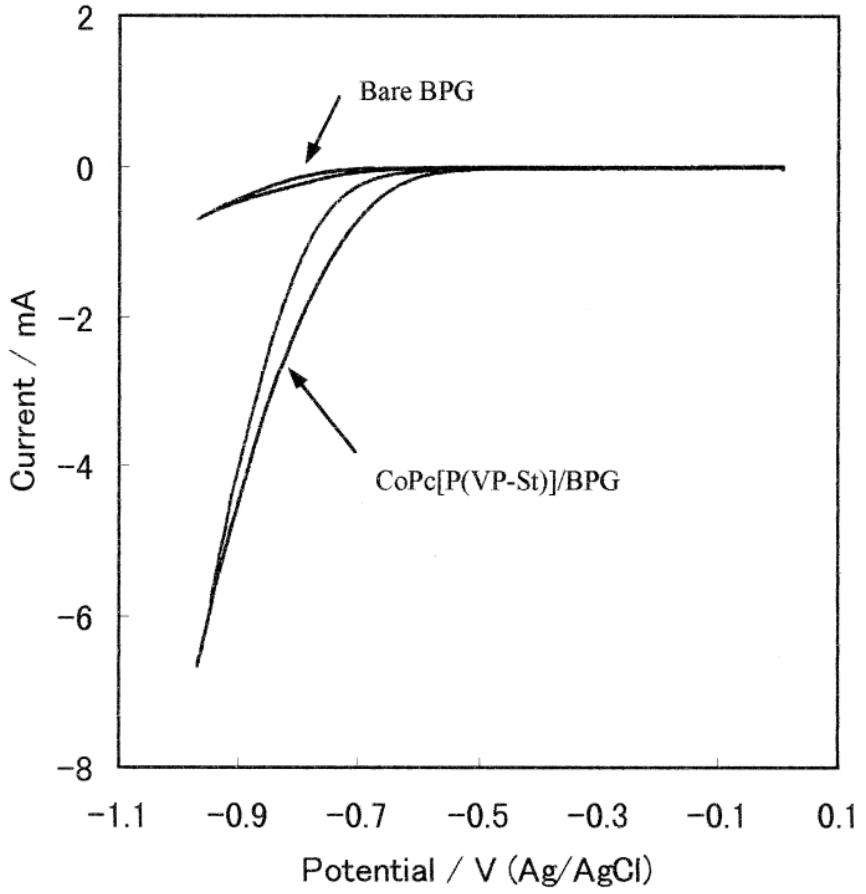

Figure 21: Catalytic onset of bare electrode compared to modified electrode as reported by Zhao 1999 et al.[91] BPG: basel plane graphite electrode, CoPc cobalt phthalocyanine, P(VP-St): poly(4-vinylpyridine:styrene)

A clear difference can be observed between the bare electrode and the modified electrode with the catalytic onset beginning at approximately -0.5 V vs Ag/AgCl when compared to -0.8 V for the bare electrode with a current 7 times greater for the modified electrode compared to the bare electrode.

Cobalt containing porphyrins and phthalocyanines show a large ability to produce hydrogen with high efficiencies and turnover numbers, much greater than that produced by Cu or Zn containing counter parts. This is attributed to the Co(II) to Co(I) process being key in the H_2 generation reaction allowing for much simpler mechanisms for the reduction of protons.

Beyene et al. investigated the cobalt porphyrin shown in Figure 22.[93] The porphyrin was designed to be water soluble to achieve hydrogen generation in neutral solutions. In 2M KPi solution a pH 7 yielded a TON of 4,900 with a TOF s^{-1} of 0.01. The FE of this catalyst approached 100% .

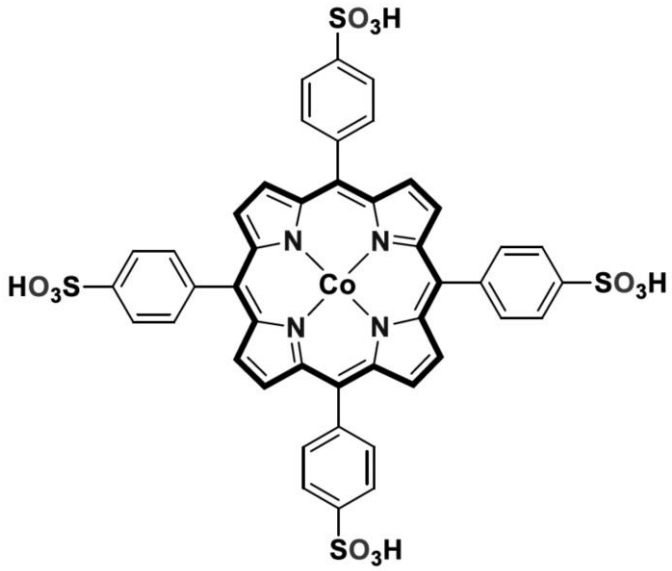

Figure 22: Catalyst investigated by Beyene et al.[93]

1.5.4 Iron containing catalysts:

Iron is a widely under-utilized metal due to its relative instability when compared to that of cobalt in the field of hydrogen evolution in aqueous solvents. However, due to the reductive process of iron (III) to iron (II) being present at approximately -0.5 V

Ag/AgCl making it an ideal candidate for electrocatalytic hydrogen evolution depending on the system.

Chebotareva et al.,[80] found that iron performed similarly to cobalt. A positive shift of approximately 175 mV to the catalytic onset was observed for an iron catalyst when compared to the cobalt analogue. It is possible with the addition of an iron (III) chloride an earlier onset would have been observed due to the iron (III) to Iron (II) process being potentially active towards H_2 generation and opening a potential binding site for formation of a metal hydride. With efficiencies of 99 % and charge values of 11.7 C making it the 3rd most efficient catalyst and the 3rd greatest charge reported by.

Bhugun et al.,[94] investigated the mechanism associated with the evolution of hydrogen, using a similar method proposed previously for cobalt. The mechanism is initiated with the reduction of iron (II) to iron (I). The iron centre is then protonated to form a hydride. The catalyst is then further reduced, and the hydride is protonated further forming a hydrogen molecule. However, with the use of iron tetraphenyl porphyrin a TON of 22 was achieved which is relatively poor compared to the other literature reported here (TOF 6,100 s^{-1}).[85] It was estimated that with better optimization the cell surface area to volume this value could be increases to 2200 however this would still not be hugely notable.

The effect of the addition of a proton source

The addition of an additional proton source has proven to alter the results of experiments in both selectivity and efficiency. In 1987 Ishida et al.,[37] noted that a variation of 0.2 pK_a units could drastically change the electrochemical selectivity and efficiency for a $[Ru(bpy)_2(CO)_2]^{2+}$ catalyst.[37] It was observed that a pK_a of 15.6 had

an efficiency of 64.1 % for formate, 19.9 % for carbon monoxide and 3.3% for molecular hydrogen. However, at the pK_a of 15.8 the efficiency for formate rose to 84.3%, carbon monoxide decreased to 2.4 % and molecular hydrogen increased to 6.8%. A comparison of this can be seen in tabe 3.

Product	**Efficiency at pK_a 15.6 (%)**	**Efficiency at pK_a 15.8 (%)**
Formate	64.1	84.3
CO	19.9	2.4
H_2	3.3	6.8

Table 1 Comparison of results at pKa 15.6 and 15.8 as reported by Ishida et al.[95]

A trend was observed throughout the paper, when the pK_a decreased so too did the selectivity for formate. Whereas, the selectivity of H_2 and CO produced was noted to increase with a decreasing pK_a[95]. Lim et al. investigated other proton sources such as frustrated Lewis pairs (FLP) on the reduction of CO_2.[96] They reportedthat with the addition of the frustrated Lewis pair, the hydride transfer barrier was greatly reduced from 25.3 kcal/mol to 3.8 kcal/mol, allowing for greater hydride interaction. Hydrides being the simplest form of Lewis aicds.[96] Saveant and co-workers have extensively published papers focusing on the use of Lewis acids and their effectiveness as a proton source (methalamine, dimethylamine, trimethylamine, phenol and benzoic acid).[97] The use of phenol as a Lewis acid has displayed a faradaic efficiency of 100 % for $Ru(bpy)_2(CO)_2$.[98] In another study by the group they reported that the use of water had shown a similar effect with a faradaic efficiency of 90 % and a turnover number of 1.25×10^6.[99] It was also noted by Ishida et al. that the use of phenol was an effective

proton source. Following the addition of phenol, an efficiency of 81 % for formate was achieved. Although this was not the greatest faradaic efficiency achieved for formate, almost no molecular hydrogen was produced with a faradaic efficiency of only 0.3 %.[95] The use of bronsted acids to replace FLPs was investigated by Smieja et al. It was found that there was a huge deviation between the additions of different bronsted acids compared to when there was no acid present. With no acid present there was no production observed. However, following the addition of methanol or trifluoroethanol the TOF increased to 130 and 340 respectively.[100] In particular, during the formation of methane (requiring 8 H^+ ions), the lack of an effective proton source could be detrimental to any possibilities of formation of reductive products. There are increasing reports that the proton source is a major contributing factor in the formation of products with high efficacy.[97]

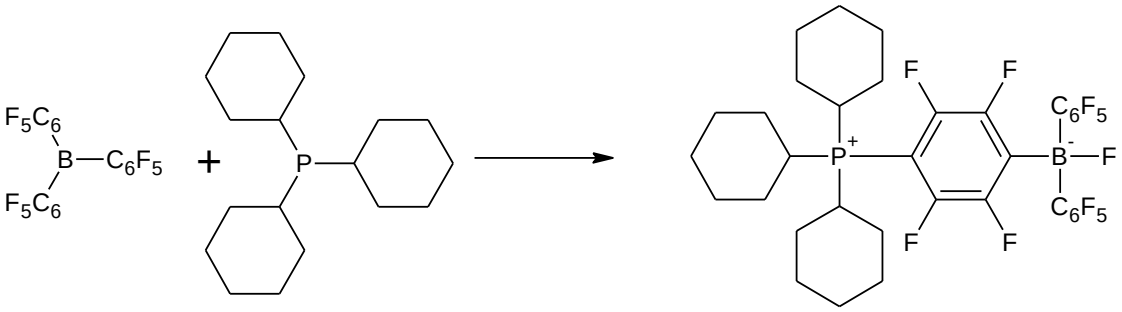

Figure 23 Synthesis of a frustrated Lewis pair[101]

Significant work has been carried out to date on both Hydrogen evolution and CO_2 reduction. This is often punctuated with 2nd and 3rd row transition metals that are cost ineffective due to their rarity. There is still a gap for the development of a cost-effective catalytic system. In the work included in this Thesis, the results from the use

of first row transition metal based porphyrins that can effectively electrocatalytically produce hydrogen will be presented.

The reduction of atmospheric CO_2 can be achieved through a process called reduction. In this process, CO_2 is reduced (gains electrons) in an attempt to form higher energy density molecules such as methane, methanol or carbon monoxide which can later be utilised in energy recovery and various chemical applications.[16] Figure 3 depicts 16 of the most commonly produced chemicals recorded in the area of electrochemical CO_2 reduction. Generally, the greater the number of electrons required, the higher the complexity of formation and the less feasible it is as a product. The conversion of CO_2 into carbon based chemicals such as methane, methanol and formic acid is both a logical and practical solution to lowering CO_2 levels. With both methanol and formic acid having common uses outside of being an energy source.

1.6 References

1 A. S. Garcia, MSc Thesis, Delft University of Technology, 2015.

2 K. Biernat, A. Malinowski and M. Gnat, in *Biofuels - Economy, Environment and Sustainability*, InTech, 2013.

3 O. Edenhofer, R. Pichs Madruga and Y. Sokona, *Renewable Energy Sources and Climate Change Mitigation (Special Report of the Intergovernmental Panel on Climate Change)*, 2012, vol. 6.

4 H. Boudet, C. Clarke, D. Bugden, E. Maibach, C. Roser-Renouf and A. Leiserowitz, *Energy Policy*, 2014, **65**, 57–67.

5 A. Vengosh, N. Warner, R. Jackson and T. Darrah, *Procedia Earth Planet. Sci.*, 2013, **7**, 863–866.

6 L. C. Best and C. S. Lowry, *J. Hydrol. Reg. Stud.*, 2014, **1**, 1–16.

7 U.S. Energy Information Administration, *Anual Energy Outlook 2014*, 2014.

8 Enviromental Protection Agency, Greenhouse Gas Emissions.

9 P. Ciais, C. Sabine and G. Bala, *Clim. Chang. 2013 Phys. Sci. Basis*, 2014, 465–570.

10 G.-K. P. Thomas Stocker , Qin Dahe, *working group I contribution to the IPCC fifth assessment report climate change 2013 : the physical science basis,* 2013.

11 NASA, NASA, global climate change, vital signs of the planet., https://climate.nasa.gov/vital-signs/carbon-dioxide/, (accessed 15 June 2017).

12 NASA, Climate change: How do we know?, https://climate.nasa.gov/evidence/, (accessed 12 July 2017).

13 D. Jenkinson, D. Adams and A. Wild, *Nature*, **351**, 304–306.

14 W. R. Emanuel, H. H. Shugart and M. P. Stevenson, *Clim. Change*, 1985, **7**, 29–43.

15 S. C. Roy, O. K. Varghese, M. Paulose and C. A. Grimes, *Am. Chem. Soc.*, 2010, **4**, 1259–1278.

16 J. L. Inglis, B. J. MacLean, M. T. Pryce and J. G. Vos, *Coord. Chem. Rev.*, 2012, **256**, 2571–2600.

17 M. Momirlan and T. N. Veziroglu, *J. Mol. Catal. A*, 2005, **30**, 795–802.

18 UNFCCC, *Conf. Parties its twenty-first Sess.*, 2015, **21932**, 32.

19 European Parliament, *Off. J. Eur. Union*, 2009, **140**, 16–62.

20 European Commission, *Eur. Comm.*, 2008, Brussels.

21 K. C. Armour and G. H. Roe, *Geophys. Res. Lett.*, 2011, **38**, 1–5.

22 K. P. Kuhl, E. R. Cave, D. N. Abram and T. F. Jaramillo, *Energy Environ. Sci.*, 2012, **5**, 7050–7059.

23 K. E. Trenberth, J. T. Fasullo and J. Kiehl, *Bull. Am. Meteorol. Soc.*, 2009, **90**, 311–

323.

24 IPCC, *Climate Change 2014: Synthesis Report. Contribution of Working Groups I, II and III to the Fifth Assessment Report of the Intergovernmental Panel on Climate Change*, 2014.

25 World Energy Council, *World Energy Resources*, 2016, vol. 1.

26 A. Paul, PhD Thesis, Dublin City University, 2012.

27 K. Harris, Photosynthesis Tutorial, https://www.hartnell.edu/biology-tutorials, (accessed 18 July 2017).

28 S. Freeman, L. A. Allison, M. Black, G. Podgorski, K. Quillin and E. Taylor, *Biological Science*, Pearson Education, Limited, 2014.

29 G. Adrian and I. E. Agency, *Key World Energy Statistics*, International Energy Agency, Paris, 2013, vol. 2013.

30 G. Adrian, G. Susan, M. John, T. Katie, S. Kay, S. John, A. Joseph, C. Connie, E. Mark, G. Karen, L. Joel, S. Patricia, S. Charles, F. Craig and W. Peggy, 2013.

31 B. Kumar, M. Llorente, J. Froehlich, T. Dang, A. Sathrum and C. P. Kubiak, *Annu. Rev. Phys. Chem.*, 2012, **63**, 541–69.

32 J. Hawecker, J.-M. Lehn and R. Ziessel, *Chem. Commun.*, 1983, 536–538.

33 J. Hawecker, J.-M. Lehn and R. Ziessel, *Helv. Chim. Acta*, 1986, **69**, 1990–2012.

34 A. H. A. Tinnemans, T. P. M. Koster, D. H. M. W. Thewissen and A. Mackor, *Recl. des Trav. Chim. des Pays-Bas*, 1984, **103**, 288–295.

35 H. Hori, F. P. a Johnson, K. Koike, O. Ishitani and T. Ibusuki, *J. Photochem. Photobiol. A Chem.*, 1996, **96**, 171–174.

36 H. Takeda and O. Ishitani, *Coord. Chem. Rev.*, 2010, **254**, 346–354.

37 H. Ishida, K. Tanaka and T. Tanaka, *Organometallics*, 1987, 181–186.

38 J.-M. Lehn and R. Ziessel, *J. Organomet. Chem.*, 1990, **382**, 157–173.

39 M. C. C.A. Craig, L.O. Spreer, J.W. Otovos, *Photochemical Reduction of Carbon Dioxide Using Nickel Tetraazamacrocycles*, 1990.

40 H. Ishida, T. Terada, K. Tanaka and T. Tanaka, *Inorg. Chem.*, 1990, **29**, 905–911.

41 E. Kimura, X. Bu, M. Shionoya, S. Wada and S. Maruyama, *Inorg. Chem.*, 1992, **31**, 4542–4546.

42 S. Matsuoka, K. Yamamoto, T. Ogata, M. Kusaba, N. Nakashima, E. Fujita and S. Yanagida, *J. Am. Chem. Soc.*, 1993, **115**, 601–609.

43 J. Grodkowski and P. Neta, *J. Phys. Chem.*, 2000, **104**, 1848–1853.

44 J. Grodkowski, P. Neta, E. Fujita, A. Mahammed, L. Simkhovich and Z. Gross, *J. Phys. Chem. A*, 2002, **106**, 4772–4778.

45 J. Grodkowski, T. Dhanasekaran, P. Neta, P. Hambright, B. S. Brunschwig, K. Shinozaki and E. Fujita, *J. Phys. Chem. A*, 2000, **104**, 11332–11339.

46 B. Gholamkhass, H. Mametsuka, K. Koike, T. Tanabe, M. Furue and O. Ishitani, *Inorg. Chem.*, 2005, **44**, 2326–2336.

47 S. Sato, K. Koike, H. Inoue and O. Ishitani, *Photochem. Photobiol. Sci.*, 2007, **6**, 454–461.

48 H. Takeda, K. Koike, H. Inoue and O. Ishitani, J. Am. Chem. Soc., 2008, 130 6708–6716.

49 Z.-Y. Bian, K. Sumi, M. Furue, S. Sato, K. Koike and O. Ishitani, *Dalton Trans.*, 2009, 983–993.

50 T. Wu, L. Zou, D. Han, F. Li, Q. Zhang and L. Niu, *Green Chem.*, 2014, **16**, 2142–

2146.

51 A. Fateeva, P. a. Chater, C. P. Ireland, A. a. Tahir, Y. Z. Khimyak, P. V. Wiper, J. R. Darwent and M. J. Rosseinsky, *Angew. Chemie - Int. Ed.*, 2012, **51**, 7440–7444.

52 J. C. Manton, C. Long, J. G. Vos and M. T. Pryce, *Dalton Trans.*, 2014, **43**, 3576–83.

53 J. Premkumar, R. Ramaraj, *J. Photochem. Photobiol. A Chem.*, 1997, **110**, 53–58.

54 J. Schneider, K. Q. Vuong, J. a Calladine, X.-Z. Sun, A. C. Whitwood, M. W. George and R. N. Perutz, *Inorg. Chem.*, 2011, **50**, 11877–89.

55 C. D. Windle, M. V Câmpian, A.-K. Duhme-Klair, E. a Gibson, R. N. Perutz and J. Schneider, *Chem. Commun.*, 2012, **48**, 8189–91.

56 R. K. Yadav, J.-O. Baeg, A. Kumar, K. Kong, G. H. Oh and N.-J. Park, *J. Mater. Chem. A*, 2014, **2**, 5068.

57 G. a. Andrade, A. J. Pistner, G. P. a Yap, D. a. Lutterman and J. Rosenthal, *ACS Catal.*, 2013, **3**, 1685–1692.

58 J. J. Teesdale, A. J. Pistner, G. P. A. Yap, Y. Z. Ma, D. A. Lutterman and J. Rosenthal, *Catal. Today*, 2014, **225**, 149–157.

59 M. Schulz, M. Karnahl, M. Schwalbe and J. G. Vos, *Coord. Chem. Rev.*, 2012, **256**, 1682–1705.

60 R. O. Reithmeier, S. Meister, B. Rieger, A. Siebel, M. Tschurl, U. Heiz and E. Herdtweck, *Dalt. Trans.*, 2014, **43**, 13259–13269.

61 A. Rosas-Hernández, C. Steinlechner, H. Junge and M. Beller, *Green Chem.*, 2017, **19**, 2356–2360.

62 A. Rosas-Hernández, P. G. Alsabeh, E. Barsch, H. Junge, R. Ludwig and M. Beller, *Chem. Commun.*, 2016, **52**, 8393–8396.

63 T. Abe, F. Taguchi, S. Tokita and M. Kaneko, *J. Mol. Catal. A Chem.*, 1997, **126**, 89–92.

64 T. Abe, T. Goto, K. Ohzeki and M. Kaneko, *Electrochim. Acta*, 2000, **45**, 4009–4014.

65 T. Abe, K. Takahashi, Y. Shiraishi, N. Toshima and M. Kaneko, *Mater. Sci.*, 2000, **106**, 102–106.

66 T. Abe, K. Hirano, Y. Shiraishi, N. Toshima and M. Kaneko, *Eur. Polym. J.*, 2001, **37**, 753–761.

67 T. Abe and M. Kaneko, *J. Mol. Catal. A Chem.*, 2001, **169**, 177–183.

68 J. L. Inglis, PhD Thesis, Dublin City University, 2013.

69 L. a Berben and J. C. Peters, *Chem. Commun. (Camb).*, 2010, **46**, 398–400.

70 X. Hu, B. S. Brunschwig and J. C. Peters, *J. Am. Chem. Soc.*, 2007, **129**, 8988–8998.

71 P. Jacques, V. Artero and J. Pécaut, Proceedings of the National Academy of Sciences of the United States of America., 2009, 106, 20627-20632

72 O. Pantani, E. Anxolabehere-Mallart, A. Aukauloo and P. Millet, *Electrochem. commun.*, 2007, **9**, 54–58.

73 M. Razavet, V. Artero and M. Fontecave, *Inorg. Chem.*, 2005, **44**, 4786–4795.

74 X. Hu, B. M. Cossairt, B. S. Brunschwig, N. S. Lewis and J. C. Peters, *Chem. Commun.*, 2005, **1**, 4723–4725.

75 G. M. Jacobsen, J. Y. Yang, B. Twamley, A. D. Wilson, R. M. Bullock, M. R. DuBois and D. L. DuBois, *Energy Environ. Sci.*, 2008, **1**, 167–174.

76 J. C. Manton, C. Long, J. G. Vos and M. T. Pryce, *Phys. Chem. Chem. Phys.*, 2014, **16**, 5229–5236.

77 S. Yu, Y. C. Rao, H. H. Wu and X. M. Duan, *Phys. Chem. Chem. Phys.*, 2018, **20**, 27970–27974.

78 J. Mahmood, F. Li, S. M. Jung, M. S. Okyay, I. Ahmad, S. J. Kim, N. Park, H. Y. Jeong and J. B. Baek, *Nat. Nanotechnol.*, 2017, **12**, 441–446.

79 P. Tong, W. Xie, D. Yang, B. Wang, X. Ji, J. Li and J. Qu, *Dalt. Trans.*, 2016, **45**, 18559–18565.

80 N. Chebotareva and T. Nyokong, *Electrochim. Acta*, 1997, **42**, 3519–3524.

81 F. Zhao, J. Zhang, D. WÖhrle and M. Kaneko, *J. Porphyr. Phthalocyanines*, 2000, **4**, 31–36.

82 A. Koca, *Int. J. Hydrogen Energy*, 2009, **34**, 2107–2112.

83 A. Koca, M. Özçeşmeci and E. Hamuryudan, *Electroanalysis*, 2010, **22**, 1623–1633.

84 A. Koca, *Electrochem. commun.*, 2009, **11**, 838–841.

85 D. Sirbu, C. Turta, E. a. Gibson and a. C. Benniston, *Dalt. Trans.*, 2015, **44**, 14646–14655.

86 J. R. McKone, S. C. Marinescu, B. S. Brunschwig, J. R. Winkler and H. B. Gray, *Chem. Sci.*, 2014, **5**, 865–878.

87 P. Du and R. Eisenberg, *Energy Environ. Sci.*, 2012, **5**, 6012.

88 R. M. Kellett and T. G. Spiro, *Inorg. Chem.*, 1985, **24**, 2373–2377.

89 A. Koca, M. Kasim Şener, M. B. Koçak and A. Gül, *Int. J. Hydrogen Energy*, 2006, **31**, 2211–2216.

90 Ö. a. Osmanbaş, A. Koca, M. Kandaz and F. Karaca, *Int. J. Hydrogen Energy*, 2008, **33**, 3281–3288.

91 F. Zhao, J. Zhang, T. Abe, D. Wöhrle and M. Kaneko, *J. Mol. Catal. A Chem.*, 1999,

145, 245–256.

92 Ö. a. Osmanbaş, A. Koca, I. Özçeşmeci, A. I. Okur and A. Gül, *Electrochim. Acta*, 2008, **53**, 4969–4980.

93 B. B. Beyene, S. B. Mane and C. H. Hung, *Chem. Commun.*, 2015, **51**, 15067–15070.

94 I. Bhugun, D. Lexa and J.-M. Savéant, *J. Am. Chem. Soc.*, 1996, **118**, 3982–3983.

95 H. Ishida, H. Tanaka and K. Tanaka, *J. Chem. Soc. Chem. Commun.*, 1987, **6**, 131–132.

96 C.-H. Lim, A. M. Holder, J. T. Hynes and C. B. Musgrave, *Inorg. Chem.*, 2013, **52**, 10062–10066.

97 I. Bhugun, D. Lexa and J. Savéant, *J. Am. Chem. Soc.*, 1996, **118**, 1769–1776.

98 C. Costentin, S. Drouet, G. Passard, M. Robert and J. M. Saveant, *J. Am. Chem. Soc.*, 2013, **135**, 9023–9031.

99 C. Costentin, S. Drouet, M. Robert and J. M. Saveant, *Science.*, 2012, **338**, 90–94.

100 J. M. Smieja, M. D. Sampson, K. A. Grice, E. E. Benson, J. D. Froehlich and C. P. Kubiak, *Inorg. Chem.*, 2013, **52**, 2484–2491.

101 D. W. Stephan, *Org. Biomol. Chem.*, 2008, **6**, 1535–1539.

2. Chapter 2: Electrochemical reduction of CO_2 using porphyrin systems.

2.1. Aim

The aim of chapter two is to investigate a suite of porphyrin systems for the photo- and electrocatalytic proton and CO_2 reduction.

The research that has been carried out to date in this area will be discussed first of as to contextualise the results. All catalysts synthesised were characterised using ^{1}H NMR, ^{13}C NMR, Mass spectroscopy, UV-vis spectroscopy, emission spectroscopy and IR spectroscopy where applicable, and subsequently be investigated for their ability to reduce protons and CO_2 through electrocatalytic means. Both solution electrochemistry and surface electrochemistry was investigated. Solution electrochemistry allows investigations into how the addition of CO_2 and proton sources effect the electrochemistry. The surface electrochemistry allows for a controlled amount of catalyst to be deposited on the electrode surface. The photocatalytic studies were carried out under inert atmosphere for hydrogen production and under a CO_2 atmosphere for CO_2 reduction. Different proton sources and mediators were investigated, their effect on the photosystems discussed.

2.2. Introduction

2.2.1. Porphyrins

Porphyrins have a variety of uses. Both in nature and in man-made applications. In nature they are contained within chlorophyll, heme, minerals and in non-natural applications porphyrins are used as electrocatalysts,[1–3] photocatalysts,[4–6] photosensitisers,[7–9] DNA tags[10,11] and to enhance imaging techniques.[12–14]

Porphyrins are attractive systems for electrochemical and photochemical studies due to their generally stable planar macrocycles which are based on a tetrapyrrole structure. They commonly display molar extinction coefficients in the region of $1x10^5$ $M^{-1}cm^{-1}$. Unsubstituted porphyrins display a planar orientation with a diameter of 8.5 Å and a height of approximately 4.7 Å. The height is attributed to the internal nitrogens. Typically, one hydrogen will be orientated below the planar symmetry of the molecule and the other hydrogen will be orientated above the planar symmetery.[15]

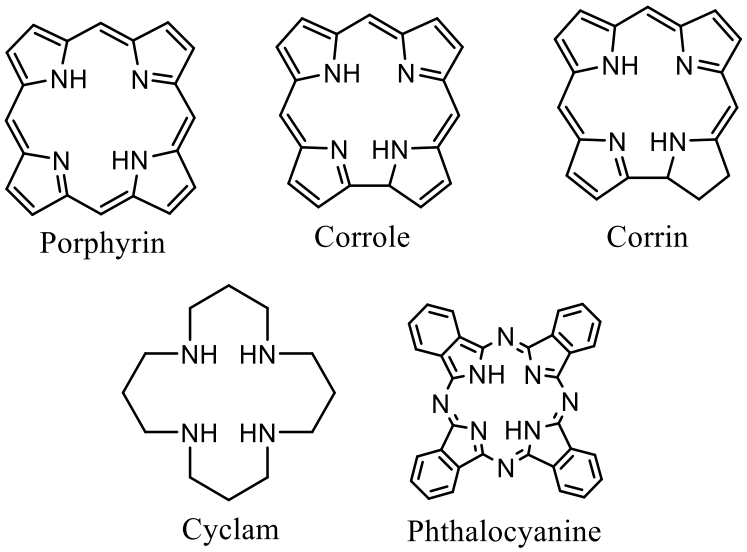

Figure 24:Structure of different tetra pyrrole macrocycles

Porphyrins, phthalocyanine, corroles and corrins all share the tetrapyrrole structure as observed in Figure 24. The most significant difference noted between phthalocyanines and the other macrocycles is the use of nitrogen in the bridging of the pyrrole groups in the phthalocyanine. Porphyrins, corroles and corrins all share carbon bridging groups. Both corroles and corrins have broken conjugation.

Porphyrins are typically classified as either a free base porphyrin or a metallo-porphyrin as seen in Figure 25. Free base porphyrins have two free hydrogens in the

centre cavity of the porphyrin. Whereas in a metallo porphyrin these hydrogens are replaced with two covalent bonds to a metal centre with additional dative bonds from the lone pair of the remaining two nitrogen.

Porphyrins have an unique UV-Vis spectrum.[15] Typically, a free base porphyrin (a porphyrin with no metal centre) will display a soret band between 300-500 nm and four much weaker Q bands in the region of 500-800 nm. The Soret band is caused by a $S_0 \rightarrow S_2$ transition while the Q bands are caused by a $S_0 \rightarrow S_1$ transition. Two Q bands are formed by the HOMO and LUMO state of the $S_0 \rightarrow S_1$ transition. The number of Q bands is doubled as a results of the asymmetry caused by the internal hydrogens .[15] A slight shift is observed to the soret peak when a metal substituent is added. Furthermore, the number of Q bands subsequently decreases to 2. This is attributed to the increased symmetry within the porphyrin.

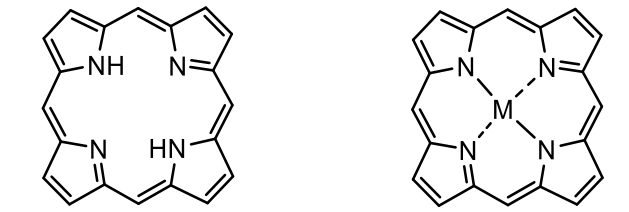

Figure 25: Structures of free-base porphyrin and metallo-porphyrin

2.1.2. Synthesis of Porphyrins:

The synthesis of porphyrins was first documented in 1935 by Rothemund.[16] He reported that the addition of pyrrole to gaseous ethanal in methanol produced porphyrins. Rothemund investigated three different procedures for the synthesis of these macrocycles. However, the yields obtained were not published.[16] Improved methods such as by Adler et al..[17] achieved yields of up to 20% by reacting aldehydes with pyrrole in propionic acid at reflux temperature. This allowed for move favourable

conditions then those described by Rothemund et al.[16] Despite Rothemund's success with the synthesis of basic porphyrins in the 1930s, but it was to lag until the early 1950s that almost exponential growth in the use of porphyrins occurred.

The first of these was by Arsenault *et al.* who reported the synthesis of several tetra substituted porphyrins.[18] Utilizing an alternative method to that proposed by Adler et al.[17] They employed pyrromethanes instead of pyrrole. This resulted in greater yields and also the simplification of ABAB substituted porphyrin synthesis (a porphyrin with two different groups in the meso position). This was due to two meso position substituents being defined by the dipyrromethenes, allowing for interaction with an additional aldehyde resulting in formation of a porphyrin ring with alternating meso substituents. There was very little advancement in porphyrin synthesis over the subsequent 20 years until Lindsey et al.[19] in the 1980's published a new method leading to greater yields than had been reported previously. Adler's method often formed a tar like substance making it difficult to purify and was ineffective for benzaldehydes with sensitive functional groups. Lindsey et al. proposed there was a reversible reaction between reactants and the porphyrinogen and the polypyrrolemethenes products. They furtherer proposed the addition of an oxidising agent would convert the porphyrinogen to a fully aromatic porphyrin allowing for much greater yields due to the reduction in the number of side products formed as seen in Figure 26.[19] Shi and Wheelhouse proposed the use of magnesium tetrabromo

porphyrin coupled with a Suzuki coupling reaction allowing for synthesis of numerous different porphyrins in yields greater the 50%.[20]

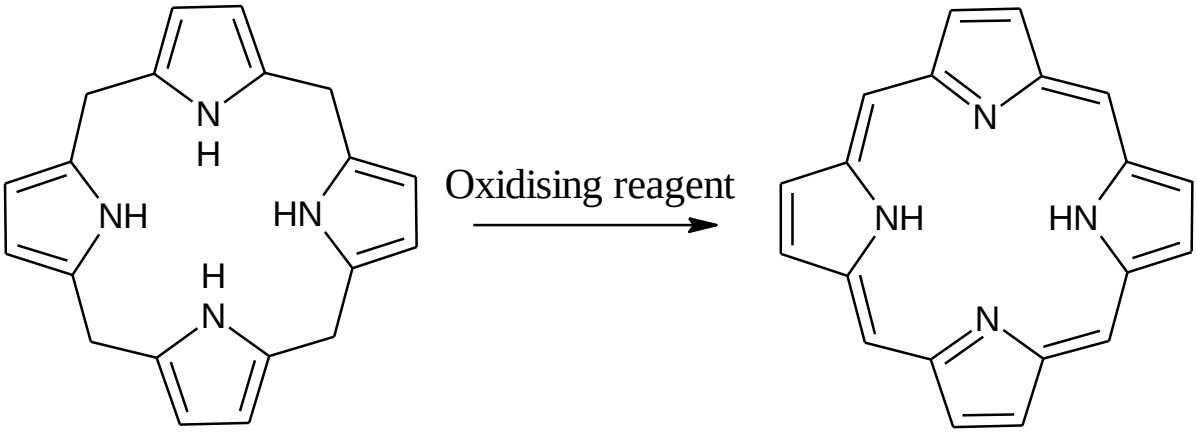

Figure 26: Porphyrinogen oxidation to porphyrin

Naik et al.[21] first proposed the use of cation exchange resins in addition to a similar methods reported previously[19] for both porphyrins and dipyrromethanes. They reported yields up to 91% for dipyrromethanes, near 70% for tetra substituted porphyrins and 23% for di-substituted porphyrins, Naik suggested that the use of a cation exchange resin instead of an acid catalyst, thus making the reactions more environmentally friendly. The resins function as a heterogeneous catalyst. Allowing adsorption to the surface and decreasing the activation energy of the reaction. Naik refers to each cation exchange resin bead as a micro reactor as each polymer chain has numerous reactive sites. Li et al.,[22] found that the addition of numerous chlorinated salts both reduced the reaction time and increased the yield of simple porphyrin systems, with the most effective salt being an equivalent of granular NaCl. It was observed that with the employment of the sodium chloride salts the length of reaction time for benzaldehyde increased 6 fold (from 1 hour to 10 minutes).[22]

2.1.3 NMR

All free base and Zinc porphyrins reported here display 3 aromatic signals. Due to the nature of the substitutions involved here they typically will integrate to 8:8:8 or 8:8:12 depending on the substitution present in the para position of the phenyl ring. With respect to the free base porphyrins only an additional signal integrating to two can be observed. Theses account for the two internal NH protons. These are typically displayed at approximately -2 ppm due to the degree of shielding experienced by the rest of the porphyrin ring.

Due to the paramagnetic nature of the other metal containing systems NMR could not be carried out. This is due to the interaction with the electric field by the unpaired electron. This greatly effects both peak area and peak placement with peaks shifting unpredictably. A typical window of proton NMR is 0 to 16 ppm. Upon the addition of Co(II) the window was increased to -50 to 200 ppm in order to account for all peaks shifts, peaks were broadened to an extent that no longer discernible as to how many signals were present.[2324]

Phenyl Porphyrin:

The ^{1}H NMRs for tetra phenyl porphyrins are well documented in the literature. A free base tetraphenyl porphyrin displays 3 aromatic signals and 1 aliphatic signal. The 3 aromatic signals integrate to 8:8:12. The furthest downfield signal occurs at 8.5 ppm this is associated with the 8 pyrrole bound protons. These appear as a singlet due to no available protons within coupling range.

Nitro porphyrin:

The ^{1}H NMR spectrum for ZnTNP, displays 3 aromatic signals. The signal at 8.74 is associated with the 8 pyrrole based protons. A singlet is observed for this as there are no protons within 3 bonds to couple with. At 8.56 ppm another signal integrating to 8 is observed this is associated with the 8 protons closest to the nitrogen. The final 8 are associated with the other 8 phenyl protons. Integration for the FbTNP shows almost identical signals. Slight variations were associated with a change is solvents.

2.2.1. UV-Vis spectroscopy

2.2.1.1. Tetra Phenyl Porphyrins

The UV-Vis spectra were in agreement with the literature.[25] A typical spectrum for a free base porphyrin consists of 1 soret peak and 4 Q bands. Upon the addition of a metal to the centre of the porphyrin the number of Q bands is typically reduced to 2. Typically, this is due to a change in symmetry from D_2h (free base) to D_4h (metalated). This is most commonly described by Gouterman's four orbital theory in which the soret band is caused by a S0-S2 transition. In a free base porphyrin, the Q bands respond to S0-S1 transitions. These porphyrins are sent to two separate excited states (commonly referred to as Q(0,0) and Q(1,0)). As mentioned previously due to the presence of the internal hydrogens on the free base porphyins, the symmetry of the system is broken. This causes the Q bands to split into two rising to the four non-degenerate Q bands.

Catalyst	Soret band (nm)	Q-band 1 (nm)	Q-band 2 (nm)	Q-band 3 (nm)	Q-band 4 (nm)
FB TPP	420	515.0	548	591	643
Zn TPP	415	555	595	N/A	N/A
Fe TPP	418	551	617	N/A	N/A
Co TPP	410	530	617	N/A	N/A
Cu TPP	419	540	615	N/A	N/A

2.3.3.2. Tetra Nitrophenyl Porphyrins

A typical spectrum for a free base porphyrin consists of 1 soret peak and 4 Q bands. Upon the addition of a metal to the centre of the porphyrin the number of Q bands is typically reduced to 2. This is due to a change in symmetry from D_2h (free base) to D_4h (metalated).

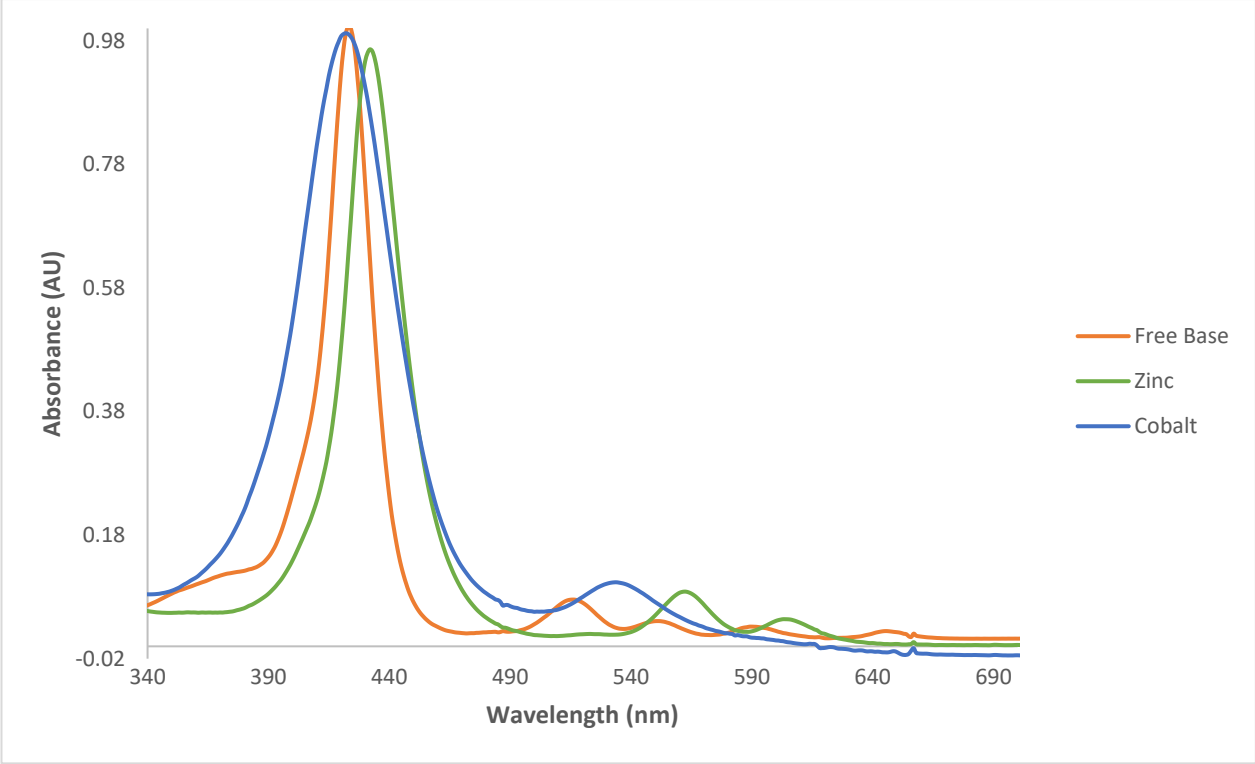

Figure 27: UV-Vis spectrums of FbTNP, CoTNP and CuTNP in anhydrous grade DMF

Free base nitro porphyrin can be seen to follow these rules. It was observed that both iron and zinc followed the expected change, with the formation of 2 Q bands. However, copper and cobalt showed the formation of a single larger Q band. Observations similar to these were made previously within the group and was attributed over concentration. Lower concentrations were investigated, showing no formation of the second Q band. Xi et al. [26] investigated the effect of different solvents on the resolution of a single Q band. It was found that in higher polarity solvents (DMSO) marginally separated the Q bands. Showing they were shifted together giving the appearance of a single Q band. Xi et al. found that upon changing to lower polarity solvents (CH_2Cl_2) a slight red shift was observed separating the Q bands allowing for an observable distinction between them. Based on the work carried out by Xi et al. the

nitro porphyrins were investigated also, they were reanalysed in DCM showing no observable difference in Q band formation.

Figure 28: UV-Vis data for all nitro porphyrin catalysts in anhydrous grade DMF.

Catalyst	Soret band (nm)	Q-band 1 (nm)	Q-band 2 (nm)	Q-band 3 (nm)	Q-band 4 (nm)
FB TNP (A)	423	516	551	590	645
Zn TNP (B)	432	562	603	NA	NA
Fe TNP (D)	425	570	614	NA	NA
Co TNP (E)	422	534	NA	NA	NA
Cu TNP (C)	421	542	NA	NA	NA

Kadish et al.[27] investigated the effect of the addition of different number of PPh_3 ligands being added to a rhodium tetraphenyl porphyrin. When a single PPh_3 was added only a single Q band was observed however upon the addition of a second PPh_3 the formation of a second Q band was observed. This is attributed to changes in symmetry of the molecule. Similar band sizes were observed with the single Q band being larger than the 2 Q bands observed in typical systems. This my indicate a symmetry effect taking place causing a single Q band to form.

2.3.4. Electrochemical catalysis

A number of nitro porphyrins were analysed for their ability to reduce CO_2 in heterogeneous systems. They were also examined for heterogeneous production of H_2 from proton rich environments. Porphryin systems are well documented for their ability to both reduce CO_2 and produce hydrogen.[28,29,30]

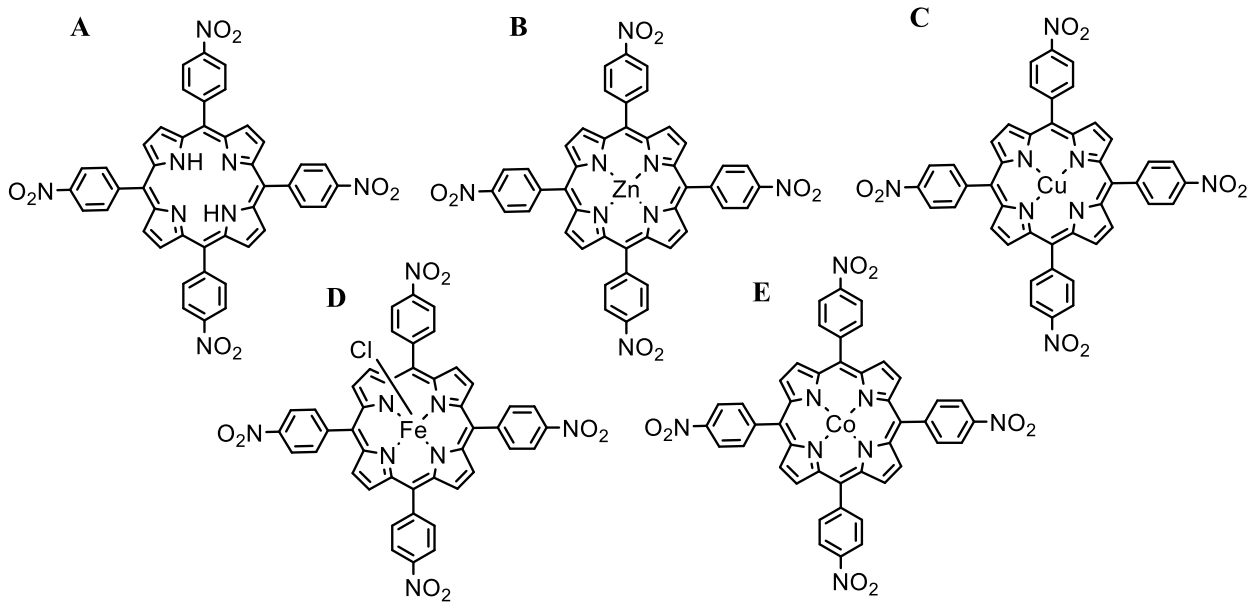

Figure 29: Porphyrin systems investigated in this chapter.

2.3.4.1. Cyclic voltammetry of nitro containing compounds.

Table 2: reduction states for all metalated nitro porphyrins (vs Fc/Fc+) at 0.1 Vs^{-1} in DMF at 1 mm

Complex	1st reduction	2nd reduction	3rd reduction	4th reduction
B	-1.5 V	-1.78 V	-2.4 V	NA
C	-1.55 V	-1.75 V	-2.0 V	NA
D	-0.5 V	-1.46 V	-1.8 V	-2.4 V
E	-1.09 V	-1.63 V	-2.2 V	-2.4 V

Tetraphenyl porphyrin were compared to which is well documented in the literature. The nitro substituted porphyrins. Free base tetraphenyl porphyrin contains two ring based electrochemical reductions, these occur at -1.7 and -2.2 V (vs Fc/Fc^{+}). Due to insolubility in all available solvents A is not reported here. Silvester et al.[31]

investigated the electrochemistry of nitrobenzene. It was found that for the polymerization of nitrobenzene 3 electrons and 3 protons were required (Figure 30).

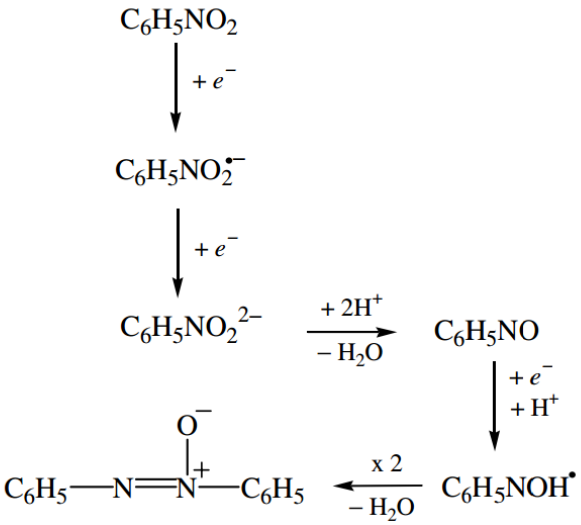

Figure 30: proposed mechanism for the reduction of nitro benzene groups [31].

2.3.4.2. Cyclic voltammetry of system ZnTNP (B):

Figure 31 shown below displays the cyclic voltammogram of zinc tetranitroporphyrin. Traditionally, free base porphyrins and zinc porphyrins show very similar electrochemistry. This is due to the lack of an observable process for zinc (II) to zinc (I) in the solvent window when using DMF. In total 3 process were observed, the first reduction taking place at -1.5 V (vs Fc/Fc^{+}) the second taking place at -1.78. It would be expected that upon the addition of electro withdrawing groups to the porphyrin that reductions would be shifter to more positive potentials. This is due to the electron density being pulled away from the porphyrin ring.[32] Li et al.[30] investigated the effect of the addition of 1, 2 and 3 nitro groups in the meso position of a corrole. It was observed that upon the addition of 1 nitro substituent an additional reduction state was observed. This peak grew upon the addition of each addition peak. They were observed at approximately -1.4 V (vs Fc/Fc^{+}) and -2.0 V. It seems that the two

processes below are associated with two porpyrin ring based reductions. The relative size of the first reduction state suggests there is also reduction of a nitro group.[30] A 3rd large reductive peak was observed that is not displayed here. Following this reduction step the electrode became passivated which suggests polymerization of the nitro groups. This was supported by literature pertaining to electrochemistry of nitrobenzene.[31] Where polymerization was observed.

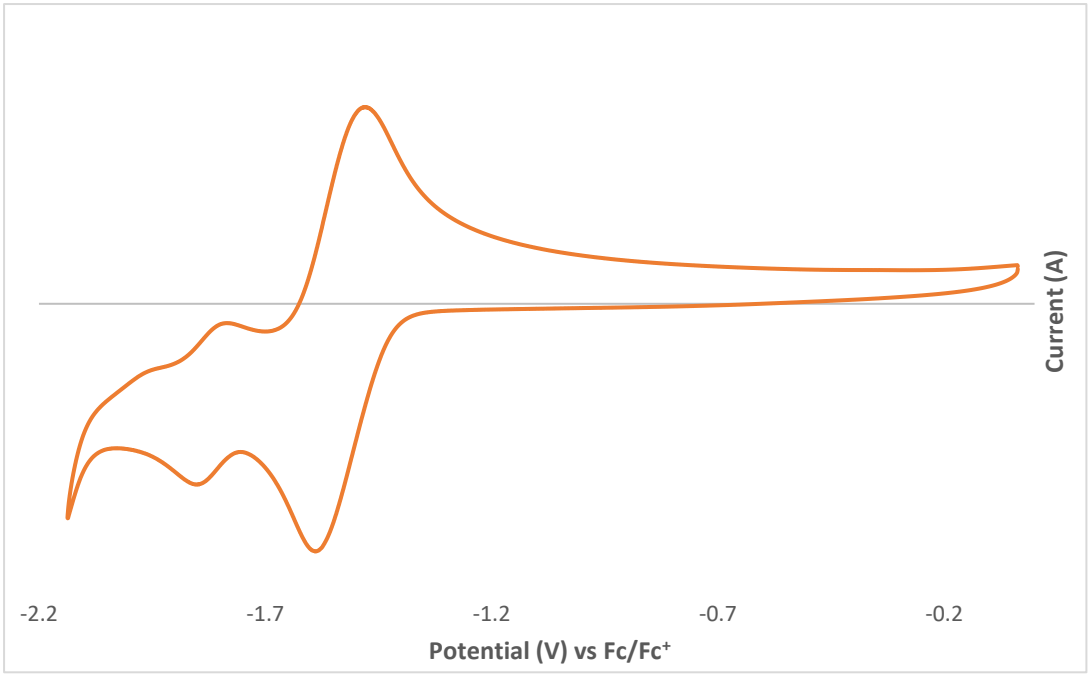

Figure 31: Cyclic voltammetry of zinc tetra nitro porphyrin at 1 mM in 0.1 M $TBAPF_6$/DMF vs Fc/Fc^+ at 100mV/sec under argon

2.3.4.3. Cyclic voltammetry of system CuTNP (C):

Due to the insolubility of compound C in DMF studies were carried out in DCM, 3 reductive states were observed. The first two reductive states appear at similar ratios and similar potentials to that of B. A 3rd process is observed at -2.0 V. Due to a change in solvent processes after this are lost in the onset of the solvent as DCM has a smaller electrocatalytic window to that of DMF. It is likely this is the beginning of a larger process similar to that observed at -2.4 V in other systems. Upon reaching the 3rd reduction state formation of a peak -1.4 V is observed. This indicates a chemical step that does not occur in DMF occurred. The process increases slowly after each subsequent scan which indicates instability in DCM.

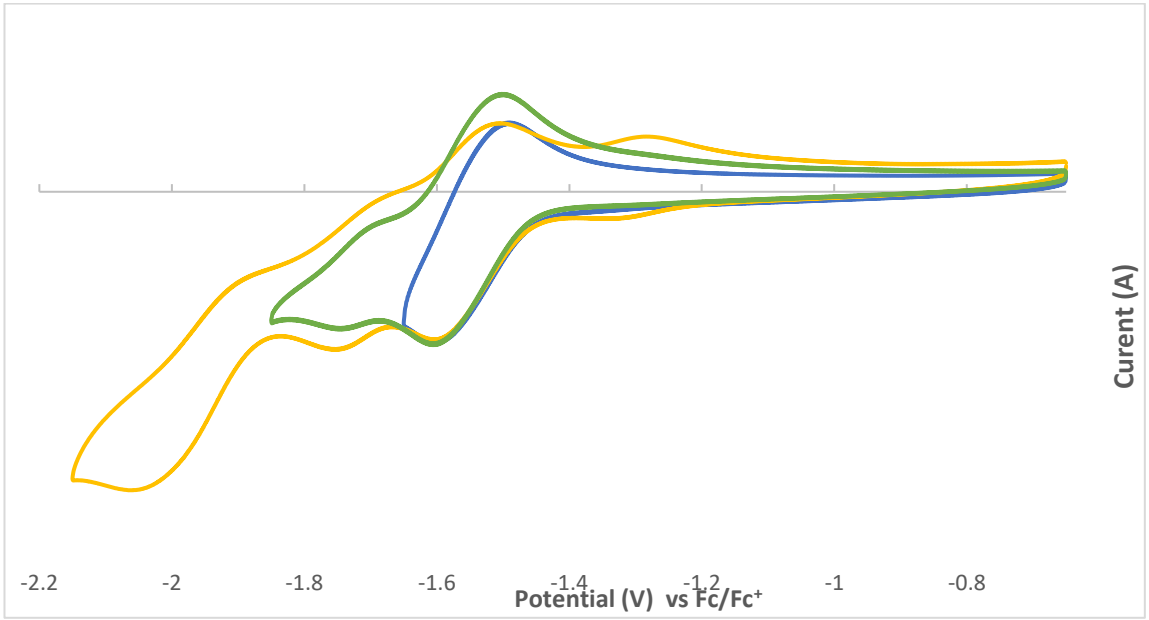

Figure 32: Cyclic voltammetry of copper tetra nitro porphyrin at 1 mM in 0.1M TBAPF6/ DCM vs Fc/Fc+ at 100mV/sec under argon

2.3.4.4. Cyclic voltammetry of system FeTNP (D):

Figure 33 shows the cyclic voltammograms for the reduction of iron (III) tetra nitro porphyrin chloride. It was observed that when scanning out to -1.3 V (vs Fc/Fc^{+}) the iron (III) to iron (II) reduction at -0.6 V was reversible. This is similar to what has been reported in the literature.[33] However, upon reaching the second reduction process the iron reduction becomes irreversible, with formation of a reversible product at -1.1 V. Two reduction states were observed similar to previous systems and as was discussed previously (–1.55 V and -1.8 V). Additionally, upon reaching the final reduction state at -2.4 V the electrode quickly became passivated indicating possible polymerization as discussed previously.

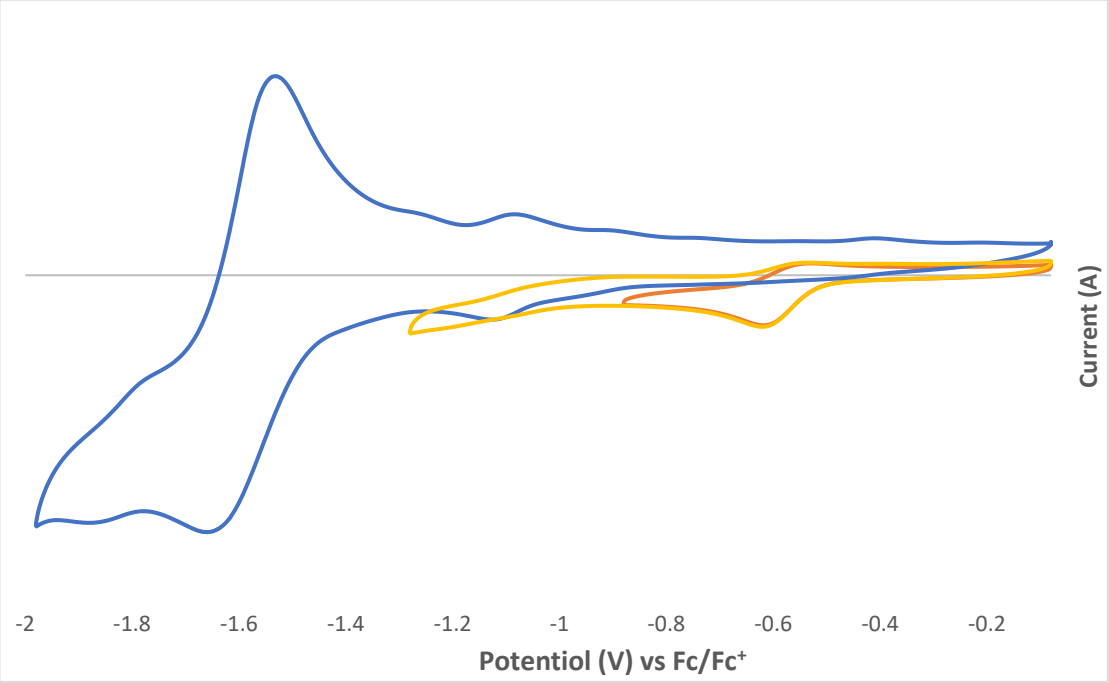

Figure 33: Cyclic voltammetry of iron tetra nitro porphyrin at 1 mM in 0.1 M $TBAPF_6$/DMF vs Fc/Fc^{+} at 100mV/sec under argon

2.3.4.5. Cyclic voltammetry of system CoTNP (E):

Similarly, to previously reported for the metalated nitro porphyrins, two processes can be observed. A reduction of Co (II) to Co (I) can be observed at 1.09 V. This is similar

to that quoted in the literature.[34,35] A lack of a second porphyrin peak was observed here. It is proposed that the peak was shifted underneath the large reduction state observed at -1.6 V. As mentioned previously; a large irreversible peak is observed at -2.4 V. Upon reaching the process all peaks became irreversible and the working electrode was passivated. A Co (II) to Co (III) was also observed at 0.095 mV. This is consistent with the literature.[34]

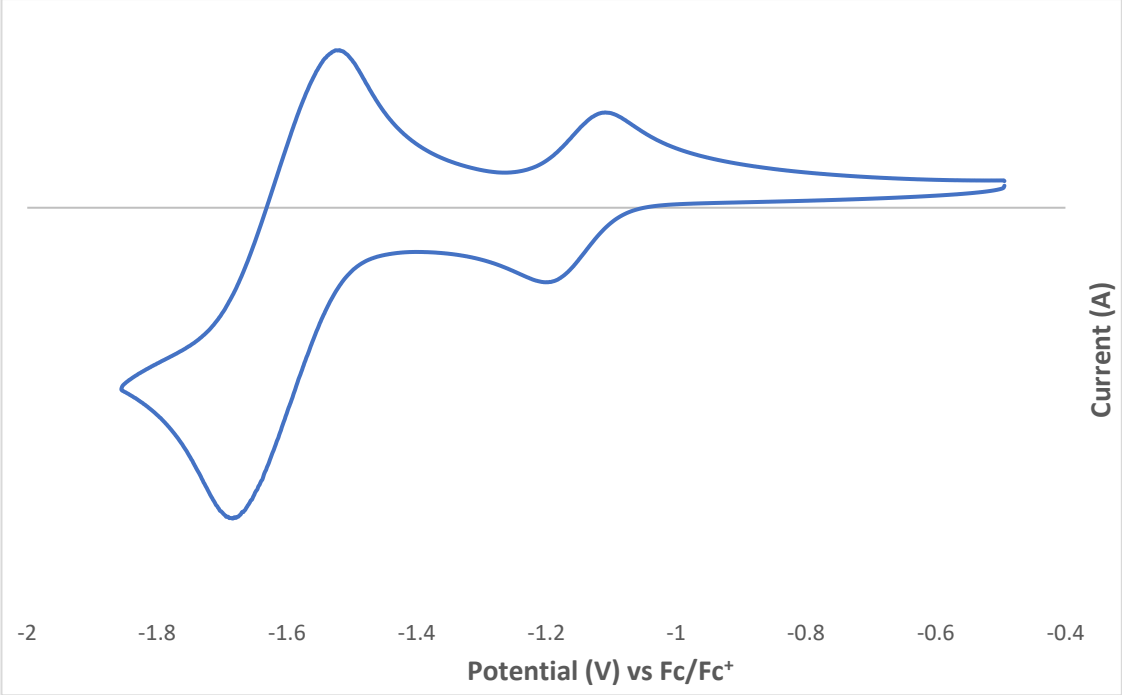

Figure 34: Cyclic voltammetry of cobalt tetra nitro porphyrin at 1 mM in DMF/TBAPF$_6$ vs Fc/Fc$^+$ at 100mV/sec under Argon

2.3.5. Electrocatalytic CO_2 reduction

All nitro porphyrins were investigated for homogeneous CO_2 reduction. Systems were purged with argon to obtain a base line and then purged with CO_2 in order to investigate a response of CO_2 binding.

2.3.5.1. CO_2 reduction of system ZnTNP (B)

A clear enhancement was observed of the second reductive process upon purging the sample with CO_2. After the first scan, the reduction state at -1.6 V was no longer electrocatalytically active and a large enhancement of the reduction state at -1.8. suggesting binding of CO_2 onto the nitro groups. This was further supported by calculations by Lie et al.[36] in which DFT was carried out showing nitro groups have a strong ability to polarize CO_2. Additionally, 5% water was added to investigate the effect of a proton source. A slight decrease in enhancement was observed and was attributed to dilution of the system. The decrease in the enhancement was consistent with the 5% dilution. Enhancements are typically an indication of activity for CO_2 reduction, suggesting that compound B should be capable of reducing CO_2.[37,38] However, B showed no activity for CO_2 reduction, which is not unusual for zinc containing macrocycles,[39] and usually favour hydrogen evolution over the formation of CO.

Upon electrolysis at -2.6 V (vs Fc/Fc^+) no observable formation of any CO_2 reduction product or hydrogen were observed.

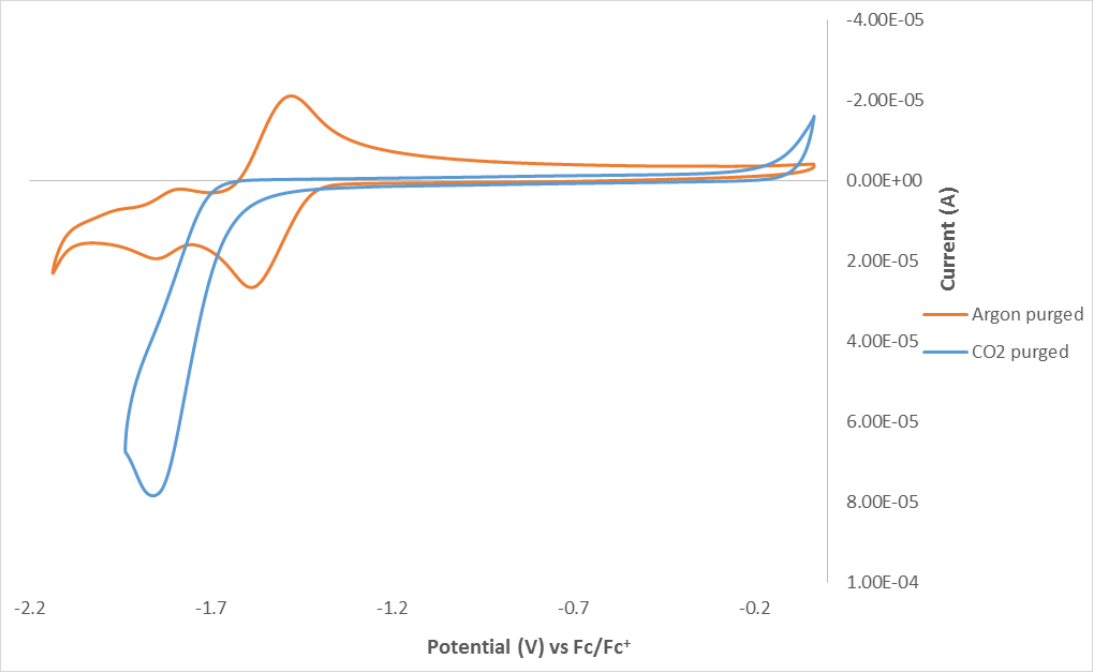

Figure 35: Cyclic voltammetry of zinc tetra nitro porphyrin at 1 mM in 0.1 M TBAPF6/DMF vs Fc/Fc+ at 100mV/sec

2.3.5.2. CO_2 reduction of using compound C CuTNP

Significant differences were observed for system C to those off all other systems discussed here. Enhancements were observed for all processes suggesting activity for both porphyrin based reductions and nitro based reductions.[37,38] Unlike the other systems studied here where a clear enhancement was observed typically on the porphyrin process. This was attributed to a solvent effect from DCM as typically Zn and Cu porphyrins should display very similar spectrums based on the litreatuer.[39] No difference could be observed upon the addition of 5% water, and this was attributed to the immiscibility of water and DCM.

Upon electrolysis at -2.6 V (vs Fc/Fc^+) no observable formation of any CO_2 reduction product or hydrogen were observed.

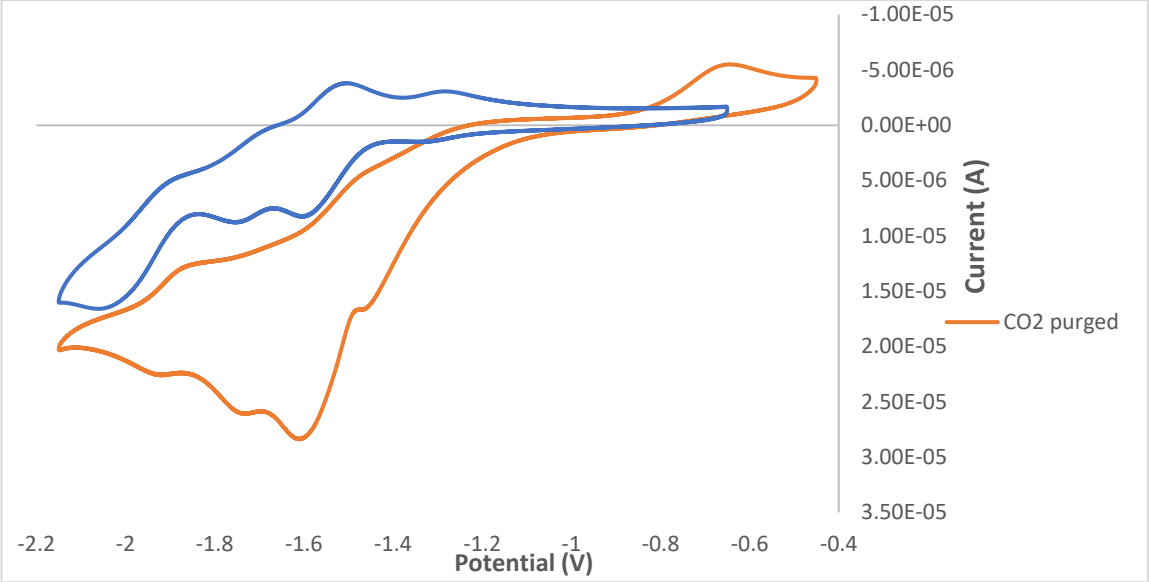

Figure 36: Cyclic voltammetry of copper tetra nitro porphyrin at 1 mM in 0.1 M TBAPF6/DCM vs Fc/Fc+ at 100mV/sec

2.3.5.3. CO_2 reduction of system compound D FeTNP

Upon purging a solution containing compound D with CO_2, formation of an irreversible reduction state was observed at -1.4 V with a second irreversible reduction state at -1.7 V. The latter was associated with the reduction of both a porphyrin and nitro groups. Only marginal enhancements were observed with all other reduction states disappearing suggesting formation of a non-electrochemically active species at those sites. However, addition of 5% water gave noticeable enhancement at -1.4 V forming a similar peak height to that observed at -1.7 V. System D was the only system discussed here that showed a positive enhancement upon the addition of water. Suggesting that the reduction state observed at -1.4 V is associated with the binding of CO_2 which is accelerated by the addition of water.

Upon electrolysis at -2.6 V (vs Fc/Fc^{+}) formation of both CO and H_2 was observed however in both cases TONs of less than one were achieved.

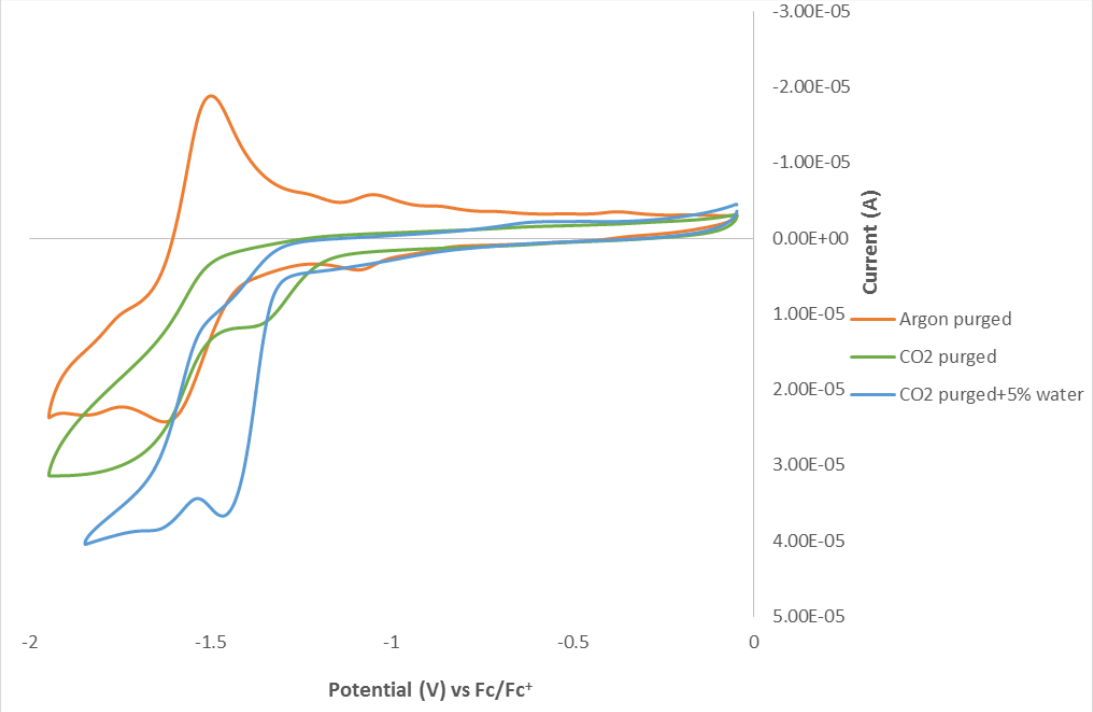

Figure 37: Cyclic voltammetry of iron tetra nitro porphyrin at 1 mM in 0.1 M TBAPF6/DMF vs Fc/Fc+

2.3.5.4. CO_2 reduction of system compound E CoTNP

Compound E showed a noticeable difference to that observed for either B or D. Displaying an enhancement for the nitro containing reduction with a loss of any reversibility. This suggests the formation of a non-electrocatalytic product. A decrease was observed for Co(II) to Co(I) with the formation of a new redox couple formed between the two reduction states. The slower rate of decreases of Co(II) to Co(I)

coupled with the formation of the new redox couple may suggest the formation of Co(I)-CO_2. Post the addition of 5% water no significant changes were observed. A slight decrease in enhancement was observed which was attributed to the dilution of the system.

Upon electrolysis at -2.6 V (vs Fc/Fc^+) formation of both CO and H_2 was observed however in both cases TONs of less than one were achieved.

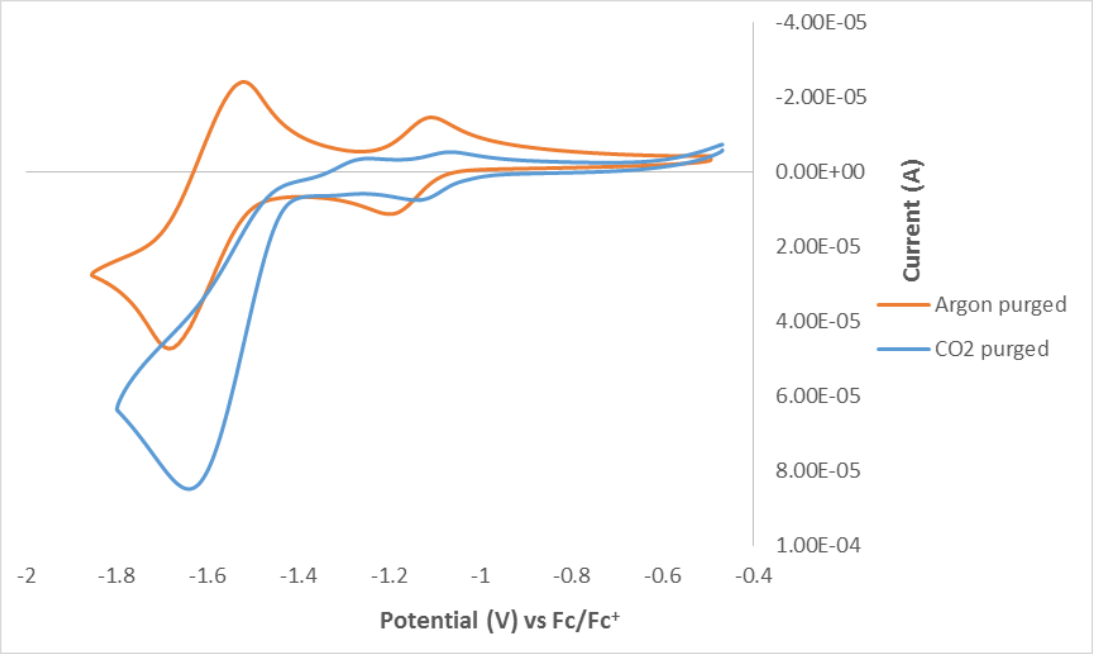

Figure 38: Cyclic voltammetry of cobalt tetra nitro porphyrin at 1 mM in 0.1 M TBAPF6/DMF vs Fc/Fc+ at 100mV/sec

2.3.6. Hydrogen Evolution:

Both cobalt and iron tetra nitro porphyrin showed highly efficient evolution of hydrogen at -1 V. Whereas at the same applied potential, zinc and copper porphyrins showed very little activity. The addition of a metal reductive process has been documented in shifting the catalytic onset for hydrogen evolution[40].

Table 3: Results reported for hydrogen electrochemical evolution over a 1 hour bulk electrolysis at -1V vs Ag/AgCl

Catalyst	Charge (C)	TON	TOF (s^{-1})	Faradic efficiency
B	0.16	128	0.03	4%
C	0.22	375	0.1	5%
D	0.5	17000	4.7	96%
E	1.8	65,000	18	98%

Assuming 100% of the catalyst is active E showed a much greater ability for hydrogen evolution when compared to other systems investigated. However, Both D and E far exceeded B and C, with B and C efficiencies of >6% compared to that of near 100% for both D and E. With regards hydrogen evolution it was observed that Co porphyrin performed better then Fe porphyrin which performed better then Cu and Zn. This is similar to that observed in the literature. [40,41]

Within the research group calculations of percentage active catalyst has been carried out previously with cobalt substituted phthalocyanines, they typically display activities of approximately 10 % or less. It was found that an activity of 6% was achieved for D. This is calculated using Faradays law which states that the number of

moles of electrons is equal to charge passed (C) divided by Faraday's constant (C mol^{-1}) for a one electro process. The peak area was calculated from Figure 39 and divided by 96487 C mol^{-1} giving a number of moles of electrons passed which is equal to the number of moles of active catalyst present.[42]

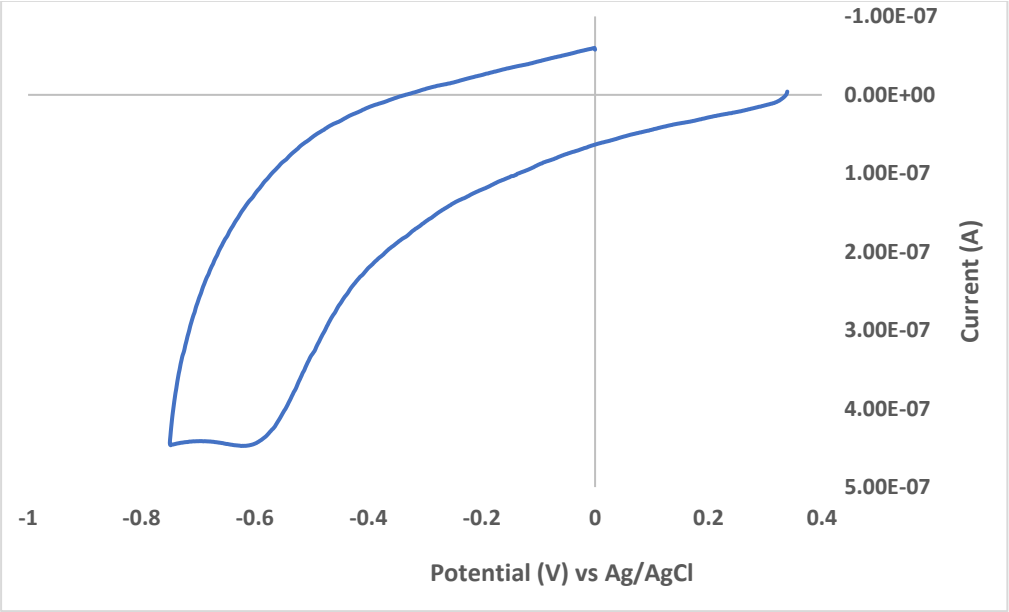

Figure 39: System D drop cast on the surface of a glassy carbon electrode (1.5x10-10 mol) in 0.1 M phosphate buffer vs Ag/AgCl

If the concentration of active catalyst is factored into the above results a TON of 17000 becomes 100,000. FeTNP was further probed in a time dependent study. In the first hour of bulk electrolysis there was a steady increase in the rate of charge of charge passed. This could indicate formation of the active catalytic species. Time intervals of 1, 3 and 16 hours were examined. It was found that after 3 hours the TON had increased almost 6 fold. After 16 hours the TON had increased 80 fold. This shows a greater than linear increase with respect to time. This further supports the indication that formation of an active catalyst was required with the greatest TOF reported was after 16 hours.

Table 4: Results for FeTNP assuming 100% active at -1 V vs Ag/AgCl at 0.1 V s^{-1} in pH 2 phosphate buffer with 1.5 x 10^{-10} mol drop cast

Time (h)	Charge (C)	TONs	TOF (s^{-1})	Faradic efficiency
1	0.5	17,000	5	98%
3	2.8	97,000	8.9	98%
16	46.8	1,380,000	24	84%

Table 5: Results for FeTNP assuming 6% percent active at -1 V vs Ag/AgCl at 0.1 V s^{-1} in pH 2 phosphate buffer with 1.5 x 10^{-10} mol drop cast

Time (h)	Charge (C)	TON	TOF (s^{-1})	Faradic efficiency
1	0.5	283,000	79	98%
3	2.8	1,616,000	150	98%
16	46.8	23,000,000	400	84%

Catalyst	Catalytic onset (V)
Bare electrode	-1.2
B	-1.2
C	-1.2
D	-1.0
E	-0.8

With a TON value of ~23,000,000 for H_2 evolution this catalyst yielded a higher TON to any porphyrin or phtalocyanine systems reported in the litreatuer.[28,43] Systems typically show high TOFs and very poor stability or high stability with poor TOFs.[44,45] It has been proposed that the use of metalated tetranitroporphyrins may strike a balance between the two, showing improved activity over time and high faradic efficiencies. These catalysts will be investigated further in larger cells as post 16 hour experiments, internal pressure is increased due to hydrogen evolution. This forced flow of solvents away from the electrode compartments leading to the experiment being ceased.

Shifts in catalytic onset were observed between different metal centres. Observations made were typical of that seen in the literature with Co and Fe showing the greatest shift in a positive direction. While Zn and Cu showed much less change compared to the blank electrode.[41] This change is typically associated with the reduction of both iron and cobalt centres allowing for protonation of the metal centre thus catalysing the formation of hydrogen production.[46]

2.3.6.1. Mechanism:

A similar mechanism is proposed to that of Kellet et al.[46] That reduction of the metal centre from Co (II) to (I) oxidation state occurs allowing for the binding of a proton to

a metal centre thus forming a metal hydride and returning it back to a (II) oxidation state. The Co centre is then protonated further forming molecular hydrogen, leaving the molecular centre in a (II) oxidation state completing the cycle. Similar mechanisms have being proposed in the literature for iron and cobalt centers.[47,48]

This mechanism is supported as the potential being applied was not at a sufficiently negative potential to allow for a porphyrin/nitro based reduction. This suggests that the reduction is caused by the reduction of the metal centre for both cobalt and iron. This was further supported by the lack of hydrogen evolved by both zinc and copper analogs.

An activation phase was observed during the first 10 minutes of the bulk electrolysis. During this phase the rate of charge passed increased significantly. The significant increase in the rate of charge passed suggests a chemical change at the catalyst occurred. This observation was not investigated further. However, it is known that the reduction of a nitro group can form an amino derivative. This would require further work to identify the catalyst post the activation phase.[49]

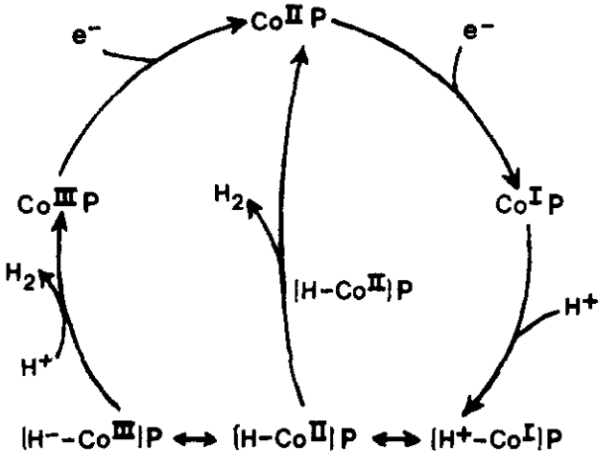

Figure 40: Mechanism proposed for hydrogen production by Kellet et al.[46]

2.4. Conclusion

The aim of Chapter 2 was to test the hypothesis that porphyrin based systems can function as an effective electrocatalyst for CO_2 reduction and/or hydrogen generation.

To achieve this, aim an array of tetra substituted porphyrins were synthesised and assessed for both H_2 and CO_2 electrocatalytically. Investigations were carried out into the cause of unusual absorbance spectrums attributing the formation of one large Q band to a shift in wavelength. Systems showed significant enhancements upon purging with CO_2. This suggests some interaction with CO_2. However, no notable results were achieved with TONs close to 1. Both cobalt and iron porphyins showed very promising results for hydrogen evolution achieving TON's of up to 23,000,000 over 16 hours and faradaic efficiencies ranging between 98 – 84 %. Leading to the highest observed results reported in the literature by any porphyrin or phtalocyanine, the percentage of active catalyst were calculated using faradays law allowing for a more accurate TON. The results pertaining to H_2 generation are very promising and these systems should be further probed to identify the mechanism and explain the lag phase, therefor leading to better performing electrocatalysts.

2.5. References

1 K. Leung, I. M. B. Nielsen, N. Sai, C. Medforth and J. a Shelnutt, *J. Phys. Chem. A*, 2010, **114**, 10174–10184.

2 D. Behar, T. Dhanasekaran, P. Neta, Hosten C. M., D. Ejeh and P. Hambright, *J. Phys. Chem. A*, 1998, **5639**, 2870–2877.

3 M. García, M. J. Aguirre, G. Canzi, C. P. Kubiak, M. Ohlbaum and M. Isaacs, *Electrochim. Acta*, 2014, **115**, 146–154.

4 A. Fateeva, P. a. Chater, C. P. Ireland, A. a. Tahir, Y. Z. Khimyak, P. V. Wiper, J. R. Darwent and M. J. Rosseinsky, *Angew. Chemie*, 2012, **124**, 7558–7562.

5 J. Rosenthal, T. D. Luckett, J. M. Hodgkiss and D. G. Nocera, *J. Am. Chem. Soc.*, 2006, **128**, 6546–6547.

6 Z. Wang, C. J. Medforth and J. a. Shelnutt, *J. Am. Chem. Soc.*, 2004, **126**, 16720–16721.

7 J. E. Van Lier, J. D. Spikes, G. Bock and S. Harnett, *Photosensitizing Compounds: Their Chemistry, Biology and Clinical Use*, Wiley Progetto Editore, Padova, 1989, vol. 146.

8 C. Pavani, A. F. Uchoa, C. S. Oliveira, Y. Iamamoto and M. S. Baptista, *Photochem. Photobiol. Sci.*, 2009, **8**, 233–240.

9 J. R. Darwent, P. Douglas, A. Harriman, G. Porter and M.-C. Richoux, *Coord. Chem. Rev.*, 1982, **44**, 83–126.

10 K. Borjesson, J. Wiberg, A. H. El-sagheer, T. Ljungdahl, J. Mårtensson, T.

Brown, B. Norde and B. Albinsson, *ACS Nano*, 2010, **4**, 5037–5046.

11 J. R. Burns, K. Göpfrich, J. W. Wood, V. V. Thacker, E. Stulz, U. F. Keyser and S. Howorka, *Angew. Chemie Int. Ed.*, 2013, **52**, 12069–12072.

12 X.-A. Zhang, K. S. Lovejoy, A. Jasanoff and S. J. Lippard, *Proc. Natl. Acad. Sci. U. S. A.*, 2007, **104**, 10780–5.

13 D. Shahbazi-Gahrouei, M. Williams, S. Rizvi and B. J. Allen, *J. Magn. Reson. Imaging*, 2001, **14**, 169–174.

14 J. E. Reeve, H. a. Collins, K. De Mey, M. M. Kohl, K. J. Thorley, O. Paulsen, K. Clays and H. L. Anderson, *J. Am. Chem. Soc.*, 2009, **131**, 2758–2759.

15 J. E. Falk, *Porphyrins and metalloporphyrins: their general, physical and coordination chemistry, and laboratory methods*, Elsevier Pub. Co., 1964.

16 P. Rothemund, *J. Am. Chem. Soc.*, 1935, **57**, 11–12.

17 A. Adler, *J Org Chem*, 1967, 1962.

18 G. Arsenault, *J. Am. Chem. Soc.*, 1960, **155**, 4384–4389.

19 J. S. Lindsey, I. C. Schreiman, H. C. Hsu, P. C. Kearney and A. M. Marguerettaz, *J. Org. Chem.*, 1987, **52**, 827–836.

20 D. Shi, R. T. Wheelhouse, W. Yorkshire and B. D. Dp, *Tetrahedron Lett.*, 2002, **43**, 9341–9342.

21 R. Naik, P. Joshi, S. P. Kaiwar and R. K. Deshpande, *Tetrahedron*, 2003, **59**, 2207–2213.

22 F. Li, K. Yang, J. Tyhonas, K. MacCrum and J. Lindsey, *Tetrahedron*, 1997, **53**, 12339–12360.

23 I. Bertini, L. Messori, G. Golub, H. Cohen and D. Meyerstein, *Inorganica Chim. Acta*, 1995, **235**, 5–8.

24 C. L. Ivono Bertini and G. Parigi, Eds., in *Solution NMR of Paramagnetic MoleculesApplications to metallobiomolecules and models*, Elsevier, 2001, vol. 2, pp. 29–73.

25 R. E. Falvo, L. M. Mink and D. F. Marsh, 1999, **76**, 237–239.

26 X. Y. Li and D. K. P. Ng, *Tetrahedron Lett.*, 2001, **42**, 305–309.

27 K. M. Kadish, Y. Hu, T. Boschi and P. Tagliatesta, *Inorg. Chem.*, 1993, **32**, 2996–3002.

28 J. L. Inglis, B. J. MacLean, M. T. Pryce and J. G. Vos, *Coord. Chem. Rev.*, 2012, **256**, 2571–2600.

29 G. F. Manbeck and E. Fujita, *J. Porphyr. Phthalocyanines*, 2015, **19**, 45–64.

30 B. Li, Z. Ou, D. Meng, J. Tang, Y. Fang, R. Liu and K. M. Kadish, *J. Inorg. Biochem.*, 2014, **136**, 130–139.

31 D. S. Silvester, A. J. Wain, L. Aldous, C. Hardacre and R. G. Compton, *J. Electroanal. Chem.*, 2006, **596**, 131–140.

32 A. Sen and V. Krishnan, *Tetrahedron Lett.*, 1996, **37**, 5421–5424.

33 M. Li, I. M. Ornelas, W. Liu, Y. Niu, J. P. Correia, A. S. Viana and G. Jin, *Electroanalysis*, 2015, **27**, 1427–1435.

34 F. D'Souza, A. Villard, E. Van Caemelbecke, M. Franzen, T. Boschi, P. Tagliatesta and K. M. Kadish, *Inorg. Chem.*, 1993, **32**, 4042–4048.

35 A. Koca, M. Kasim Şener, M. B. Koçak and A. Gül, *Int. J. Hydrogen Energy*,

2006, **31**, 2211–2216.

36 Y. Liu, J. Liu, M. Chang and C. Zheng, *J. Phys. Chem. C*, 2012, **116**, 16985–16991.

37 A. J. Morris, R. T. McGibbon and A. B. Bocarsly, *ChemSusChem*, 2011, **4**, 191 – 196.

38 M. Keshavarz-k, K. T. Potts and H. D. Abruila, *Inorg. Chem.*, 1992, **31**, 3680–3682.

39 N. Sonoyama, M. Kirii and T. Sakata, *Electrochem. commun.*, 1999, **1**, 213–216.

40 P. Du and R. Eisenberg, *Energy Environ. Sci.*, 2012, **5**, 6012.

41 N. Chebotareva and T. Nyokong, *Electrochim. Acta*, 1997, **42**, 3519–3524.

42 A. J. Bard, L. R. Faulkner, N. York, C. @bullet, W. Brisbane and S. E. Toronto, *ELECTROCHEMICAL METHODS Fundamentals and Applications*, 1944.

43 J. R. McKone, S. C. Marinescu, B. S. Brunschwig, J. R. Winkler and H. B. Gray, *Chem. Sci.*, 2014, **5**, 865–878.

44 P. V Bernhardt and L. a Jones, *Inorg. Chem.*, 1999, **38**, 5086–5090.

45 D. Sirbu, C. Turta, E. a. Gibson and a. C. Benniston, *Dalt. Trans.*, 2015, **44**, 14646–14655.

46 R. M. Kellett and T. G. Spiro, *Inorg. Chem.*, 1985, **24**, 2373–2377.

47 I. Bhugun, D. Lexa and J.-M. Savéant, *J. Am. Chem. Soc.*, 1996, **118**, 3982–3983.

48 A. Koca, *Int. J. Hydrogen Energy*, 2009, **34**, 2107–2112.

49 N. L. Weinberg, *Chem. Rev.*, 1968, **68**, 449–523.

3. Chapter 3. Materials and methods

3.1 **Synthesis**

3.1.1.1. 5,10,15,20-tetraphenylporhyrin (TPP)

Into a clean dry 500ml round bottom flask 240 ml of propionic acid was added. A further 50.1 mmol of benzaldehyde were added and 63 mmol of acetic anhydride were added to the solution. 43 mmol of pyrrole was diluted with 10 ml of propionic acid and added slowly once the solution reached reflux temperature (160 ^{o}C). The reactant mixture was allowed to stir for 1 hour. The mixture was then allowed to cool to room temperature and placed in the freezer overnight.

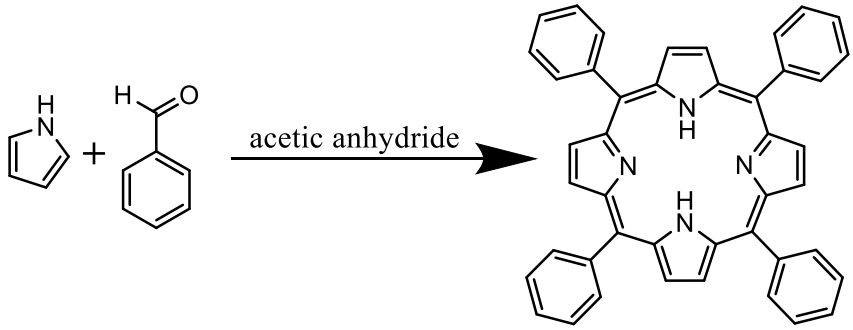

Figure 41: Reaction for the formation of TPP

The solution was filtered under vacuum and washed with water and methanol until the washing became clear. No further purification was required. This resulted in the formation of a purple powder.

Yield: 12%

NMR: (400 MHz, CDCl3), 8.84 ppm(s, 8H), 8.29ppm (d, 8H), 7.77 ppm (d, 12H), -2.73 ppm (s, 2H)

UV-Vis (**λ max**): **420,** 515, 548, 591, 643 nm

4.1.1.2. Zinc 5,10,15,20-tetraphenylporhyrin (ZnTPP):

Solutions containing DCM and methanol were purged individually for 10 minutes. Into a clean dry round bottom flask 40 ml of DCM and 10 ml of methanol were added carefully under a nitrogen atmosphere. A further 0.33 mmol of TPP and 0.1 mmol of zinc (II) acetate were added and allowed to stir under a nitrogen atmosphere overnight.

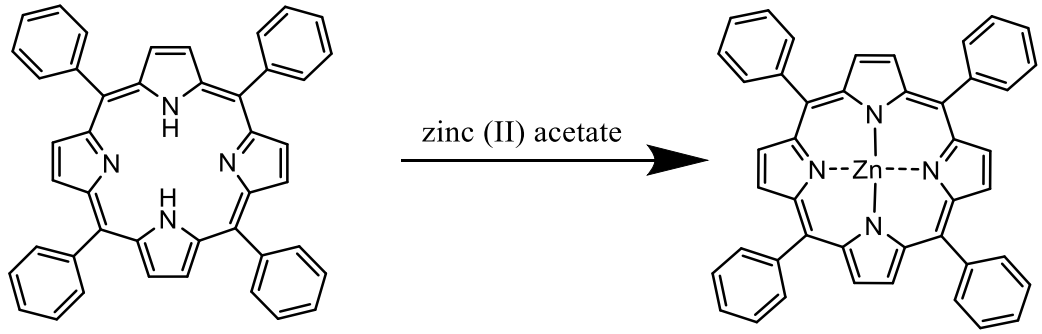

Figure 42: Synthesis of ZnTPP

The DCM was removed under reduced pressure. Once all DCM was removed a precipitate could be observed. The solution was then filtered under vacuum. The precipitate was further washed with methanol until washing became clear. No further purification was required. A purple powder was obtained.

Yield: 95%

NMR: (400 MHz, CDCl3), 8.94 ppm(s, 8H), 8.32ppm (d, 8H), 7.81 ppm (d, 12H),

UV-Vis (**λ max**): **425,** 556, 598 nm

4.1.1.3. Cobalt 5,10,15,20-tetraphenylporhyrin (CoTPP):

Solutions containing DCM and methanol were purged individually for 10 minutes. Into a clean dry round bottom flask 40 ml of DCM and 10 ml of methanol were added carefully under a nitrogen atmosphere. A further 0.33 mmol of TPP and 0.1 mmol of cobalt (II) chloride hexahydrate were added and allowed to stir under a nitrogen atmosphere overnight.

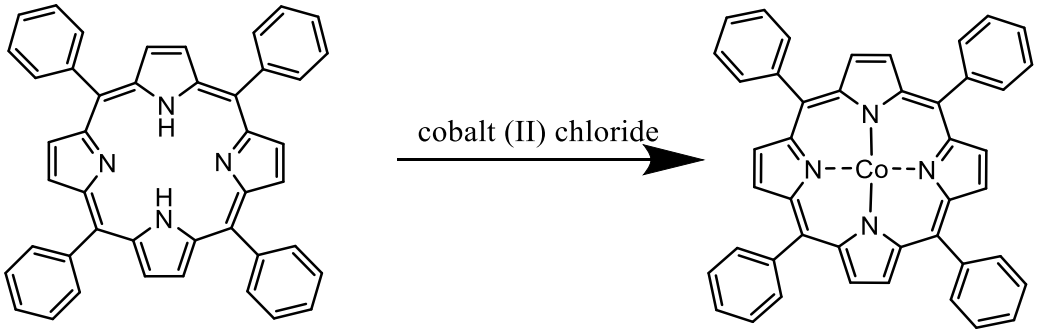

Figure 43: Synthesis of CoTPP

The DCM was removed under reduced pressure. Once all DCM was removed a precipitate could be observed. The solution was then filtered under vacuum. The precipitate was further washed with methanol until washing became clear. The resulting residue was placed on a silica column and eluted with 100% dichloromethane. Only one distinct band was observed. The eluent was collected and solvent was removed under vacuum. Resulting in a fine purple powder.

Yield: 75%

NMR: (400 MHz, CDCl3), 8.94 ppm(s, 8H), 8.32ppm (d, 8H), 7.81 ppm (d, 12H),

UV-Vis (**λ max**): **410,** 530, 617 nm

4.1.1.4. Copper 5,10,15,20-tetraphenylporhyrin (CuTPP):

Solutions containing DCM and methanol were purged individually for 10 minutes. Into a clean dry round bottom flask 40 ml of DCM and 10 ml of methanol were added carefully under a nitrogen atmosphere. A further 0.33 mmol of TPP and 0.1 mmol of Copper (II) chloride were added and allowed to stir under a nitrogen atmosphere overnight.

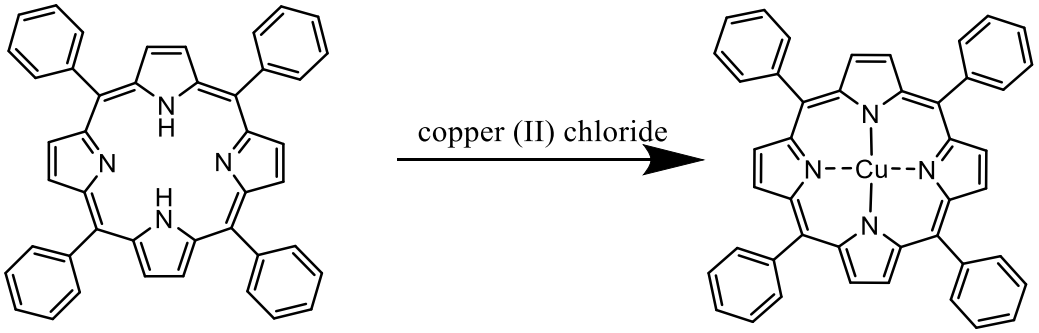

Figure 44: Synthesis of CuTPP

The DCM was removed under reduced pressure. Once all DCM was removed a precipitate could be observed. The solution was then filtered under vacuum. The precipitate was further washed with methanol until washing became clear. No further purification was required. A purple powder was obtained.

4.1.1.5. Iron 5,10,15,20- tetraphenylporhyrin (FeTPP):

Solutions containing DCM and methanol were purged individually for 10 minutes. Into a clean dry round bottom flask 40 ml of DCM and 10 ml of methanol were added carefully under a nitrogen atmosphere. A further 0.33 mmol of TPP and 0.1 mmol of Iron (III) chloride were added and allowed to stir under a nitrogen atmosphere overnight.

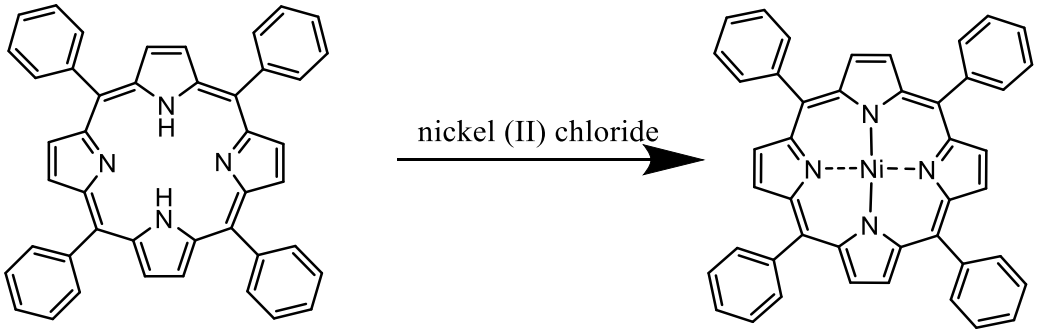

Figure 45: Synthesis of NiTPP

The DCM was removed under reduced pressure. Once all DCM was removed a precipitate could be observed. The solution was then filtered under vacuum. The precipitate was further washed with methanol until washing became clear. No further purification was required. A purple powder was obtained.

4.1.1.6. Iron tetramethyl 4,4',4'',4'''-(porphyrin-5,10,15,20-tetrayl)tetrabenzoate (FeTEP):

Into a clean dry round bottom flask 25 ml of DMF was added. The solution was purged with N_2 for 10 minutes. A further 0.1 mmol of TEP and 0.3 mmol of Iron (III) chloride were added and purged for an additional 5 minutes. The reaction mixture was then brought to reflux temperature and allowed to stir under a nitrogen atmosphere overnight.

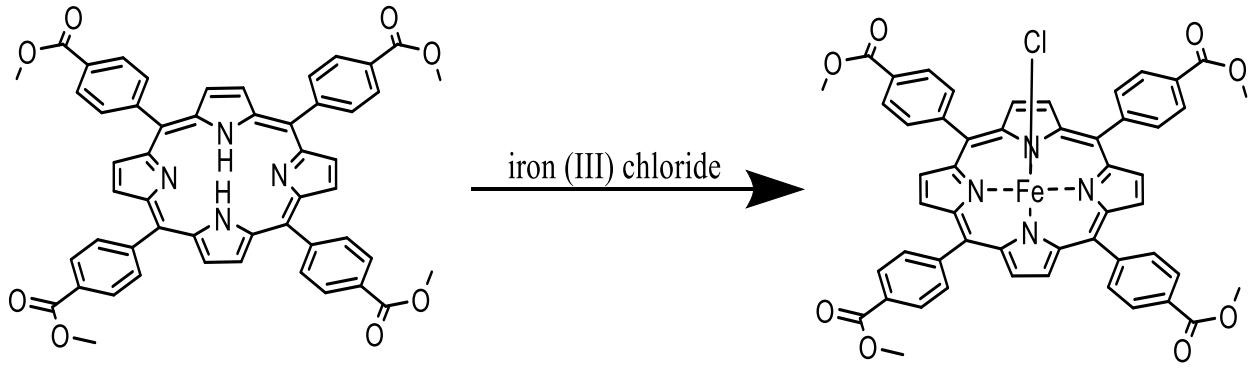

Figure 46: Synthesis of CuTEP

DMF was added to 400 ml of cyclohexane. The solution was stirred vigorously to allow a precipitate to form. The solution was then filtered under vacuum. The precipitate was further washed with methanol until washing became clear. No further purification was required. A purple powder was obtained.

4.1.1.7. 5,10,15,20-tetrakis(4-nitrophenyl)porphyrin (TNP)

Into a clean dry 500ml round bottom flask 100 ml of propionic acid was added. A further 16.7 mmol of 4-nitro benzaldehyde was added and 21 mmol of acetic anhydride were added to the solution. 14.3 mmol of pyrrole was diluted with 10 ml of propionic acid and added slowly one the solution reached reflux temperature (160 ^{o}C).

The reactant mixture was allowed to stir for 1 hour. The mixture was then cooled to room temperature and placed in the freezer overnight.

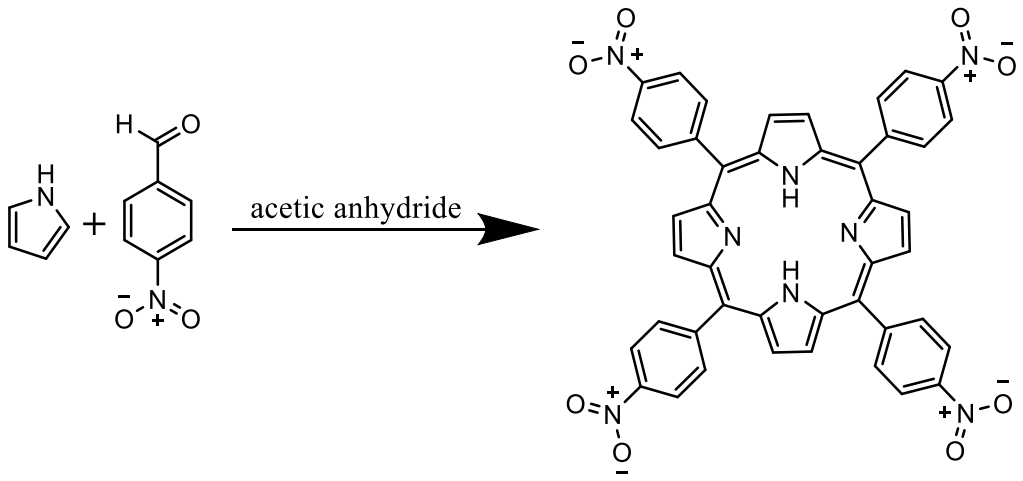

Figure 47: Reaction for the formation of TNP

The solution was filtered under vacuum and washed with water. The resultant solid was then added to 50 ml of pyridine and brought to reflux temperature for 1 hour. The solution was then cooled to room temperature, filtered and washed with methanol. No further purification was required. This resulted in the formation of a purple powder.

Yield: 16%

NMR: (400 MHz, $CDCl_3$), 8.80 ppm(s, 8H), 7.66ppm (d, 8H), 7.38 ppm (d, 8H), -2.14 (s, 2H)

UV-Vis: **432**, 516, 551, 590, 645 nm

4.1.1.8. Zinc 5,10,15,20-tetrakis(4-nitrophenyl)porphyrin(ZnTNP):

Into a clean dry round bottom flask 25 ml of DMF was added. The solution was purged with N_2 for 10 minutes. A further 0.1 mmol of TEP and 0.3 mmol of zinc (II) acetate

were added and purged for an additional 5 minutes. The reaction mixture was then brought to reflux temperature and allowed to stir under a nitrogen atmosphere overnight.

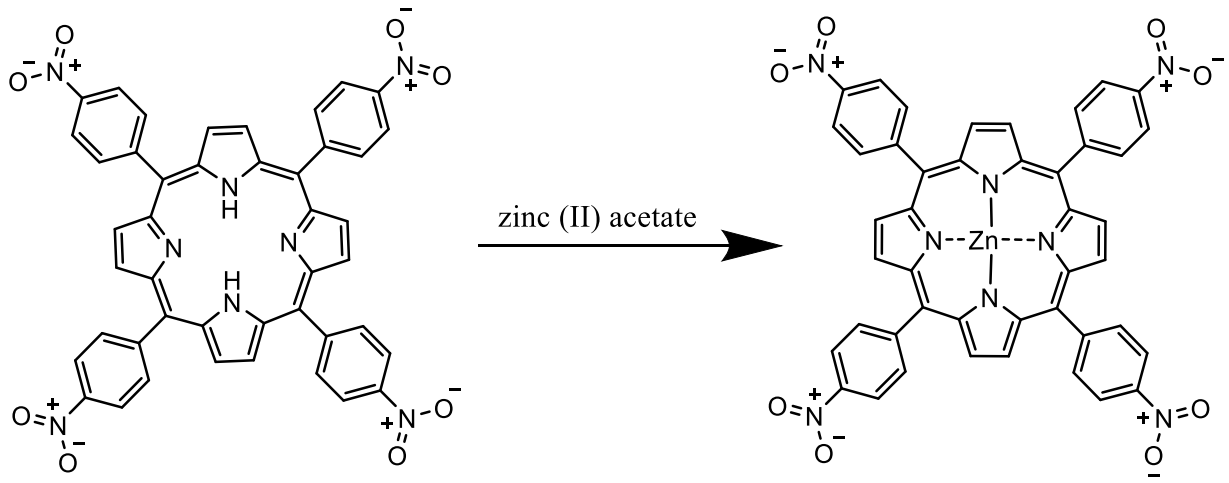

Figure 48: Synthesis of ZnTNP

The mixture was then cooled to room temperature. DMF was added to 400 ml of deionized water. The solution was stirred vigorously to allow a precipitate to form. The solution was then filtered under vacuum. The precipitate was further washed with methanol until washing became clear. No further purification was required. A purple powder was obtained.

Yield: 83%

NMR: (400 MHz, DMSO), 8.74 ppm(s, 8H), 7.56ppm (d, 8H), 7.36 ppm (d, 8H)

UV-Vis: **432**, 562, 602 nm

4.1.1.9. Cobalt5,10,15,20-tetrakis(4-nitrophenyl)porphyrin (CoTNP):

Into a clean dry round bottom flask 25 ml of DMF was added. The solution was purged with N_2 for 10 minutes. A further 0.1 mmol of TEP and 0.3 mmol of cobalt (II) chloride

hexahydrate were added and purged for an additional 5 minutes. The reaction mixture was then brought to reflux temperature and allowed to stir under a nitrogen atmosphere overnight.

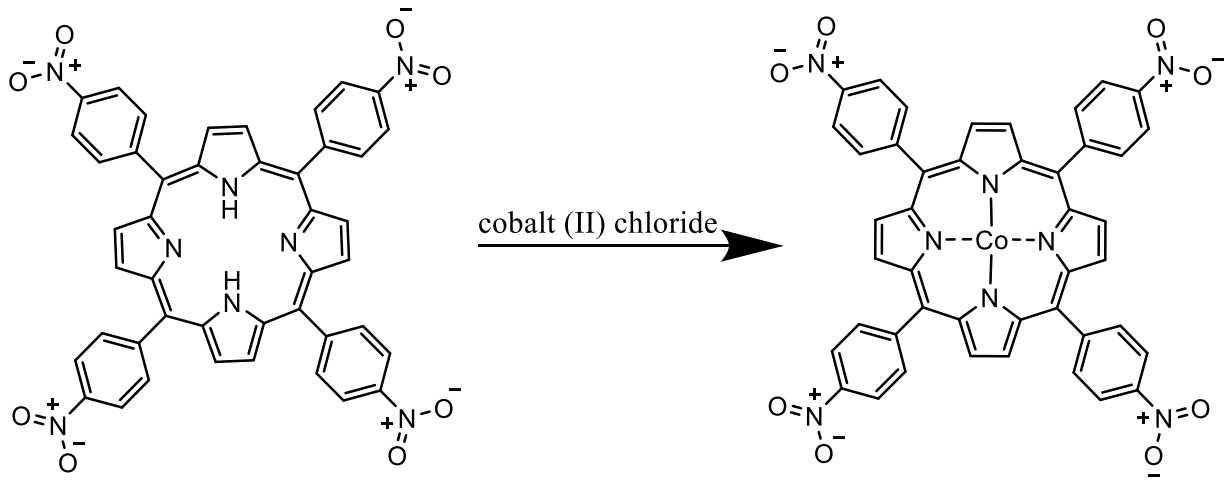

Figure 49: Synthesis of CoTNP

The mixture was then cooled to room temperature. DMF was added to 400 ml of deionized water. The solution was stirred vigorously to allow a precipitate to form. The solution was then filtered under vacuum. The precipitate was further washed with methanol until washing became clear. No further purification was required. A purple powder was obtained.

Yield: 72%

UV-Vis: **422**, 534 nm

4.1.1.10. Copper 5,10,15,20-tetrakis(4-nitrophenyl)porphyrin (CuTNP):

Into a clean dry round bottom flask 25 ml of DMF was added. The solution was purged with N_2 for 10 minutes. A further 0.1 mmol of TEP and 0.3 mmol of copper (II)

chloride were added and purged for an additional 5 minutes. The reaction mixture was then brought to reflux temperature and allowed to stir under a nitrogen atmosphere overnight.

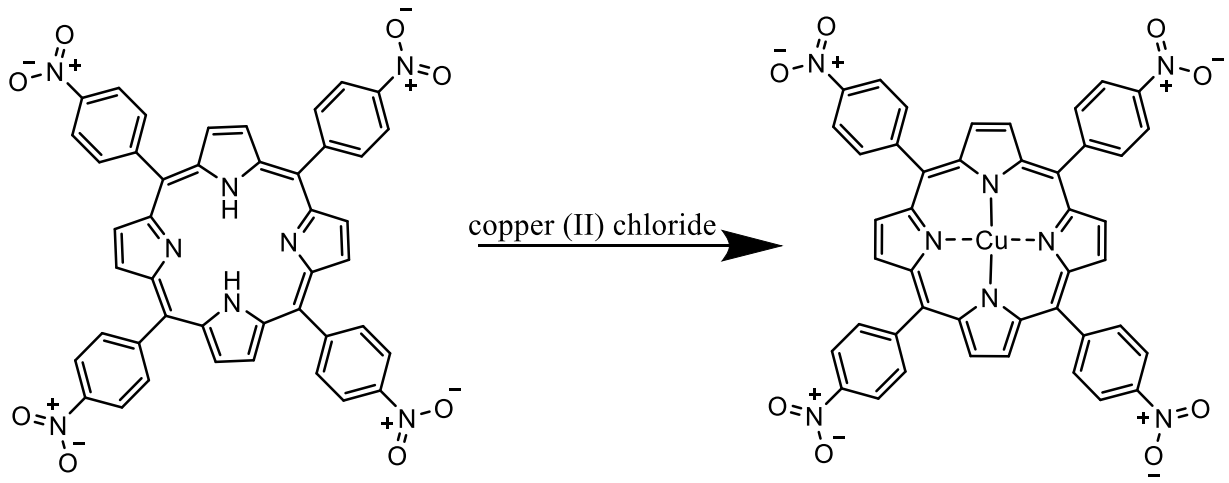

Figure 50: Synthesis of CuTNP

The mixture was then cooled to room temperature. DMF was added to 400 ml of deionized water. The solution was stirred vigorously to allow a precipitate to form. The solution was then filtered under vacuum. The precipitate was further washed with methanol until washing became clear. No further purification was required. A purple powder was obtained.

Yield: 74%

UV-Vis: **421**, 542 nm

4.1.1.11. Iron 5,10,15,20-tetrakis(4-nitrophenyl)porphyrin (FeTNP):

Into a clean dry round bottom flask 25 ml of DMF was added. The solution was purged with N_2 for 10 minutes. A further 0.1 mmol of TNP and 0.3 mmol of iron (III) chloride

were added and purged for an additional 5 minutes. The reaction mixture was then brought to reflux temperature and allowed to stir under a nitrogen atmosphere overnight.

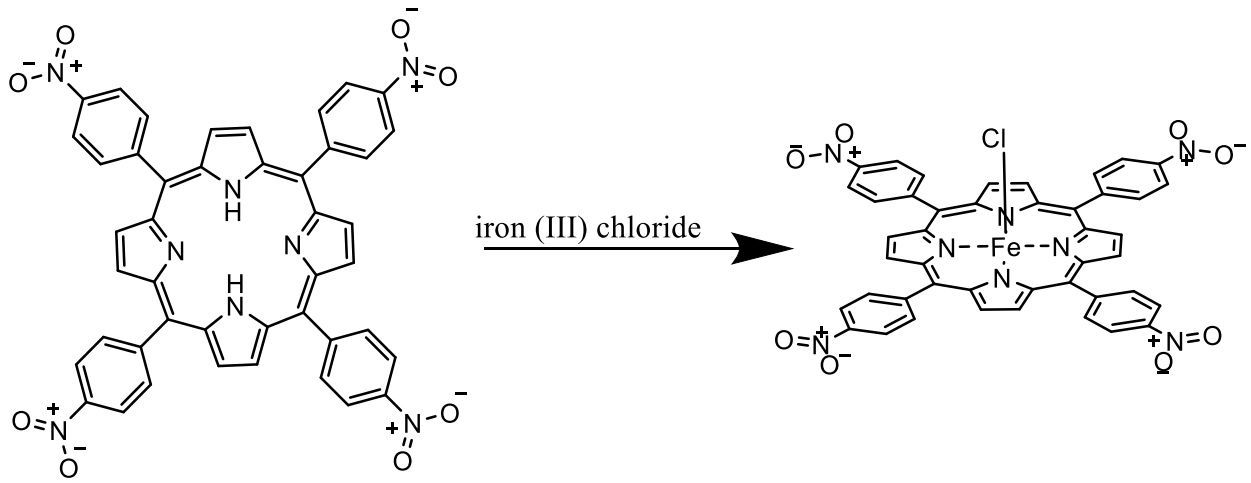

Figure 51: Synthesis of CoTNP

The mixture was then cooled to room temperature. DMF was added to 400 ml of deionized water. The solution was stirred vigorously to allow a precipitate to form. The solution was then filtered under vacuum. The precipitate was further washed with methanol until washing became clear. No further purification was required. A purple powder was obtained.

Yield: 42%

UV-Vis: **425**, 570, 614 nm

3.1.1.12. 3-((trimethylsilyl)ethynyl)benzaldehyde

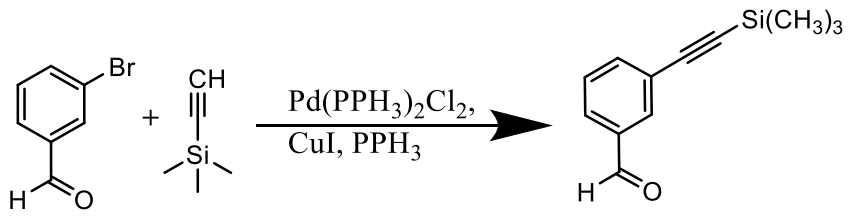

Figure 52: Synthesis of 3-((trimethylsilyl)ethynyl)benzaldehyde

25 ml of diisopropylamine was purged with N_2 for 10 minutes in a 50 ml round bottom flask. 1.82 mmol of 3-bromobenzaldehyde was added, the mixture was allowed to purge for an additional 10 minutes. 0.072 mmol (4%) of $Pd(PPh_3)_2Cl_2$, 0.072 mmol (4%) of CuI and 0.144 mmol (8%) were all added to the mixture. Lastly 2.73 mmol of ethynylTMS was added to the reaction flask. The reaction mixture was brought to reflux temperature and allowed to reflux under a nitrogen atmosphere overnight.

The solvent was removed by reduced pressure and extracted with 20 ml portions of a DCM:Hexane (5:1) mixture. The DCM hexane mix was decanted. This process was repeated until the liquid was clear. Solvent was dried under reduced pressure and purified using a kugelrohr at 125 ^{o}C. A clear liquid resulted in the collection flask. Spectroscopic data was in agreement with the literature.[24]

HNMR:(400 MHz, DMSO), 9.99 ppm(s, 1H), 7.97ppm (t, 1H), 7.90 ppm (dt, 1H), 7.77 ppm (dt, 1H), 7.60 ppm(t, 1H), 0.28 ppm (s, 9H)

3.1.1.13. 2,8-diethyl-5,5-difluoro-1,3,7,9-tetramethyl-10-(3-((trimethylsilyl)ethynyl)phenyl)-5H-4l4,5l4-dipyrrolo[1,2-c:2',1'-f][1,3,2]diazaborinine (F)

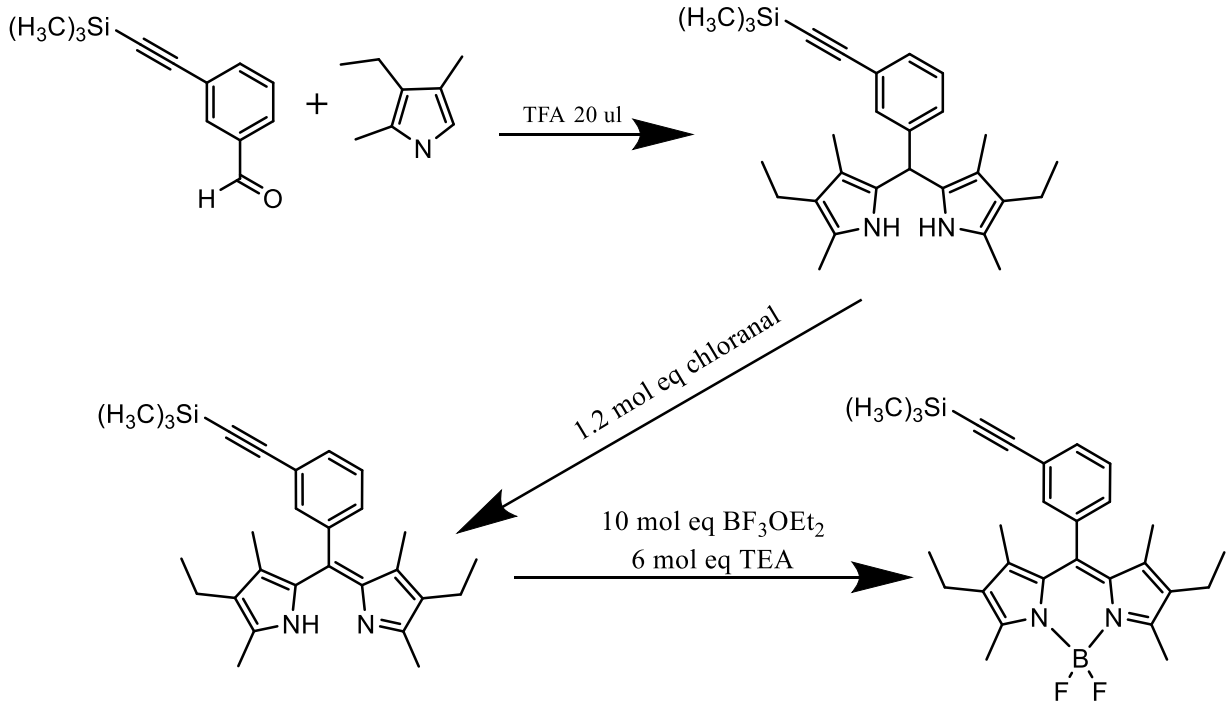

Figure 53: Synthesis of F

20 ml of DCM was placed in a clean and dry 50 ml round bottom flask. The solutions were purged for 15 minutes. 2.94 mmol if kryptopyrrole and 1.47 mmol of 3-ethynyl TMS aldehyde were added and purged for a further 5 minutes. 20 ul of TFA was added and the solution was allowed to stir overnight at room temperature under a N_2 atmosphere. 5ml of DCM was purged for 5 minutes .1.76 mmol of chloranil was added to the purged DCM and this solution was added to the reaction mixture. The mixture was then allowed to stir for an additional 4 hours at room temperature under a N_2 atmosphere. Finally 8.8 mmol of TFA and 14.7 mmol of BF_3OEt_2 were added and the reaction mixture was allowed to stir overnight at room temperature under a N_2 atmosphere.

The resultant mixture was washed with saturated sodium hydrogen carbonate and the organic phase was collected. This was repeated until the aqueous fraction remained clear. The product was further purified using silica column chromatography with a solvent mixture of 9:1 hexane:ethyl acetate as mobile phase. This resulted in a fine red powder being formed.

Yield: 20%

HNMR : (400 MHz, DMSO), 7.62 ppm(d, 1H), 7.56ppm (t, 1H), 7.48 ppm (s, 1H), 7.41 ppm (d, 1H), 2.43ppm(s, 6H), 2.28 ppm(q, 4H), 1.26ppm(s, 6H), 0.93ppm(t, 6H), 0.24 ppm (s, 9H)

3.1.1.14. 3 2,8-diethyl-10-(3-ethynylphenyl)-5,5-difluoro-1,3,7,9-tetramethyl-5H-4l4,5l4-dipyrrolo[1,2-c:2',1'-f][1,3,2]diazaborinine (G)

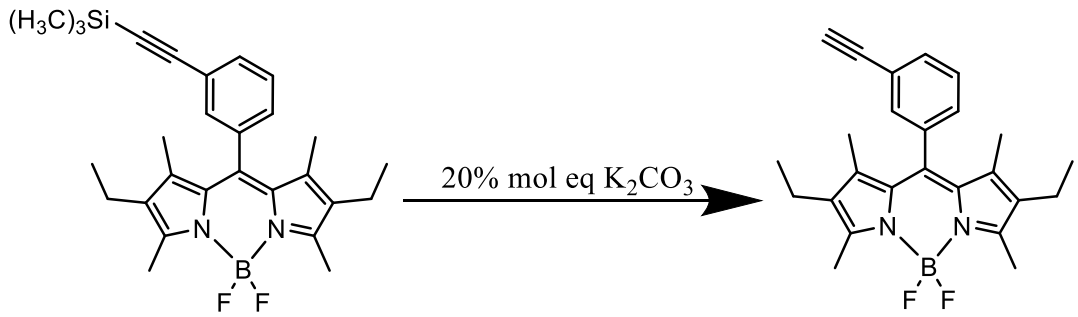

Figure 54: Synthesis of G

20 ml of methanol was added to a clean dry round bottom flask and allowed to purge for 15 minutes. 0.37 mmol of 3-ethynyl TMS phenyl bodipy was added and allowed to purge for a further 5 minutes. Finally a 20% molar equivalent of K_2CO_3 was added. The reaction was allowed to stir at room temperature for 4 hours under atmosphere of N_2.

The resultant mixture was washed with saturated sodium hydrogen carbonate and the organic phase was collected. This was repeated until the aqueous fraction remained clear. The product was further purified using silica column chromatography with a solvent mixture of 9:1 hexane:ethyl acetate as mobile phase. This resulted in the formation of a fine red powder.

Yield: 90%

HNMR: (400 MHz, DMSO), 7.66 ppm(d, 1H), 7.60ppm (t, 1H), 7.48 ppm (s, 1H), 7.41 ppm (d, 1H), 4.30 ppm (s, 1H), 2.43ppm(s, 6H), 2.28 ppm(q, 4H), 1.26ppm(s, 6H), 0.93ppm(t, 6H).

3.1.1.15. 5,5-difluoro-1,3,7,9-tetramethyl-10-(3-((trimethylsilyl)ethynyl)phenyl)-5H-4l4,5l4-dipyrrolo[1,2-c:2',1'-f][1,3,2]diazaborinine (H)

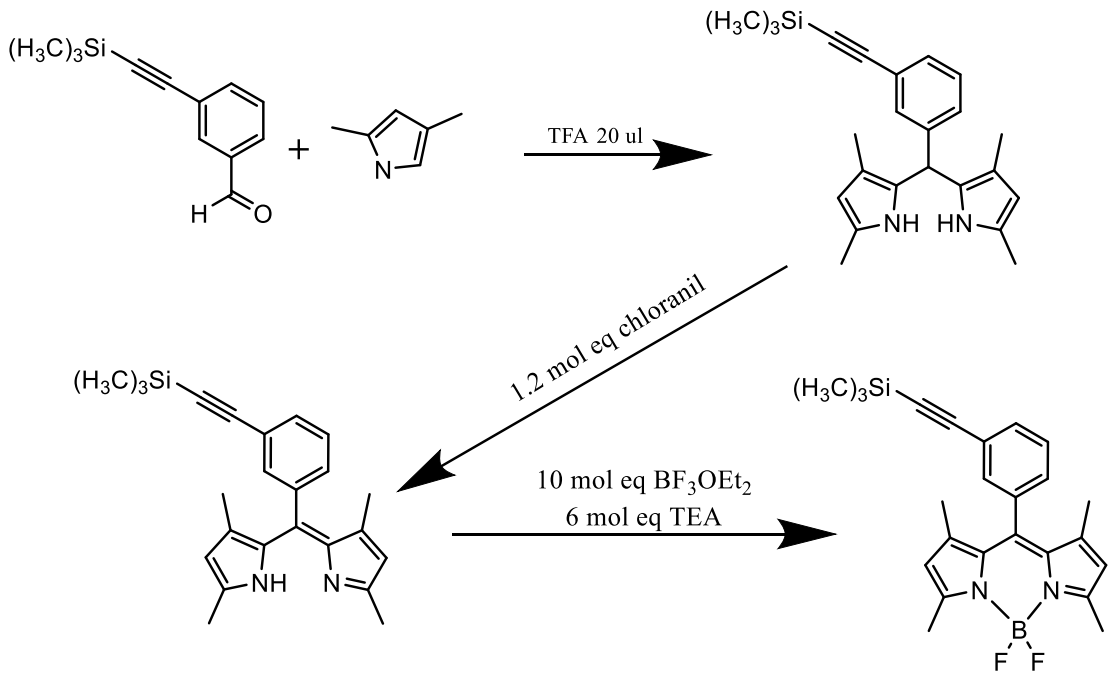

Figure 55 Synthesis of H

20 ml of DCM was placed in a clean and dry 50 ml round bottom flask. The solutions were purged for 15 minutes. 2.94 mmol of 2, 4-dimethyl pyrrole and 1.47 mmol of 3=ethynyl TMS aldehyde were added and purged for a further 5 minutes. 40 ul of TFA was added and the solution was allowed to stir overnight at room temperature under a N_2 atmosphere. 5 ml of DCM was purged for 5 minutes and used to add 1.76 mmol of chloranil to the reaction mixture. The mixture was then allowed to stir for an additional 4 hours at room temperature under a N_2 atmosphere. Finally 8.8 mmol of TFA and 14.7 mmol of BF_3OEt_2 was added and allowed to stir overnight at room temperature under a N_2 atmosphere.

The resultant mixture was washed with saturated sodium hydrogen carbonate and the organic phase was collected. This was repeated until the aqueous fraction remained clear. The product was further purified using silica column chromatography with a solvent mixture of 1:1 hexane:ethyl acetate. This resulted in the formation of a fine orange powder.

Yield: 18%

HNMR: (400 MHz, CDCl3), 7.57 ppm(dt, 1H), 7.44ppm (m, 2H), 7.24 ppm (dt, 1H), 5.98 ppm (s, 2H), 2.55 ppm (s, 6H), 1.41ppm(s, 6H), 0.24 ppm(s, 9H).

3.1.1.16. 10-(3-ethynylphenyl)-5,5-difluoro-1,3,7,9-tetramethyl-5H-4l4,5l4-dipyrrolo[1,2-c:2',1'-f][1,3,2]diazaborinine (I)

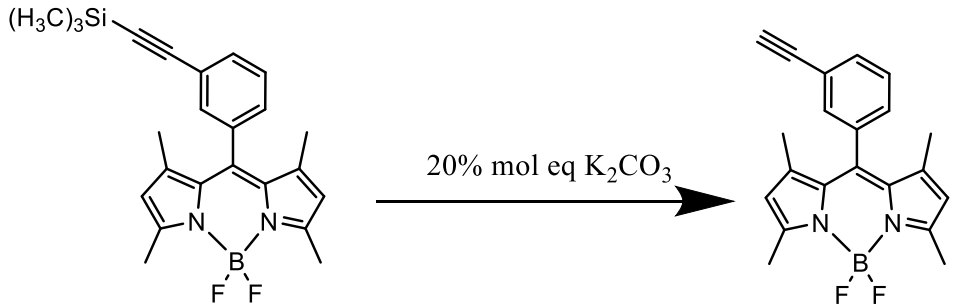

Figure 56: Synthesis of I

20 ml of methanol was added to a clean dry round bottom flask and allowed to purge for 15 minutes. 0.37 mmol of 3-ethynyl TMS phenyl bodipy was added and allowed to purge for a further 5 minutes. Finally a 20% molar equivalent of K_2CO_3 was added. The reaction was allowed to stir at room temperature for 4 hours under atmosphere of N_2.

The resultant mixture was washed with saturated sodium hydrogen carbonate and the organic phase was collected. This was repeated until the aqueous fraction remained clear. The product was further purified using silica column chromatography with a solvent mixture of 9:1 hexane:ethyl acetate.

Yield: 92%

HNMR: (400 MHz, CDCl3), 7.61 ppm(dt, 1H), 7.44ppm (m, 2H), 7.28 ppm (dt, 1H), 5.98 ppm (s, 2H), 3.14 ppm (s, 1H), 2.55 ppm (s, 6H), 1.41ppm(s, 6H).

3.1.1.17. Rhenium Bipyridine Tricarbonyl Chloride

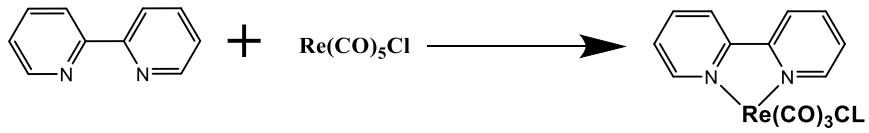

Into a dry and clean round bottom flask, 30 ml of toluene was purged with N_2. 0.7 mmol of pentacarbonylchlororhenium was added to the round bottom flask. 0.7 mmol of 2, 2'-bipyridine was added to the flask. The solution was brought to reflux temperature and allowed reflux for 4 hours.

The solution was allowed to cool to room temperature. The solid yellow precipitate was collected by vacuum filtration. The solid was washed with water and ethyl acetate. No further purification was required. A fine yellow powder was collected. Spectroscopic data reported here is in agreement with the literature.[15]

Yield: 87%

HNMR : (400 MHz, CDCl3), 9.02 ppm(d, 2H), 8.77ppm (d, 2H), 8.35 ppm (t, 2H), 7.77 ppm (t, 2H).

IR: (DCM) 2025, 1917, 1900

3.1.1.18. Bromobipyridine

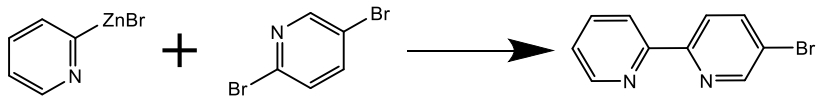

Into a clean dry 2 necked round bottom flask under a trickle flow of nitrogen 5mmol of 2, 5-dibromopyridine, 0.2 mmol of Pd $(PPh_3)_2Cl_2$, 0.4 mmol of PPH_3 and 0.2 mmol of CuI were all placed in round bottom flask (insure nitrogen flow is low). This was followed by 11 mmol of pyridyl zinc bromide (0.5 M in THF) (use cautions pyrophoric) and placed in the round bottom flask. The reaction flask was allowed to stir over night under a nitrogen atmosphere.

The solution was purified by washing with 500 ml portions of a saturated EDTA and Na_2CO_3 solution. A small quantity of the reaction mixture was added to each portion. This mixture was washed with 100 ml aliquots of DCM three times. The DCM portions were combined, dried over$MgSO_4$ and allowed to evaporate in the fume hood due to the low temperature sublimation point of the product. The product was purified using alumina with a mobile phase of 9:1 hexane:ethyl acetate. The solutions were left to evaporate in a fume hood due to the sublimation temperature of the product.

Yield: 38%

HNMR: (400 MHz, CDCl3), 9.12 ppm(s, 1H), 9.07ppm (d, 1H), 8.17 ppm (s, 2H), 8.08 ppm (m, 2H), 7.58 ppm (t, 1H)

3.1.1.19. Rhenium Bromobipyridine Tricarbonyl Chloride

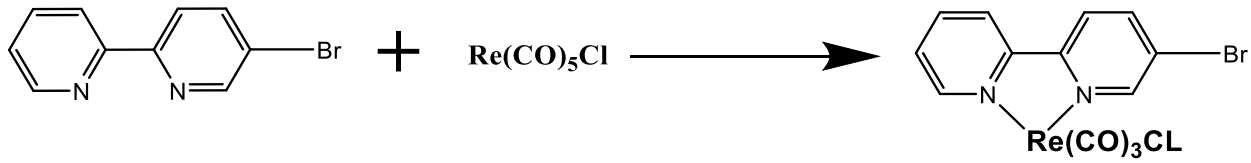

Into a dry and clean round bottom flask, 30 ml of toluene was purged with N_2. 0.7 mmol of Pentacarbonylchlororhenium was added to the round bottom flask. 0.7 mmol of 2, 2’ bipyridine was added to the flask. The solution was brought to reflux temperature and left for 4 hours.

The solution was allowed to cool to room temperature. The solid yellow precipitate was collected by vacuum filtration. The solid was washed with water and ethyl acetate. The solid was allowed to by vacuum filtration. No further purification was required. Spectroscopic data reported here is in agreement with the litreatuer.[15]

Yield: 80%

NMR: (400 MHz, CDCl3), 9.12 ppm(s, 1H), 9.07ppm (d, 1H), 8.16 ppm (d, 2H), 8.08 ppm (m, 2H), 7.57 ppm (t, 1H)

IR: (DCM) 2025, 1920, 1900

3.2 Instrumentation and methods

3.2.1 Gas chromatography

Gas chromatography experiments results within this thesis were all carried out on a Shimadzu GC2010 with a Restek ShinCarbon ST (2 m x 0.53mm) and a BID (barrier ionisation detector). The carrier gas used was BIP grade Helium (Air Products) Each run took approximately 24 minutes, the column oven was maintained at 30^{o}C throughout the run. Each run was carried out with a flow rate of 10ml/min. The elution order observed was H_2, CO, CH_4 and CO_2 respectively.

3.2.2 Standards and sample injection

1000 ppm standards were used as reference standards. Each standard was made up with a mix of six gases (H_2, O_2, CO, CH_4, CO_2, He) by Scientific and Technical Gases (STG). 1 ml of sample was withdrawn from the standard vessel and injected into the 250 ul sample loop 100 and 10,000 ppm standards were also available for experiment that produced far more or less than a standard experiment to ensure that the concentration of the standard was equivalent to the actual value. Experimental samples were injected in the same manner as standards.

3.2.3 Calculation of gas generated, TON and Faradaic efficiency (FE)

For calculation of TON and FE the ideal gas law was used. It was assumed that the vessels were at 1 atm of pressure and the temperature of the lab was measured in real time for each experiment (typically between 19 and 21 ^{o}C). The total volume of each vessel was calculated. The total volume of solution was then subtracted from this value to calculate the headspace.

3.3 Electrochemistry

3.3.1. Cyclic voltammetry and bulk electrolyses

Cyclic voltammetry and bulk electrolysis were carried out on a CH instruments 600C. The working electrode used was a 3mm diameter glassy carbon electrode o The reference electrode was Ag/Ag^{+} made up in the electrolyte of the experiment. The Counter electrode was a 1.5 x 1.5 cm platinum mesh . Glassy carbon electrodes were cleaned with polishing with 0.3 and 0.05 um alumina with rinsing in between.

The electrochemical cell used throughout this thesis was a custom H-cell. It contained a glass frit separating two compartments that would allow flow of charge between both compartments. The volume of each compartment was approximately 34 ml.

3.3.2 Electrochemical cyclic voltammetry procedure:

All CVs were carried out in DMF with 0.1M TBAPF6 with a glassy carbon electrode (3 mm diameter) silver silver ion in ACN reference electrode and a platinum gauze counter electrode. All concentrations of catalyst were at 1 mM. Pure DMF was purged with argon and analysed prior to the addition of catalyst to insure a clean background. A stepwise investigation was observed with purging of argon post the addition of catalyst and investigated. Followed by purging with CO_2 and reanalysed. This was concluded by the addition of 5% water and finally analysed a 3rd time.

3.3.3 Electrochemical surface procedure:

Electrodes were coated by dropcasting from 0.1mM DMF solutions, 1.5 uL of each sample were placed on electrodes and allowed to dry overnight. In each side of an H-cell 15 mls of the desired solution was placed. Reference and working electrodes were placed in one compartment of the cell with the counter electrode placed in the other. CVs were carried out prior to all bulk electrolysis being carried out.

3.4 Photocatalysis

1) Two stock solutions were prepared Firstly a stock solution of ACN and TEOA in a 2:1 mixture was prepared, a secondary solution of 0.133 mM rhenium bipyridine tricarbonyl chloride and 3-ethynyl bodipy was prepared in ACN. All solutions were deaerated under vacuum and placed under a blanket of CO_2 using Schlenk techniques. This was step was repeated in triplicate to ensure samples were fully deaerated. Samples were irradiated with LED lights sources; with λ >400nm, 470nm and 525nm, for 18 hours. The amount of CO in head space was confirmed by GC injection of the headspace. All results presented assume negligible CO dissolved in solution. The samples were examined by gas chromatography coupled with a barrier discharge ionization detector (GC-BID). Results were compared to mixed standards prepared by Scientific and Technical Gases (STG) at 1000ppm.

2) Method 2 was carried out as per 1 with the adjustments: TEOA was replaced by TEA. 10% water was also added to each sample and purging was carried out with argon.

3) Method 3 was carried out as per 1 with the adjustments: ACN was replaced by DMF

4) Three solutions were made up prior to the experiment. First being a stock solution of DMF and TEOA in a mixture of 2 parts DMF to 1 part TEOA. A secondary solution of 0.2mM catalyst and photosensitiser were prepared in DMF. A third solution was prepared containing 0.15.M benzyl-1,4-dihydronicotinaminde in DMF. All solutions were deaerated under vacuum and placed under a blanket of CO_2. This was carried out in triplicate to ensure samples were fully deaerated. Samples were irradiated at different wavelengths (>400nm; one at 470nm; and one at 525nm) for 18

hours. Post photolyzing, the samples were examined by gas chromatography coupled with a barrier discharge ionization detector (GC-BID). Results were compared to mixed standards prepared by Scientific and Technical Gases (STG) at 1000ppm. All results presented assume negligible CO dissolved in solution

3.5 Chemicals and materials

All solvents were purchased from Sigma Aldrich. Solvents for use in photochemistry were freshly distilled prior to use. Acetonitrile (ACN) was dried by distillation over calcium hydride. Triethylamine (TEA) was dried by distillation over potassium hydroxide. Methanol was dried by distillation over magnesium turnings and iodine. DMF was purchased at anhydrous 99%, no further purification was carried out. TEOA was purchased at 99% GC grade. No further purification was carried out. All solvents used from chromatography were dried over magnesium sulphate ($MgSO_4$). All solvents used for spectroscopy were spectrophotometric grade solvents or of equal purity. Column chromatography was carried out using neutral silica gel pH 6.5 – 7.5 or neutral aluminium oxide. Silica Gel (Merck) was used as received. All other chemicals were obtained commercially and were used without further purification.